Electronic Thesis and Dissertation Repository

11-17-2022 10:30 AM

Production of cellulose-based superabsorbent polymers for soil water retention

Rosa Maria Arredondo Ramirez, *The University of Western Ontario*

Supervisor: Rehmann, Lars, *The University of Western Ontario*
A thesis submitted in partial fulfillment of the requirements for the Doctor of Philosophy degree in Chemical and Biochemical Engineering
© Rosa Maria Arredondo Ramirez 2022

Follow this and additional works at: https://ir.lib.uwo.ca/etd

Part of the Other Chemical Engineering Commons

Abstract

Superabsorbent polymers (SAPs) have attracted tremendous attention, with researchers noting that their high water absorption capacity (AC) is valuable for various applications, especially in agricultural contexts. Two types of materials can be used to produce SAPs: fossil-based (which are harmful to the environment) and bio-based (which are significantly more environmentally friendly, given their biodegradability and minimal toxic side effects). Although bio-based SAPs (Bio-SAPs) are preferable due to their environmental merits, their preparation tends to be time consuming and labour intensive, and their AC is still far below expectations. To address these problems, a novel, eco-friendly, cellulose-based superabsorbent polymer (Cellulo-SAP) was developed in this study through facile preparation via free radical synthesis using esterified pure cellulose. First, pure cellulose was esterified with maleic anhydride to evaluate the effects of the catalyst, solvent, and cellulose–maleic anhydride molar ratio. Second, an approach for graft copolymerization of esterified pure cellulose with acrylic acid was developed; this involved free radical synthesis using polyethylene glycol diacrylate as the crosslinker, resulting in the production of Cellulo-SAP. Third, the absorbency, thermal/pH stability, reusability, and biodegradability of Cellulo-SAP were evaluated. This new polymer demonstrated reusability as a water reservoir, in addition to high thermal and pH stability. More importantly, Cellulo-SAP achieved an AC of 475 g/g and exhibited superior biodegradability compared to a commercial, fossil-based SAP (Sigma-Aldrich sodium polyacrylate). These results suggest that Cellulo-SAP can be used in agriculture as an effective alternative to fossil-based SAPs. Finally, crude cellulose was obtained via organosolv fractionation with a mixture of acetic acid, formic acid, and water added to the biomass from cornstalk residues. The crude cellulose consisted of 13.87% lignin, 27.58% hemicellulose, and 57.46% α-cellulose, and it had a 0.41 degree of esterification after fractionation. This crude cellulose was used as a raw material to obtain a Bio-SAP (CrudeCellulo-SAP) via the methodology developed for graft copolymerization and crosslinking of Cellulo-SAP. CrudeCellulo-SAP demonstrated an AC of 369 g/g.

Keywords

Summary for lay audience

Materials with a high absorption capacity (AC) have many applications, which makes them very useful. A common application of such materials is in diaper granules, which absorb large amounts of liquid and expand greatly. Materials of this sort—which absorb more than 300 times their weight—are called "superabsorbent polymers" (SAPs). SAPs also have applications in industries such as construction (e.g., concrete additive), medical care (e.g., drug releaser), and agriculture (e.g., water releaser for plants).

The first step in the agricultural applications of SAPs is hydrating them; a hydrated SAP is known as a "hydrogel." The second step is mixing the hydrogel with the soil, where it functions as a water reservoir for a plant's roots. Finally, the water contained in the hydrogel is released; the roots absorb the water, enhancing the plant's growth and optimizing water irrigation. Since the hydrogel is durable, it can absorb and desorb water several times. After the SAP/hydrogel has been used, it remains in the soil. In the case of fossil-based SAPs—the only SAPs available on the market—this is problematic because they biodegrade very slowly and leave harmful residues in the soil.

SAPs have been benefitting agriculturalists for more than 30 years, and they are increasingly in demand in this industry. SAPs are imperative, but it is also vital to use alternative, natural sources to produce them and make them biodegradable. To this end, the present dissertation explains the development of a methodology to obtain bio-based SAPs, or "Bio-SAPs" (i.e., SAPs that contain natural materials in their composition), as alternatives to fossil-based SAPs. The Bio-SAPs formulated in this study were cellulose-based (Cellulo-SAP) and crude cellulose-based (CrudeCellulo-SAP). Evaluations of Cellulo-SAP and CrudeCellulo-SAP showed high AC in both, highlighting their viability as alternatives to fossil-based SAPs.

Co-authorship statement

This dissertation was completed under the supervision of Dr. Charles Xu and Dr. Lars Rehmann. The research was conducted under the technical supervision of Dr. Sean Yuan at Western University's Institute for Chemicals and Fuels from Alternative Resources (ICFAR) and Western Maple BioResources's laboratory. The extent of the collaboration in each chapter is stated below.

Chapter 1

Introduction

Rosa Arredondo: Wrote the chapter.

Dr. Spencer Moyes: Edited the text.

Dr. Qiang Wei: Edited the text.

Dr. César Medina: Edited the text.

Dr. Lars Rehmann: Edited the text.

Chapter 2

Cellulose modification: esterification

Rosa Arredondo: Designed and conducted experiments, analyzed samples, interpreted data, and wrote the chapter.

Dr. Sean Yuan: Assisted in experiment design and data interpretation, oversaw experiments, and edited the text.

Dr. Charles Xu: Oversaw experiments and edited the text.

Dr. Spencer Moyes: Edited the text.

Dr. Qiang Wei: Edited the text.

Dr. César Medina: Edited the text.

Dr. Lars Rehmann: Edited the text.

Chapter 3

Bio-SAP synthesis and the effects of its variables

Rosa Arredondo: Designed and conducted experiments, analyzed samples, interpreted data, and wrote the chapter.

Dr. Sean Yuan: Assisted in experiment design and data interpretation, and edited the text.

Dr. Spencer Moyes: Edited the text.

Dr. Qiang Wei: Edited the text.

Dr. César Medina: Edited the text.

Dr. Lars Rehmann: Edited the text.

Chapter 4

Performance of Cellulo-SAP: absorbency, stability, reusability, and biodegradability

Current Status: Accepted article, published online.

Arredondo, R., Yuan, Z., Sosa, D., Johnson, A., Beims, R.F., Li, H., Wei, Q. and Xu, C.C. (2022), Performance of a novel, eco-friendly, cellulose-based superabsorbent polymer (Cellulo-SAP): Absorbency, stability, reusability, and biodegradability. Can J Chem Eng. Accepted Author Manuscript. https://doi.org/10.1002/cjce.24601

Rosa Arredondo: Designed and conducted experiments, analyzed samples, interpreted data, and wrote the text.

Dr. Qiang Wei: Provided technical advice regarding property characterization, assisted in data interpretation, and edited the text.

Dr. Spencer Moyes: Edited the text.

Dr. Hongwei Li: Edited the text and figures.

Dr. Charles Xu: Acted as the corresponding author for the submission of the manuscript.

Dr. Lars Rehmann: Mediated communication for manuscript publication.

Chapter 5

CrudeCellulo-SAP

Rosa Arredondo: Designed and conducted experiments, analyzed samples, interpreted data, and wrote the chapter.

Dr. Qiang Wei: Provided technical advice regarding property characterization, assisted in data interpretation, and edited the text.

Dr. Spencer Moyes: Edited the text.

Dr. César Medina: Edited the text.

Dr. Lars Rehmann: Edited the text.

Acknowledgments

Table of contents

List of tables

List of figures

Nomenclature

Abbreviations and acronyms

ANOVA, analysis of variance

Bio-SAP, bio-based superabsorbent polymer

CAS, chemical abstracts service

CCD, central composite design

Cell-MA, esterified cellulose with maleic anhydride with (degree of substitution = 1.2)

Cellulo-SAP, esterified cellulose-based superabsorbent polymer obtained with optimal formulation

CrudeCellulo-SAP, crude cellulose-based superabsorbent polymer obtained with optimal formulation

DON, degree of neutralization

DS, degree of substitution

FESEM, field emission scanning electron microscope

FTIR, Fourier transformed infrared

FWHM, full width at half-maximum

ICFAR, Institute for Chemicals and Fuels from Alternative Resources

PEG, polyethylene glycol

RSM, response surface methodology

SAP, superabsorbent polymer

SEM, scanning electron microscopy

XRD, X-ray diffraction

Chapter 1

1 Introduction

1.1 Background

Water-absorbent polymers are hydrophilic networks capable of absorbing and retaining water within their structure [1]. It is possible to find compounds in nature that present such properties. Based on their origin, they can be organic (e.g., cellulose-based materials such as cotton and starch), inorganic (e.g., zeolites), or synthetic (e.g., polymers derived from fossil resources). Chemically, hydrophobicity can be attributed to the functional groups attached to the polymeric structure. The polymeric network is bonded by connectors known as crosslinkers, which provide water solubility resistance to the water-absorbent polymer. Water-absorbent polymers capable of absorbing more than 300 g/g of deionized water are called "superabsorbent polymers" (SAPs) [2].

The interaction between an aqueous solution and a SAP involves the following mechanisms: i) hydration [3], ii) hydrogen bonds [3], iii) swelling of ionic polymers [4–7], and iv) osmosis and osmotic pressure [8,9]. These mechanisms play a fundamental role in the relationship between the swelling capacity and the stiffness of the polymer. By modifying the polymeric chain's neutralization and controlling the crosslinking degree in the polymer, it is possible to design the desired behaviour of the SAP [5,10].

Typically, fossil-based raw materials such as the following are used to synthesize SAPs: hydroxyethyl methacrylate, hydroxyethoxyethyl methacrylate, hydroxydiethoxyethyl methacrylate, methoxyethyl methacrylate, methoxyethoxyethyl methacrylate, methoxydiethoxyethyl methacrylate, ethylene glycol dimethacrylate, N-vinyl-2-pyrrolidone, vinyl acetate, acrylic acid, and N-(2-hydroxypropyl) methacrylamide. The main crosslinkers in SAP synthesis are epichlorohydrin; ethylene glycol; polyethylene glycol (PEG) acrylate; PEG methacrylate; PEG diacrylate; PEG dimethacrylate; N, N'-Methylene-bis-acrylamide; and divinyl sulfone. Depending on the type of synthesis, an

initiator, such as 2,20-azobis (isobutyronitrile), ammonium persulfate (APS), or potassium peroxydisulfate, may be required [1].

SAPs can be classified based on the following attributes: i) origin (i.e., natural, synthetic, or hybrid), ii) monomeric unit (e.g., polyacrylates/polyacrylamides and cellulose/starch graft copolymers), iii) polymeric composition (i.e., single or multiple monomers in the polymeric chain), iv) configuration (i.e., amorphous [11], semi-crystalline, or crystalline) [1], v) crosslinking type (i.e., chemical or physical) [12], vi) presence of electrical charges in the crosslinked chains (i.e., ionic, non-ionic, ampholytic, or polybetaines) [2], and vii) physical appearance (e.g., matrix, film, or microsphere).

The high water absorption capacity (AC) is a feature that makes SAPs attractive materials for application in different areas. They have been widely used in the hygiene industry to fabricate diapers and feminine pads. Other industries that frequently use SAPs include medical care [13–17], agriculture [18,19,28–37,20,38,21–27], and construction [39–43]. Novel applications of SAPs include the prediction of environmental phenomena through the analysis of swollen SAPs [5], adsorption–degradation of organic waste in water [44], and oil spillage cleanup [45].

Over the last 50 years, the ease of production and chemical modification of fossil-based SAPs have made them popular products on the market. However, over the last two decades, interest has grown in developing bio-based SAPs (Bio-SAPs, i.e., SAPs that contain natural materials in their composition) to replace fossil-based SAPs [11]. The production of absorbent materials from natural sources has become more important due to the need for non-toxic, biodegradable products to diminish the environmental impact of fossil-based reactant usage. This requirement has engendered more research and technology pertaining to bio-absorbent production, which involves using compounds made of biomass instead of by-products from a petroleum source. Nevertheless, biomass compounds present challenges as raw materials for SAP production (e.g., low reactivity in the synthesis resulting in lower AC compared to fossil-based SAPs). This study aims to develop an effective technique (functionalization and copolymerization) for using a

bio-based raw material—cellulose—to produce a Bio-SAP whose AC is comparable to that of fossil-based SAPs.

1.2   Literature review

1.2.1   Classification of SAPs

SAPs are often classified according to their attributes [46]. Figure 1 shows a compilation of SAP categories. The most commonly used categories in research on SAPs are origin, polymeric composition, crosslinking type, and electrical charge.
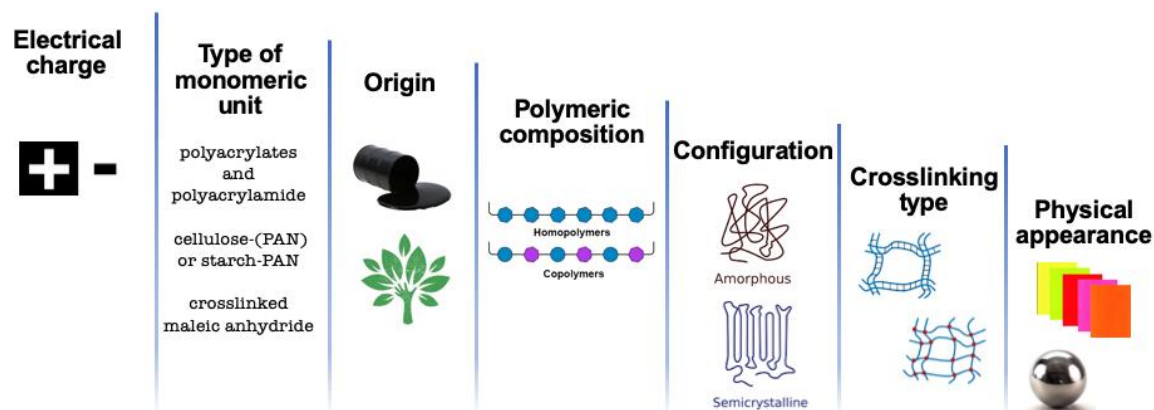
Figure 1: Classification of SAPs: electrical charge (anionic, cationic), type of monomeric unit (acrylates, acrylamides), origin (fossil, natural), polymeric composition (homopolymers, copolymers), configuration (amorphous, semicrystaline), crosslinking (physical, chemical), and physical appearance (spheric, films)

1.2.1.1 Origin

According to the origin of the raw materials, SAPs are classified as fossil-based (synthetic), natural, or hybrid. Fossil-based SAPs are generally synthesized from vinyl structure monomers from fossil sources, such as acrylic acid and acrylonitrile. Both are obtained from propylene, a by-product of ethylene and gasoline production. Acrylic acid is mainly obtained via oxidation reaction [47], and acrylonitrile via catalytic

ammoxidation [48]. Natural raw materials that produce SAPs are classified as polysaccharides (e.g., cellulose, starch, chitosan, carrageenan, and gelatin) or proteins (e.g., collagen-based proteins and soy protein) [49].

Hybrid SAPs have both synthetic and natural elements [12,50]. They are prepared by adding synthetic compounds to natural polymeric chains (e.g., polysaccharide graft copolymerization of vinyl monomers).

1.2.1.2 Polymeric composition

SAPs of homopolymers are prepared from a single type of monomer, and they can be crosslinked depending on the monomer structure and polymerization process [51]. Copolymeric SAPs are formed by replicates of units of two or more monomer types. According to the order and position of the replicated units, copolymeric SAPs can be classified into the following groups: alternate copolymers, random copolymers, block copolymers, and graft copolymers [52]. Multipolymer SAPs are made of two independent crosslinked polymers, whereas semi-multipolymer SAPs are formed by one crosslinked polymer and another non-crosslinked polymer [2].

1.2.1.3 Crosslinking types

SAPs can be formed by chemical and/or physical crosslinking. Chemical crosslinking has covalent bonds between polymeric chains; therefore, this type of bond plays a significant role in the final mechanical strength property of the SAP [53]. In contrast, physical crosslinking occurs only within transient junctions, such as ionic and electrostatic interactions, hydrogen bonds, Van der Waals forces, and hydrophobic interactions [12]. Generally, physical crosslinking results in a lower degree of crosslinking compared to chemical crosslinking. The physical crosslinking reaction is held on the surface of the material, whereas the chemical crosslinking reaction (e.g., emulsion polymerization, radical polymerization, and photo-induced reaction) extends to a greater area, resulting in a higher degree of crosslinking [54]. Figure 2 shows a summary of the chemical and physical crosslinking reactions [55].
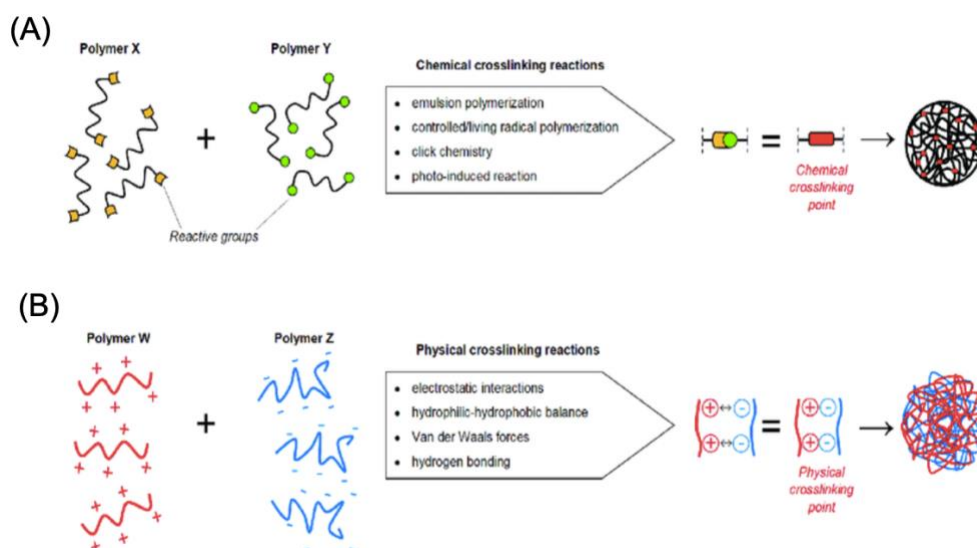
Figure 2: Summary of crosslinking types: (A) covalent bonds forming crosslinking points (in red) between reactive moieties (yellow and green) of polymers X and Y; (B) physical interactions between polymers W and Z, forming a self-assembled scaffold [55]

1.2.1.4 Electrical charge in polymeric chains

Depending on their functionalization, polymeric chains can bear different electrical charges. Therefore, they are classified as neutral, ionic, or ampholytic. Neutral SAPs, also known as non-ionic or non-charged SAPs, lack functional groups containing ions or charges, and they interact minimally with polar solvents [56]. In contrast, ionic SAPs can include positive (cationic) or negative (anionic) charges. In an aqueous medium, ionic SAPs' charges dissociate; therefore, their absorption efficiency depends on the pH characteristics of aqueous media [1]. Generally, cationic SAP dissociation is favoured by low pH solutions, whereas anionic SAPs present a higher degree of dissociation in a neutral to acidic medium. Ampholytic SAPs, also known as amphoteric SAPs, have acidic and basic groups in each unit of their molecules, resulting in the same number of positive and negative charges (not net charges) reaching its isoelectric point. Therefore, an alteration in the pH level of the aqueous medium may lead to a change in the electrical charge of the ampholytic SAP [57]. The electrical charges in SAPs influence the performance of AC and their mechanical strength properties [58].

1.2.2   Water absorption mechanism of SAPs

Several mechanisms of the swelling process in ionic SAPs are caused by negative and positive charges. When water is added to a SAP (Figure 3) [59], the water's interaction with the polymeric chain leads to hydration and hydrogen bond formation [5].
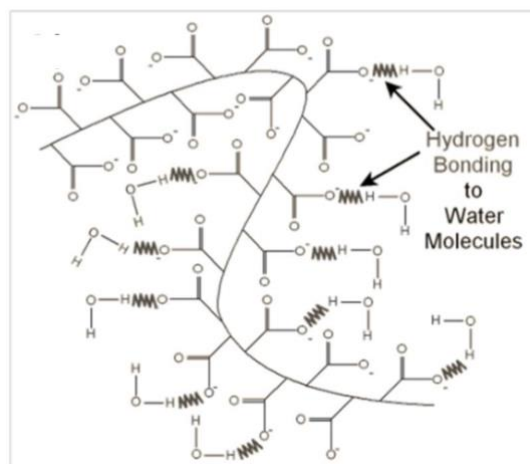
Figure 3: Molecular interaction between water molecules and a polymeric chain of sodium polyacrylate [59]

1.2.2.1   Hydration

Hydration occurs within the SAP's chain structure, whose charged chemical groups enable the interaction of water molecules in the polymeric chain network due to the attraction of opposite charges [3].

1.2.2.2   Hydrogen bonds

When a water molecule is inside a SAP network, it is surrounded by other water molecules or functional groups attached to a polymeric chain; therefore, the water molecule's electronegative atoms, such as oxygen, bond with hydrogen electrons [3].

A SAP's hydrophobicity stimulates the dispersion of polymeric chains into water. When such dispersion occurs, the energy of the SAP–water system decreases, and entropy increases. However, the dissolution of the SAP is prevented by its three-dimensional

network created by the crosslinks between polymeric chains [60]; these crosslinks also limit the amount of water that can be absorbed by the SAP network. This phenomenon can be seen when the SAP swells in water, becoming a hydrogel (i.e., a SAP in a hydrated state); the hydrogel is less stiff than the original collapsed SAP, and the water is retained due to the crosslinking, which acts as a trap. Therefore, the crosslinking density controls the amount of water inside the SAP network. There are two possible scenarios: (i) high crosslinking density results in increased mechanical strength and decreased AC and (ii) low crosslinking density results in decreased mechanical strength and increased AC [12]. Figure 4 presents a schematic representation of a SAP network.
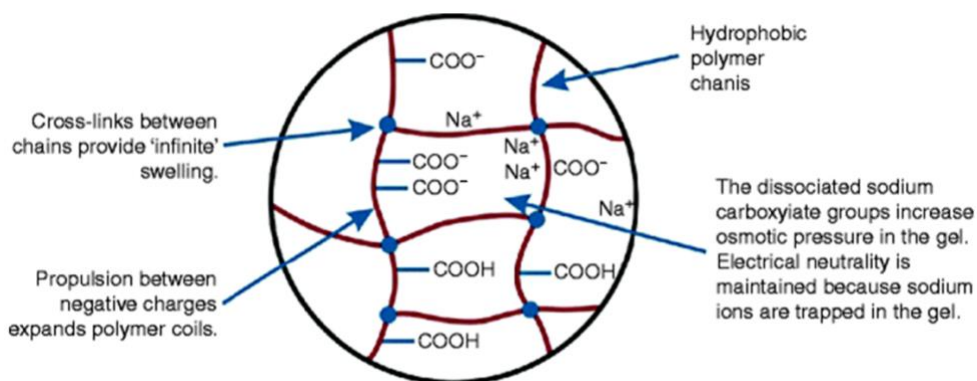
Figure 4: Structural network of a SAP [61]

In the case of a SAP with a neutral chain, when the number of anions and cations is equal, swelling may occur due to the interaction between the polymeric chains' anions and the water molecules' hydrogen atoms. Consequently, the attraction between the anions and cations decreases, and the cations move freely across the polymeric chains but become trapped within the SAP network. This effect is characteristic of a semipermeable membrane; the cations inside the membrane increase the osmotic pressure, allowing water molecules to pass through the membrane, which results in the swelling of the SAP network. The opposite case may occur: when more cations are outside the SAP network, the osmotic pressure and the SAP's swelling capacity decrease [4,5]. The driving force of swelling is defined as the difference between the osmotic pressure inside and outside the hydrogel. Swelling capacity is at its maximum in deionized water [6]. When

interconnected pores are introduced to a hydrogel during synthesis in which bubbles are captured inside the polymeric chain, absorption time can increase [7].

1.2.2.3 Osmosis and osmotic pressure

When a semipermeable membrane separates two aqueous solutions with different salt concentrations, water—but not salts—can pass through the membrane. Therefore, equilibrium in salt concentration between the two solutions is achieved [8]. Thus, osmotic pressure is balanced with the solution, providing the pressure needed to prevent water from moving within the membrane [9]. In the case of a SAP, the crosslinked polymeric chains act as a membrane, providing the driving force that allows the entrance of water molecules while also preventing infinite swelling [24,62].

The swelling of a SAP balances the electrical charge in a polymeric chain. When this occurs, the osmotic pressure inside the SAP becomes higher than the pressure in the external media.

1.2.3 Applications of SAPs

SAPs were first applied in the hygiene industry, mainly in disposable products such as diapers and feminine pads. Nowadays, this conventional application continues, but SAPs are also used in agriculture, pharmaceuticals, biomedicine, tissue engineering, biosensors, food additives, construction additives, coal dewatering, artificial snow, wastewater treatment, etc. These applications can be grouped into four main categories: hygiene, construction, medical care, and agriculture (see Figure 5).

Figure 5: Four main categories of SAP application

1.2.3.1 Agricultural application of SAPs

The growing global population increases food demand and, consequently, the demand for arable lands. It is necessary to develop technology that helps ensure soil nutritiveness and moistness [24,63] and that improves water irrigation so that the global population can grow enough food. Over the past two decades, SAPs' agricultural utility has been widely demonstrated; their water retention properties have positively impacted the development of the agricultural industry.

Soil tends to degrade after several agricultural cycles. Soil degradation involves organic matter depletion, which hinders soil's water absorption, causing soil erosion.

SAPs have been used as soil amendments; they provide moisture and increase soil's water retention capacity (Senna and Botaro, 2017). SAPs are particularly helpful in increasing the water retention capacity of soil that is porous and/or under conditions of excessive rainfall in which the loss of fertilizer due to leaching is severe [63].

Moreover, SAPs can absorb, retain, and release water when in close contact with a plant root in the soil [24]. By acting as water reservoirs for plants, SAPs enhance plant growth and improve water irrigation [64,65].

SAPs can also be applied to the controlled release of nutrients; chemicals and fertilizers, such as nitrogen, phosphorous, and potassium [65]; agrochemicals (Senna and Botaro, 2017); and herbicides [66].

Several environmental factors limit the AC performance of SAPs in soil. For instance, the content and type of salts in soil contribute to the concentration of ions [67], which can neutralize the polymeric chain and reduce a SAP's AC. Osmosis is negatively correlated with salt concentration in the surroundings [6]. Therefore, SAP's neutralization has been studied with the aim of developing high-AC SAPs under high-salt-concentration conditions [63,68]. Temperature and water conditions can also affect SAPs [20].

1.2.4   SAP production

1.2.4.1   Polymerization techniques and SAP manufacturing

In the production of a SAP, the following components are present: an initiator, a crosslinker, and monomers. Sometimes, copolymers are also present. The selection of a technique for obtaining a SAP depends on several factors, such as the raw material to be used (i.e., natural, synthetic, or hybrid), application (e.g., hygiene, construction, medical care, and agriculture), and desired properties (e.g., AC, cost, biodegradability, and mechanical strength).

1.2.5   Fossil-based SAP synthesis

Fossil-based SAP synthesis can be achieved via different polymerization techniques [69]. Four polymerization techniques are particularly common: suspension, solution, bulk, and radiation. Other recent techniques, such as in situ polymerization, have been used to obtain composite hybrid hydrogels [70].

In industrial manufacturing, the most commonly used methods are suspension polymerization and solution polymerization. The use of each technique depends mainly on the raw materials, desired properties, and cost [55,71]. Suspension polymerization involves the production of a primary polymer particle in a reactor via the suspension of a hydrophilic reactant in an organic solvent, which results in a final engineered product

without the need for a mechanical post-reaction stage. In solution polymerization, a mass of polymerized gel is obtained; this process, due to its exothermic nature, reduces manufacturing costs. However, this process necessitates a post-reaction stage that involves chopping, drying, and grinding the obtained gel [71].

Free radical polymerization is the most commonly used reaction for SAP production [11,27] in which crosslinking occurs via a chemical reaction or physical means, such as ionization or hydrogen bonding. Water and other solvents are employed to regulate the heat of the reaction in SAP preparation. At the end of the reaction, impurities such as left-over monomers, initiators, or crosslinking agents are washed off the final product in preparation for further gel processing to form the final product [11].

In the commercial production of SAPs, the most common raw material is sodium polyacrylate, a product derived from acrylic acid neutralized with sodium hydroxide.

1.3   Bio-SAPs

1.3.1   Components of SAPs

SAPs—whether fossil-based or bio-based—are collapsed networks resulting from the connection of three components: i) a matrix polymeric chain that contains hydrophilic groups, such as $-CONH_2$, $-CONH$, $-OH$, $-COOH$, and $-SO_3H$ [56]; ii) a crosslinker; and/or iii) a copolymer. Although SAP networks are initially collapsed, they show three-dimensional characteristics when they absorb water, increasing in volume due to water retention.

1.3.2   Bio-SAP synthesis

Fossil-based SAPs have commercial appeal because of their chemical stability, low solubility, and high molecular weight. Additionally, they are relatively easy to modify in their synthesis. However, due to their chemical stability, they have low biodegradability, and they may introduce pollutants into the systems where they are applied [72]. Nevertheless, pollution concerns can be diminished if bio-based materials that have high

biodegradability are included in the composition of SAPs. Therefore, a combination of bio-based and fossil-based reagents has been proposed to obtain Bio-SAPs that have similar AC levels and superior biodegradability to fossil-based SAPs [73].

Unlike fossil-based raw materials, bio-based raw materials often require modification to obtain SAPs.

Table 1 shows a compilation of the types of polymerization and synthesis used to obtain fossil-based SAPs and Bio-SAPs, as well as each type's advantages and disadvantages. In addition to the common methods for obtaining Bio-SAPs, new methods have been developed, such as fast contact between solid and liquid interfaces to control the size and increase the mechanical strength of hydrogels [74].

Table 1: Compilation of common synthesis techniques for obtaining fossil-based SAPs and Bio-SAPs

Process	Process description	Advantage	Disadvantage	Examples of fossil-based SAPs	Examples of Bio-SAPs
Chemical polymerization					
Bulk polymerization	Monomers are polymerized by initiators, light, heat, or radiation without the presence of solvents and dispersants.	High rate and degree of polymerization occur because of the high concentration of monomer. Product with high molecular weight and high purity.	Viscosity of reaction increases markedly and the heat result from polymerization is difficult to spread.	Poly(2-hydroxyethyl methacrylate) and poly(acrylic acid).	Graft copolymers of starch and polyacrylamide (polyacrylate acrylamide) prepared via reactive extrusion using a co-rotating twin-screw extruder.
Solution polymerization	There are two types of solutions according to the resultant polymer: homogeneous (soluble in water) and heterogeneous (insoluble in water).	The viscosity in the system is lower than in bulk polymerization.	Less concentrated system, which decreases the polymerization degree.	Fullerene (C60) containing crosslinked poly(2-hydroxyethyl methacrylate).	Chitosan-based hydrogels and resin with pectin grafted acrylic acid.

Suspension polymerization	Initiators are dissolved in aqueous solution to form a droplet shape; therefore, their thermal decomposition generates radicals that initiate the polymerization.	Possible to obtain spherical product of a small particle size in the range of 1 μm to 1 mm.	The monomers may be enwrapped by the particles and difficult to remove.	Microparticles of poly (hydroxyethyl methacrylate.	Cellulose-g-polyacrylamide/ hydroxyapatite.
Irradiation polymerization	Radiation (alpha, beta, gamma, electron beams) is used as initiator of aqueous polymer solutions, resulting in the formation of radicals in the polymeric chains. Radiolysis may occur, resulting in hydroxyl radicals that form covalent bonds and crosslinked structures.	No initiator or catalyst is needed. Operating costs are low. It requires less time than grafting induced by chemicals; thus, time is not wasted on processing.	Low solvent tolerance to radiation of some solvents reduces the polymerization rate. Radiation-induced cationic polymerization of isobutylene–isoprene systems has advantages and disadvantages compared to catalytic initiation.	Poly(vinyl alcohol), PEG, and poly(acrylic acid).	Starch-graft-poly (ethylene glycol)-co-poly(methacrylic acid) and starch-g-PEG-co-polymethyl methacylate.
Physical polymerization					
Crosslinking hydrogen bonds	Crosslinking results from the attractive force between a hydrogen atom covalently bonded to a high electronegative atom (N, O, or F). Strong hydrogen bonds may also be formed in cellulose under cryogenic conditions.	Can occur spontaneously.	Crosslinks are formed by weak interactions, which are mechanically and thermally less stable than the interactions in chemical crosslinking.	Poly (vinylphenol) and bisphenol A, (phenoxy) polyhydroxyether, and (phenoxy) polymer blends.	Hemicellulose polyvinyl alcohol hydrogels and chitin nanowhiskers.
Crosslinking ionic bonds	Usually occurs between two oppositely charged molecules or polyelectrolytes. Gelation phenomena of hydrogels can occur in situ via ionic crosslinking.			Polyvinyl alcohol gels upon the addition of borax, which causes hydrogen bonding.	Sodium alginate, pectin, or chitosan gels upon exposure to calcium ion (e.g., protein–protein interaction as gelatin).

1.3.3 Bio-SAPs for soil water retention

SAPs are used for soil water retention. In this application, SAPs fulfill two principal roles: i) water reservoir for soil amendment and ii) slow releaser of water and agrochemicals, such as pesticides, chemical fertilizers, and other growth or amendment agents. Furthermore, SAPs minimize the agrochemical losses that typically occur due to soil leaching, volatilization, and degradation. Fossil-based SAPs can be environmentally harmful in this application; due to their petroleum origin, they have low biodegradability and, therefore, remain in the substrate as pollutants [75]. Moreover, when fossil-based SAPs that contain monomers derived from acrylamide and aldehyde biodegrade, they release environmentally harmful formaldehyde by-products [76]. Consequently, Bio-SAPs—which have high biodegradability and do not release environmentally harmful by-products—are preferable.

Bio-SAPs are environmentally compatible with soil and plants; they do not have any adverse effects when applied [37]. Polysaccharides are among the common bio-based raw materials used in Bio-SAP synthesis [37]. The biodegradability and non-toxicity advantages of polysaccharide-derived Bio-SAPs over fossil-based SAPs for slow release and water-retention applications have been demonstrated (Senna and Botaro, 2017). Polysaccharide-derived Bio-SAPs have been shown to be competitive with fossil-based SAPs in terms of the following properties: AC, biodegradability, cost of production, and yield of harvest [30,75].

Polysaccharide compounds (Figure 6) are often used as natural sources for Bio-SAP production. According to their source, they are grouped into four categories: i) alginate (from algae), ii) cellulose, pectin, cyclodextrin, and starch (from plants), iii) dextran (from microorganisms), and iv) chitosan (from animals).
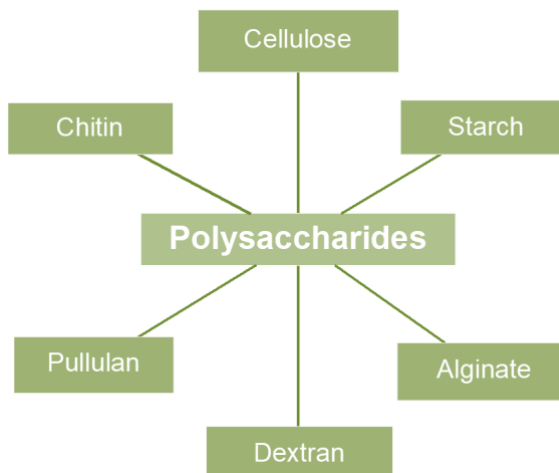
Figure 6: Polysaccharide compounds from natural sources

Table 2 summarizes some previous research pertaining to the agricultural applications of Bio-SAPs.

Table 2: Agricultural applications of Bio-SAPs

Bio-basedraw material	Agricultural application	References
Cellulose	Water retention in soil and slow release of fertilizers	[18,20,30,65,77–79]
Guar gum	Soil amendment material	[20,26]
Corn starch/biochar	Improving plant growth and nutrient uptake	[21,25]
Starch	Slow release of fertilizers	[25,80]
Chitosan	Water retention in soil and slow release of fertilizers	[31,36,77]
Wheat	Soil water retention	[33]
Sugar	Soil water retention	[37]
Collagen	Controlled release of agrochemicals	[38]

1.4 Cellulose-based Bio-SAP

Due to the wide variety of the above-mentioned bio-based raw materials, cellulose—the most abundant biopolymer on the planet—has captured the attention of SAP researchers (Heinze, 2015). Furthermore, cellulose is available as a residue produced by the forestry and agriculture industries. Cellulose's popularity as a raw material for SAPs has also increased because, as a carbohydrate and polymer, it has dual chemical properties. Consequently, according to the ScienceDirect database (Figure 7), over the last two decades (2000–2020), a growing number of research articles related to the use of cellulose for SAP production has been published; five such articles were published in 2000, and 119 in 2020. Research on SAP production has been developing in diverse fields of study, especially biochemistry, genetics, and molecular biology (254 articles published), chemistry (208), material science (177), and environmental Science (141).
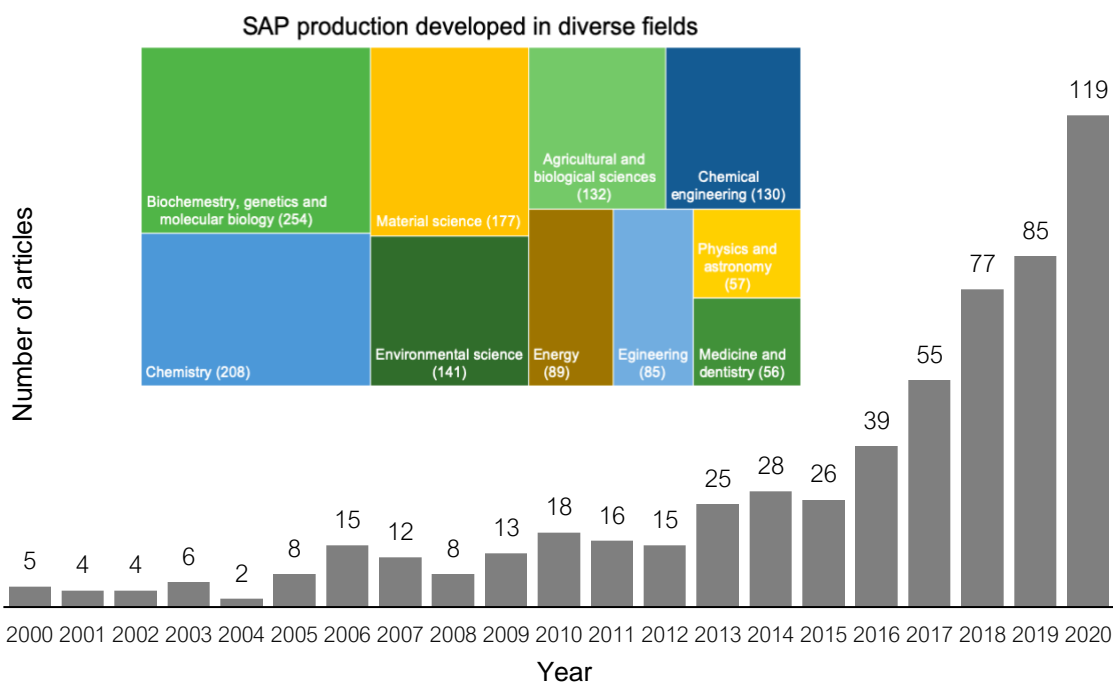
Figure 7: Published research articles related to the use of cellulose for SAP production, categorized by year and field of study

1.4.1   Cellulose

Cellulose constitutes the plant's cell wall. Due to the linear structure of cellulose, its microfibrils provide tensile strength to the plant, and they play a structural role in the layering of cell walls. Each microfibril has a diameter of 10–20 nm and consists of up to 40 cellulose chains. Microfibrils can be crystalline or paracrystalline (i.e., amorphous), and they are enfolded by plant components such as hemicellulose, a mixture of primarily pentose sugars (e.g., xylose and arabinose), and several hexoses (e.g., mannose, galactose, and glucose). The crosslinker between microfibrils and hemicellulose is a rigid aromatic polymer known as lignin. Figure 8 shows the structure of cellulose.

Biomass is composed of the following: cellulose (35–45%), hemicellulose (25–30%), and lignin (15–20%) [81]. Cellulose is a macromolecule composed of repeating glucose units, and it possesses a fusion of the chemical properties of carbohydrates and synthetic polymers. Cellulose is a biopolymer that contrasts with low molar mass carbohydrates due to its intermolecular structure, capacity to have crosslinking reactions, chain lengths, chain length distribution, and functional group distribution within the repeating anhydroglucose unit (AGU) and along the polymeric chain [82]. Cellulose also contrasts with synthetic polymers due to its high chain stiffness and capacity to form acetal groups via hydrolysis and oxidation [83]. Cellulose is a linear syndiotactic homopolymer constituted of AGU linked by β-(1-4)-glycosidic bonds. Each AGU has three hydroxyl groups: the primary group (at C6) and two secondary groups (at C2 and C3, respectively) [82].
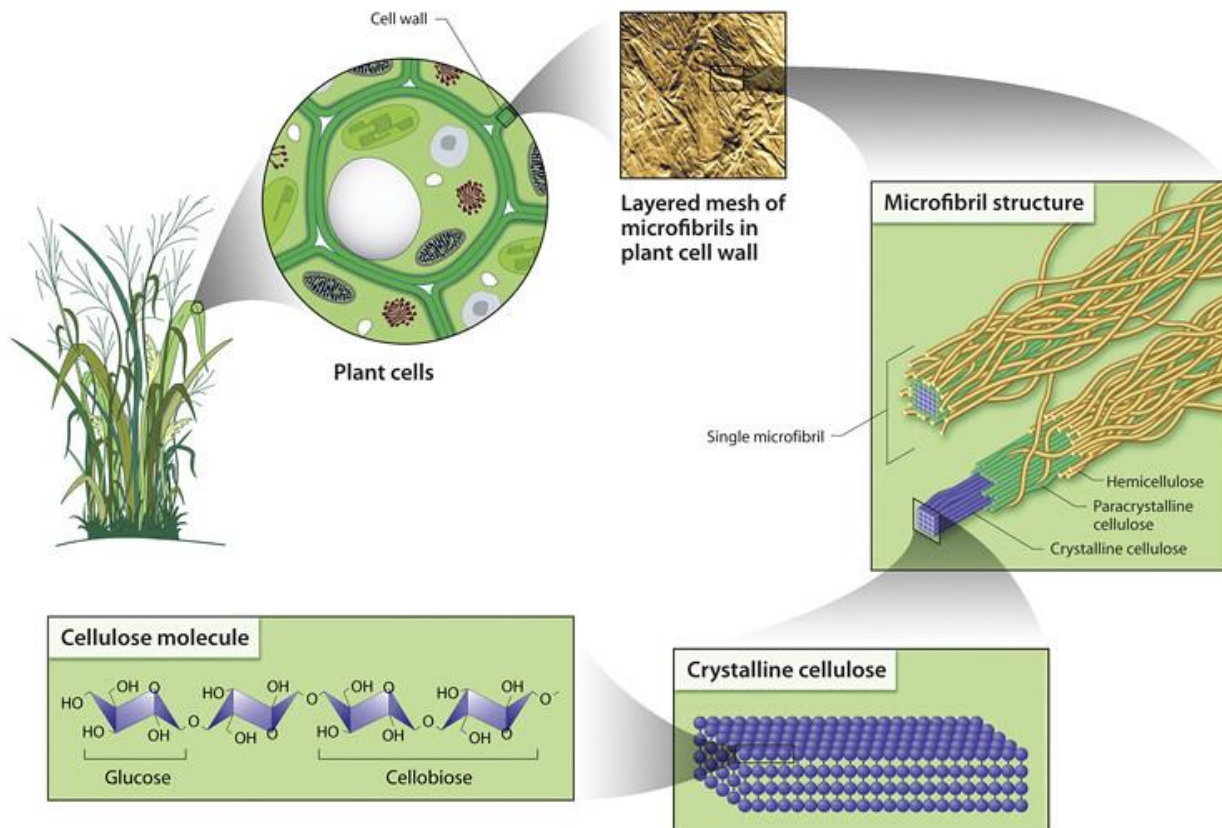
Figure 8: Structure of cellulose [84]

1.4.2   Cellulose surface modification

Hydroxyl groups are susceptible to modifications such as esterification, etherification, oxidation, sialyation, and polymer grafting [82]. In most cases, however, cellulose is highly stable during its use in SAP production [85]. Surface modification of cellulose can result in functional groups becoming attached to the cellulose, which endows it with functionality and increases its reactivity. The three main categories of surface treatments for cellulosic fibres are chemical, physical/physicochemical, and biological.

There are six types of chemical surface treatment: i) alkaline treatment, which increases amorphous regions and decreases crystallinity; ii) silane treatment, in which chemical bonds are formed with organosilanes acting as coupling agents, resulting in stronger tensile fibres; iii) esterification treatment, in which hydroxylic groups are substituted by ester bonds, which increases fibre–matrix compatibility; iv) maleation treatment, in

which a maleated polymer becomes a coupling agent, forming a chemical bond in a hydroxyl group of cellulose; v) polymer grafting treatment, which is used to introduce polymeric chains into cellulose fibre, creating bio-composites; and vi) other chemical treatments, such as bleaching with sodium chlorite, sodium hypochlorite, or hydrogen peroxide to enhance whiteness and delignify fibres.

Physical/physicochemical treatments are considered less severe than the bulk structure properties and surface composition of cellulose. Typical physical treatments are mechanical, heating, and stream explosion; typical physicochemical treatments are laser, γ-ray, and UV irradiation.

Biological treatments have become popular due to their environmental friendliness; they waste little to no energy, and they do not involve solvent usage. In these treatments, biological agents, such as enzymes and fungi, biodegrade pectin binds that isolate cellulose fibres [86]. The advantages of these treatments include the separation between fibres and clean surfaces.

Ether functionalization is a popular modification of cellulose used to produce SAPs. The most common ether-functionalized cellulose is carboxymethyl cellulose (CMC), which is soluble in water. It is the foremost commercial cellulose derivate and has been applied in various industries, such as pharmaceutics, cosmetics, textiles, and paper [18]. Bio-SAPs made with CMC generally have a high AC. CMC has been used for the following: copolymerization with starch [87] and chitosan [88]; bonding with divalent metals such as Zn^{+2} [89]; grafting to synthetic vinyl molecules such as acrylic acid and polyacrylamide [90]; and bonding with crosslinkers, such as PEG [91] and N, N'-methylenebisacrylamide [92].

Ether functionalization can be performed on pure cellulose but not on untreated crude cellulose. When crude cellulose (with lignin residues) is treated via ether functionalization, it is necessary to add a pretreatment process such as bleaching with sodium hypochlorite and sodium chlorite—a non-environmentally friendly process due to the low biodegradability and toxic derivate chemicals [93]—before proceeding with the ether functionalization [94]. Therefore, when crude cellulose is used as the raw material

in SAP production, ether functionalization—which necessitates a pretreatment process that reduces environmental friendliness and raises production costs—is not a viable treatment.

1.4.3 Esterification

The presence of hydroxyl groups in cellulose makes it easy to esterify. Esterification aims to functionalize the cellulose surface by inserting –COOH groups into the cellulose. Cellulose esterification occurs due to an acetylation reaction in which the acetylating agents (e.g., carboxylic acid anhydrides) substitute an acetoxyl group for a hydroxyl group. This substitution occurs due to the presence of a strong acid catalyst (e.g., p-toluenesulfonic acid and hydrochloric acid) or Lewis acids (e.g., $ZnCl_2$, $AlCl_3$). Figure 9 shows the process of cellulose esterification.
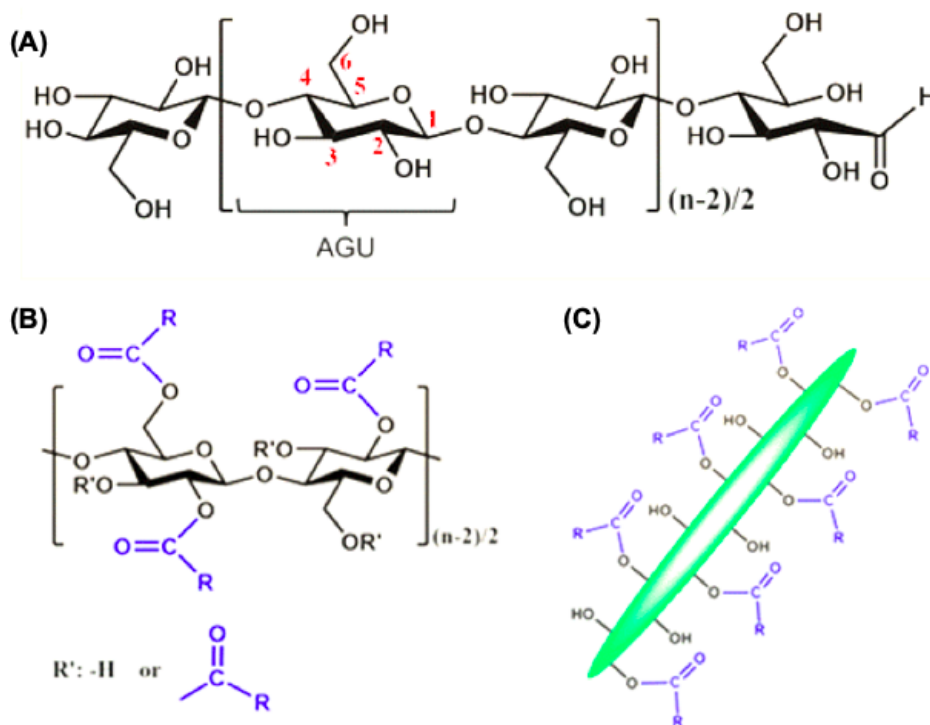
Figure 9: (A) molecular structure of cellulose; (B) molecular structure of esterified cellulose; (C) esterified cellulose surface [82]

Typically, esterification involves mixing cellulose with reagents such as acid chloride, acetic anhydride, acetic acid, maleic anhydride, and benzoyl chloride [95]. Hydroxyl

groups are easier to esterify in amorphous cellulose regions than in crystalline cellulose regions. In crude cellulose fibres—compared to pure cellulose fibres—it is easier to esterify lignin and hemicellulose, and it is more difficult to reach closely packed regions of crystalline cellulose. Esterification in cellulosic fibres has been shown to improve composites' stability and moisture resistance. Conversely, it has been observed that excess esterification can cause cellulose degradation [86].

Through esterification, cellulose increases in hydrophobicity and decreases in water absorption. Esterification also enhances reactive regions and increases the mechanical performance of bio-composites in cellulose [86].

1.5 Cellulose functionalization

1.5.1 Cellulose esterification with maleic anhydride

Maleic anhydride is often used for the esterification of polysaccharides, a treatment widely applied in the textile industry. In clothing manufacturing, esterification of polysaccharides has been used to make cotton fibres less disposed to wrinkling after water absorption–dry cycles [96]. In this treatment, the esterification reaction occurs in short grafts that maintain the physical and mechanical properties of the cellulose. However, the anhydride group in maleic anhydride reduces the electron concentration in the cellulose's structure, lowering the cellulose's reactivity. The use of catalysts such as pyridine [97] or Lewis acids significantly increases the cellulose's reactivity. Figure 10 shows the esterification reaction between cellulose and maleic anhydride.
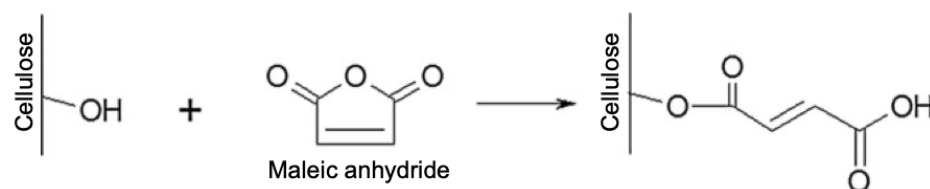
Figure 10: Esterification reaction between cellulose and maleic anhydride [98]

A bifunctional maleic anhydride structure connects with cellulose on one side; the other side is free to interact with an additional polymeric chain, which allows for crosslinking with other polymer molecules and for expansion of the polymeric chain's dimensional stability [99]. The nature of maleic anhydride makes promotes nucleophilic attacks (e.g., of hydroxyl groups). Because cellulose has three hydroxyl groups per AGU, it can react with maleic anhydride. Furthermore, the success of an esterification reaction is likely when the following conditions are met: a catalyst is present, a convenient solvent media (e.g., organic solvent) is present, and the mixture is adequately heated and stirred.

1.5.2   Cellulose esterification with citric acid

Citric acid is a bio-based polycarboxylic acid monomer with three –COOH groups [100]. Its non-toxicity and environmental friendliness make it a popular reagent in the esterification of cellulose. Citric acid can efficiently react with cellulose's hydroxyl groups by obtaining five or six cyclic anhydride intermediates. The esterification reaction involves a two-step ester bond formation mechanism between cellulose and polycarboxylic acids, as shown in Figure 11. The first step is the dehydration of two citric acid –COOH groups, which forms an intermediate-cycle anhydride, and the second step is the esterification of the cellulose with the cycle anhydride.

Polycarboxylic acid

Cyclic anhydride

Polycarboxylic acid bonded to cellulose through ester linkage
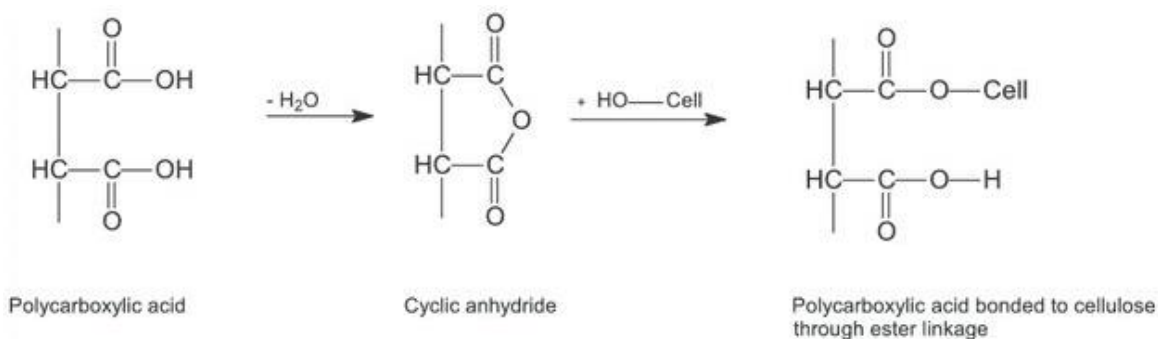
Figure 11: Esterification reaction mechanism between polycarboxylic acid and cellulose [101]

These two steps take place under a particular temperature condition known as the curing temperature. Curing temperatures vary according to whether a catalyst is used. Typically, sodium hypophosphite (SHP) is employed as an efficient catalyst in reactions with citric

acid at curing temperatures ranging from 120–170°C. SHP increases the formation of anhydride intermediates without degrading cellulose during the curing process. Figure 12 shows the cellulose esterification mechanism in the presence of SHP and a polycarboxylic acid.
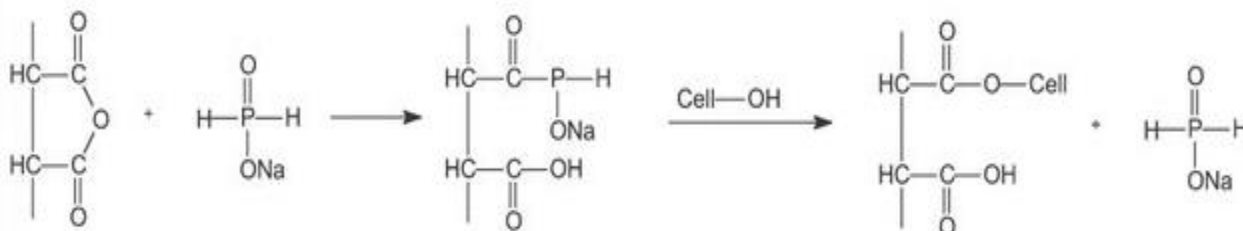
Figure 12: Cellulose esterification mechanism in the presence of SHP and a polycarboxylic acid [101]

In addition to the esterification reaction, crosslinking between esterified cellulose units forms a three-dimensional SAP network that is capable of absorbing and retaining water molecules [102].

1.5.3 The roles of NaOH and urea

Anhydrous NaOH is a chemical compound that is soluble in water. When a NaOH crystalline structure combines with water, various hydrates are formed; the types of hydrates depend on the temperature and concentration of the solution in which they are formed. The interaction between water and NaOH lead to the formation of eight hydrates and the destruction of NaOH crystalline structure [103]. For example, the concentrated solutions (70–100% w NaOH) have one stable crystalline hydrate with seven molecules of water and another metastable crystalline hydrate with five molecules of water. The region with concentrations between 25 and 70% w NaOH have the following stable and metastable hydrates: NaOH•4H$_2$O and NaOH•5H$_2$O [104]. In the low NaOH concentrations (below 25% w NaOH), two hydrates can be found. In addition, a stable hydrate (NaOH•7H$_2$O) can be formed when the temperature rapidly drops. Additionally, when the temperature slowly decreases, a metastable hydrate (NaOH•5H$_2$O) is formed [104].

NaOH solutions have been used as alkali solvents to react with cellulose. For cellulose dissolution [104], the NaOH concentration must be below 20% w/w. Figure 13 shows the NaOH concentration region in which cellulose dissolves, which indicates a eutectic mixture of 20% w NaOH and 80% w water. The eutectic mixture's corresponding hydrate is NaOH•$5H_2O$;$4H_2O$. The melting temperature of this compound is -33.4°C, and the melting enthalpy of the pure eutectic is 187 J/g [104].
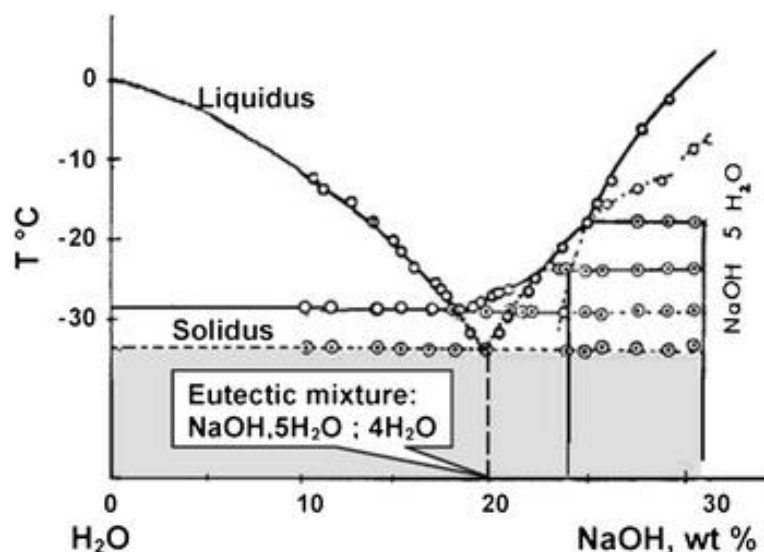
Figure 13: Binary phase diagram of a low-concentration region of NaOH–water solution [105]

A model of the organization between water and NaOH-dissociated ions was proposed [105]. Figure 14 shows this model; the water molecules surround the ions—Na^+ and OH^-—forming primary solvation cages (represented by the grey rings) and secondary solvation cages (represented by the larger, white rings).
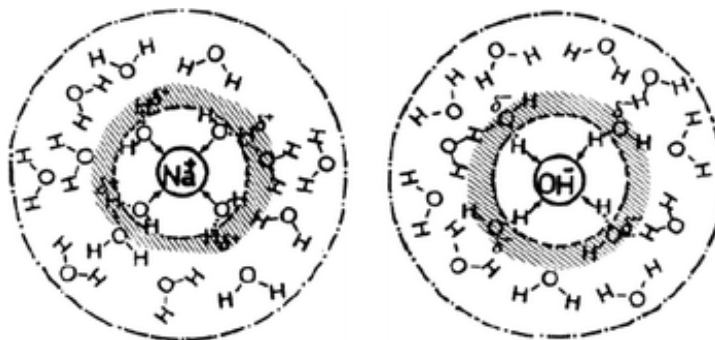
Figure 14: Model of organization between water molecules and ions in a 9% w/w NaOH–water solution [105]

The caustic role of NaOH involves rearranging cellulose molecules and breaking hydrogen bonds between cellulose chains, which results in the swelling of cellulose fibres. This swelling starts on the cellulose surface in the superficial chains in contact with the solution. Once these chains are swollen, they can move freely and transfer inside the solid cellulose [105]. This transference continues until the cellulose reaches solubility. At the same time, the concentration of hydroxyl groups increases on the cellulose surface, which changes the cellulose's properties and improves its water absorption. Furthermore, NaOH penetrates cellulose's amorphous and crystalline regions, weakening interchain interactions. Consequently, the cellulose crystallinity is decreased, leaving cellulose chains accessible for subsequent chemical treatment [105] and making them reactive for graft copolymerization and further SAP synthesis. Figure 15 shows a model of dissolved cellulose in a NaOH–water solution.
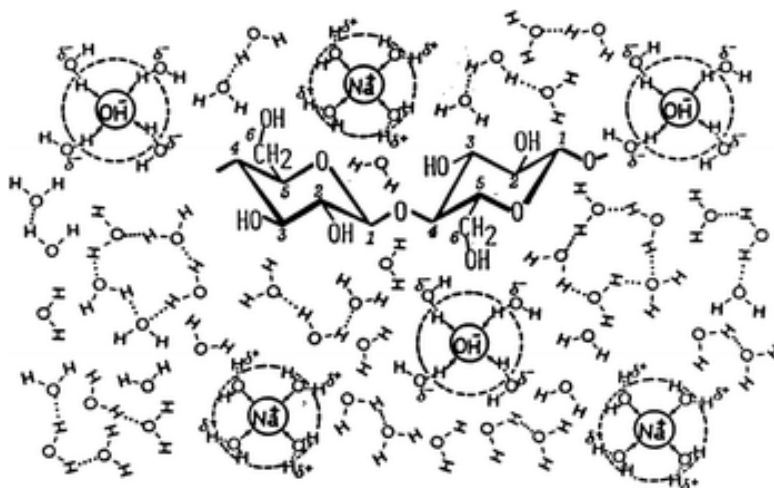
Figure 15: Model of dissolved cellulose in a NaOH–water solution [105]

Studies have shown that additives in cellulose solutions can increase the swelling of cellulose. One of the most commonly used additives is urea, a non-toxic, highly water-soluble compound that promotes the solution of cellulose in NaOH–water [106]. A cellulose–NaOH aqueous solution requires a minimum of four NaOH molecules to dissolve one AGU of cellulose; such dissolution results in a cellulose–weight ratio of approximately 1:1. When urea is added to a cellulose–NaOH aqueous solution, this 1:1 ratio remains constant; the free NaOH hydrates do not bond to the cellulose, and urea does not interact with the cellulose or NaOH [107].

Urea's presence decreases the enthalpy of the eutectic point of NaOH–water. Consequently, urea stabilizes the alkali-swollen cellulose by binding water [108] located in the hydrophobic region of the cellulose, avoiding the agglomeration of the dissolved cellulose chains [109]; as a result, cellulose crystallinity is decreased. Figure 16 shows the dissolution of cellulose in a NaOH–urea aqueous solution.
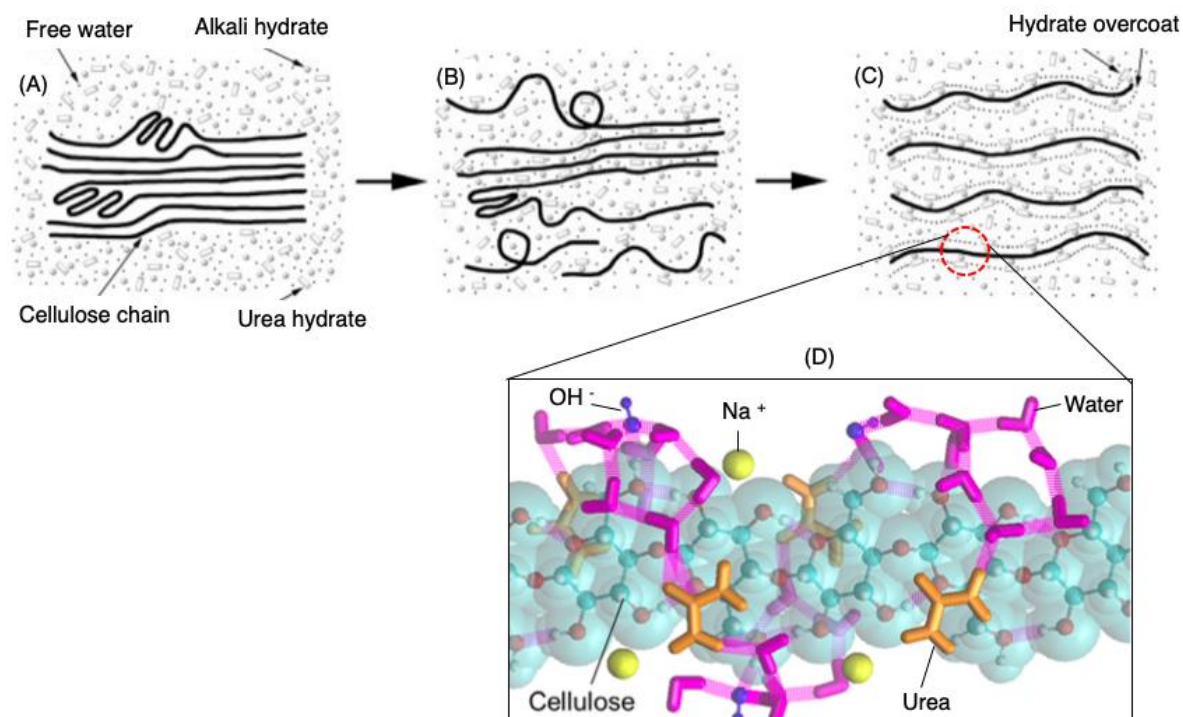
Figure 16: Dissolution of cellulose in a NaOH–urea aqueous solution: (A) cellulose in the solvent; (B) swollen cellulose in the solution; (C) transparent cellulose solution [109]**; (D) helical cluster of NaOH, urea, and water around a single cellulose molecule (van der Waals transparent surface indicated in turquoise)** [107]

Other studies have shown that additives such as acrylamide, acrylic acid, and acrylonitrile can influence the stability of cellulose dissolution in NaOH aqueous solutions. In one study, for example, the dissolved cellulose fraction increased with acrylamide and remained stable with acrylic acid and acrylonitrile [110]. Moreover, research on additives such as PEG has shown that PEG facilitates the cellulose solubility of NaOH–urea–PEG aqueous solutions [111] with 1% w/w PEG, 6% w/w NaOH, and 4% w/w urea.

1.6 Copolymerization

Regardless of the polymer's macromolecule nature (natural or synthetic), most have solid-like properties and are comprised of simpler molecules called monomers. A group of monomers arranged in a regular structure is crystalline, whereas a group of monomers arranged in an irregular structure is amorphous.

Polymers can be categorized according to chain morphology. A chemical descriptor known as "degree of polymerization" defines the number of repeating units in an average polymeric chain. The repeating units can be a single monomer or a combination of several monomers. If the repeating units are a single monomer, the polymer is called a "homopolymer." If the repeating units are a combination of several monomers, the polymer is called a "copolymer." Copolymers have various arrangements; they can be alternating, random, block, or graft copolymers (Figure 17).

A SAP is classified as a graft copolymer when its backbone polymeric chain is attached to one or more sides of another polymeric chain. The chemical nature of a graft copolymer depends on the type of backbone polymeric chain and the attached polymeric chain. Therefore, there is a large variety of graft copolymers; they differ according to their synthetic preparation [112,113]. Figure 18 shows the formation of a graft copolymer molecule.
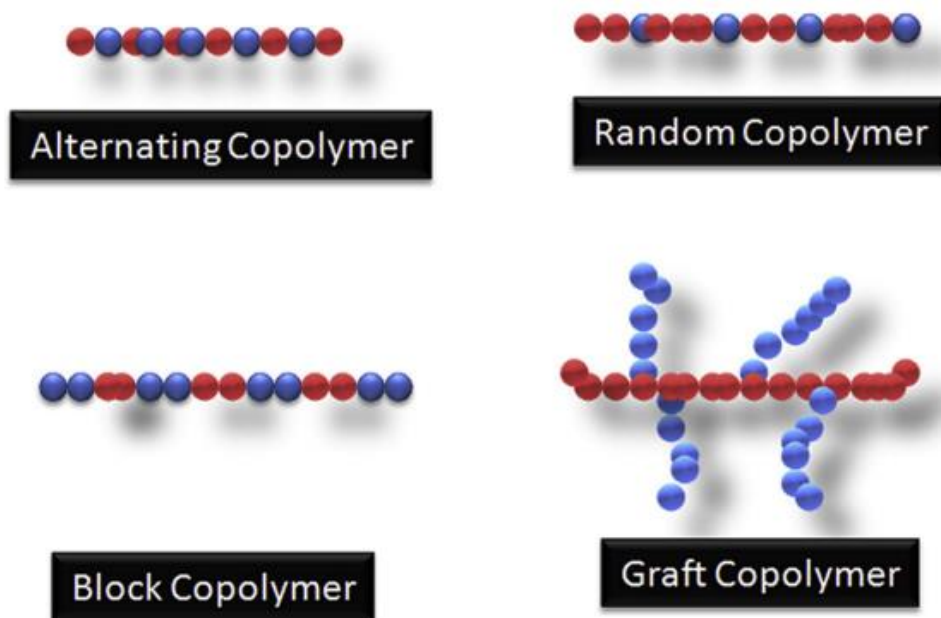
Figure 17: Configuration of monomers in a copolymer [113]
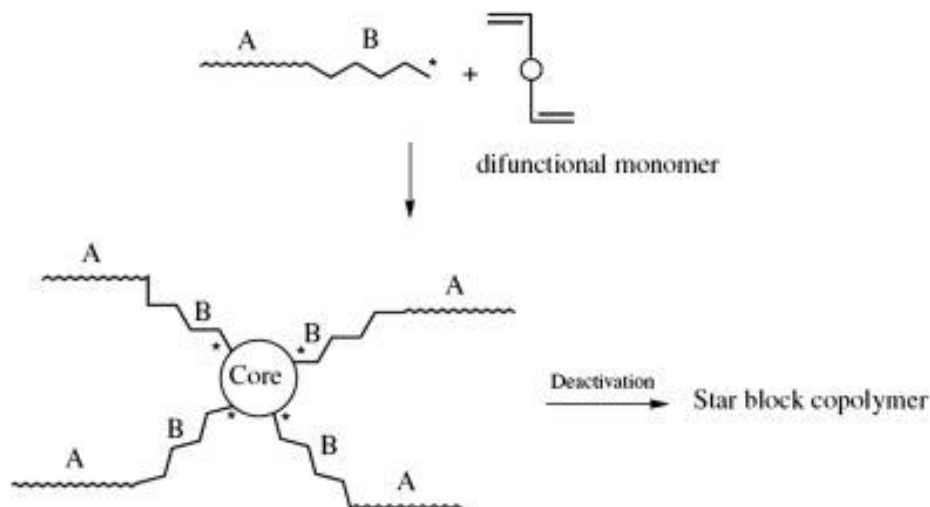
Figure 18: Formation of a graft copolymer molecule [112]

1.6.1 Acrylic acid

Acrylic acid is an organic vinyl monomer typically used to copolymerize with other monomers or polymers. Its chemical formula is $CH_2=CHCOOH$, an unsaturated carboxylic acid that polymerizes into polyacrylates. At room temperature, acrylic acid is a liquid that is fully miscible in water. It polymerizes to form homopolymers, and it copolymerizes with these homopolymers' esters and with other vinyl monomers. Due to its carboxylic functionality, acrylic acid is reactive to alcohols and epoxides. It is commonly used in the production and manufacture of superabsorbent paints, plastics, and other products. It is a popular compound due to its biocompatibility [114].

1.6.2 Free radical formation and graft copolymerization

Free radical polymerization is the most commonly used reaction for SAP production. crosslinking occurs via a chemical reaction or physical means, such as ionization or hydrogen bonding. Water and other solvents are employed to regulate the heat of the reaction in SAP preparation. At the end of the reaction, impurities such as left-over monomers, initiators, or crosslinking agents are washed off of the final product in preparation for further gel processing to form the final product [11].

Free radical graft copolymerization is a chemical reaction of addition that is thermodynamically favoured and is considered an effective technique to add hybrid properties to both agents in the reaction: the polymeric backbone (i.e., cellulose) and the monomer (sodium acrylate). A previous study evaluated the efficiency of initiators in grafting monomers into natural polymers [115]. Some of the best-performing initiators are azobisisobutyronitrile, potassium, and ammonium persulfate. Remarkably, APS was shown to have strong oxidizing power, to have high solubility in water, and to quickly produce radicals in temperatures above 70°C [116]. Formation of radical and free radical species are crucial for initiating polymerization.

Free radical graft copolymerization starts after APS has been added to the solution and the solution's temperature has reached 70°C. It involves three stages: initiation, propagation, and termination. In the first stage of graft copolymerization (initiation), cellulose radicals are produced. In the second stage (propagation), acrylic acid monomers attach to cellulose, forming a macromer. In the final stage (termination), a graft copolymer is formed, as shown in Figure 19.

Initiation

$$2SO_4^{--} \longrightarrow 2SO_4^{\cdot -}$$

$$2SO_4^{\cdot -} + H_2O \longrightarrow HSO_4^- + \overset{\cdot}{O}H$$

$$P\text{-}O\text{-}H + SO^{\cdot -} \longrightarrow P\text{-}O + HSO_4^-$$

$$P\text{-}OH + \overset{\cdot}{O}H \longrightarrow P\text{-}O + H_2O$$

$$M + \overset{\cdot}{O}H \longrightarrow \overset{\cdot}{M}\text{-}O\text{-}H$$

$$M + SO_4^{\cdot -} \longrightarrow \overset{\cdot}{M}\text{-}SO_4^-$$

Propagation

$$P\,OH + \overset{\cdot}{M}\text{-}OH \longrightarrow P\text{-}O\text{-}\overset{\cdot}{M} + H_2O$$

$$P\text{-}O\text{-}\overset{\cdot}{M} + n\overset{\cdot}{M} \longrightarrow P\text{-}O\text{-}(M)_n\text{-}\overset{\cdot}{M}$$

$$P\text{-}\overset{\cdot}{O} + nM \longrightarrow P\text{-}O\text{-}(M)n\text{-}_1\overset{\cdot}{M}$$

$$\overset{\cdot}{M}\text{-}O\text{-}H + nM \longrightarrow H\text{-}O\text{-}(M)_n\text{-}\overset{\cdot}{M}$$

Termination

$$P\text{-}O\text{-}(M)_n\text{-}\overset{\cdot}{M} + \overset{\cdot}{M}\text{-}(M)_n\text{-}O\text{-}P \longrightarrow P\text{-}O\text{-}(M)n\text{-}M_2\text{-}(M)_n\text{-}O\text{-}P$$

Graft Copolymer

$$P\text{-}O\text{-}(M)_{n+1}\overset{\cdot}{M} + \overset{\cdot}{M}\text{-}(M)n_{+1}\text{-}O\text{-}P \longrightarrow P\text{-}O\text{-}(M)_{n+1}\text{-}M_2\text{-}(M)_{n-1}O\text{-}P$$
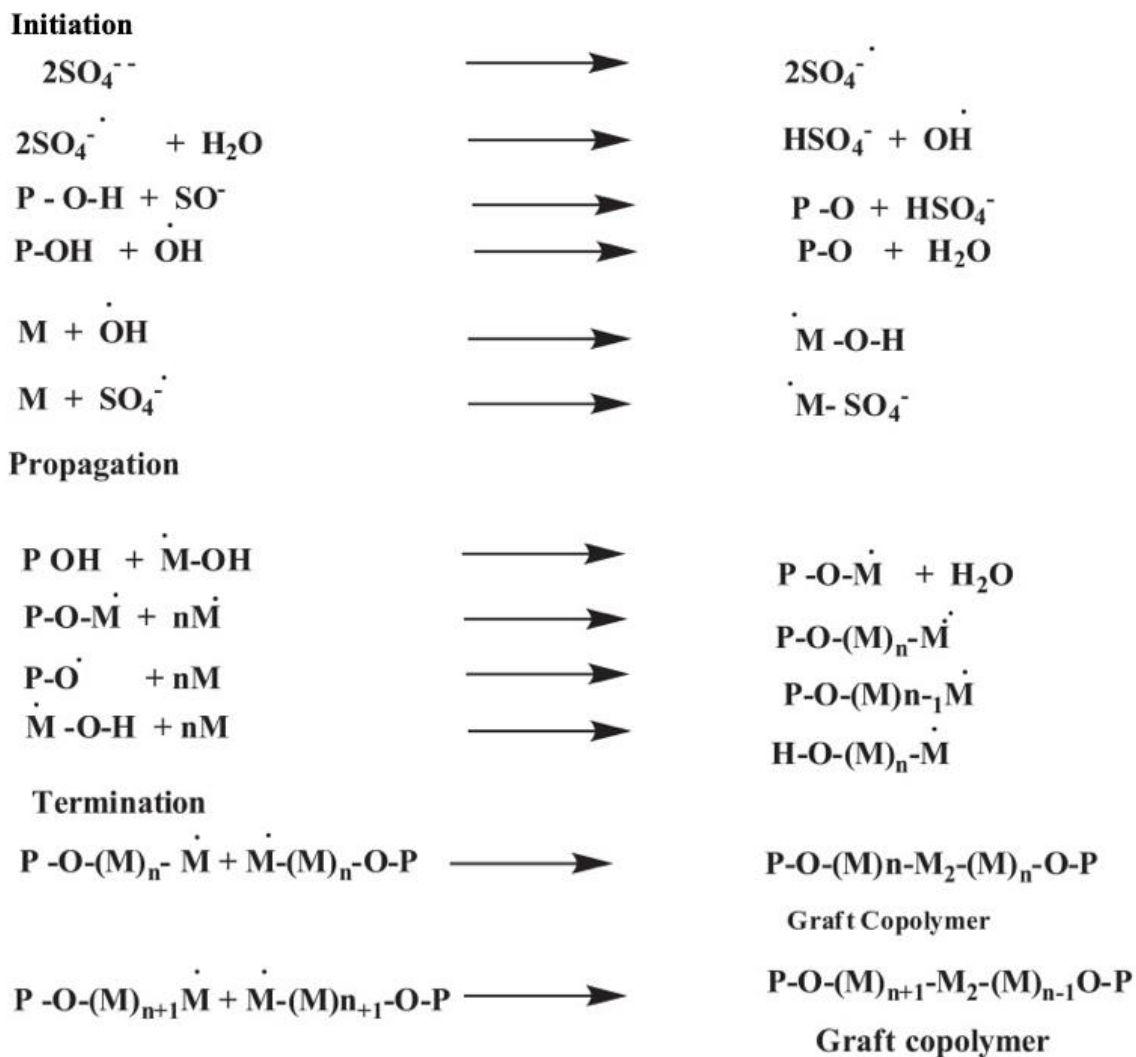
Graft copolymer

Figure 19: Free radical graft copolymerization mechanism of cellulose-g-poly(sodium acrylate) or -poly(acrylate) , where P is the cellulose (polymeric backbone chain), M is the acrylic acid (monomer), and C is the crosslinker [117]

The graft copolymers cellulose-g-poly(sodium acrylate) and cellulose-g-poly(acrylate) are macromer products that are crosslinked with other macromers to form three-dimensional structures. Figure 20 shows a graft copolymer network formed by cellulose and a copolymer.
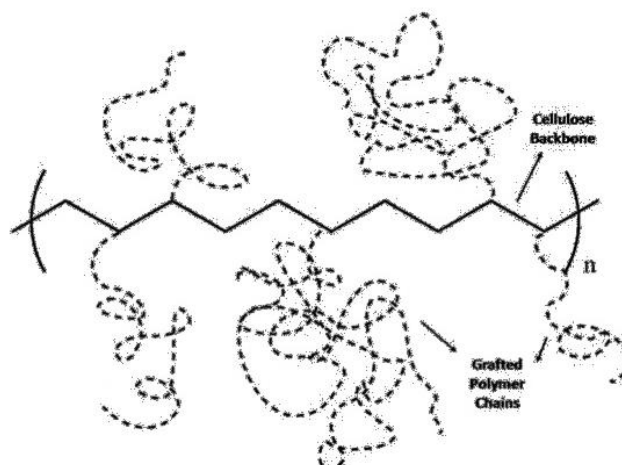
Figure 20: Graft copolymer network formed by cellulose and a copolymer [86]

1.7 Crosslinking

In SAP production, the selection of the crosslinker is based on the chemical functional groups of the macromer, such as –COOH, in an esterified cellulose or a poly(acrylate) polymer. The crosslinker acts as a bond between –COOH units, producing a SAP network. Depending on the crosslinker bond, the SAP can be either chemical (covalent and ionic bonds) or physical (hydrogen and other bonds). As shown in Table 3, SAPs can be classified according to their crosslinking type.

Table 3: SAP classification according to crosslinking type [118]

Gel type	Cross-linking mechanism	Backbone polymer		Example
Chemical gel	Covalent bond and ionic bond	Synthetic polymer		Cross-linked sodium polyacrylate
				Cross-linked sodium poly(vinyl sulfonate)
				Cross-linked poly(methacryloxyethyl ammonium chloride)
				Cross-linked poly(ethylene glycol)
		Natural polymer	Polysaccharide	Cross-linked carboxymethyl cellulose
				Cross-linked hyaluronic acid
				Cross-linked chitosan
				Cross-linked hydroxyethyl cellulose
			Polyamino acid	Cross-linked poly(glutamic acid)
				Cross-linked poly(lysine)
				Cross-linked poly(aspartic acid)
		Natural/synthetic hybrid		Starch–*graft*–sodium polyacrylate
				Saponified starch–*graft*–polyacrylonitrile
Physical gel	Hydrogen bond and others	The same as above		Poly(vinyl alcohol) treated by freezing and thawing
				Saponified poly(vinyl acetate-co-methyl [meth]acrylate)
				Mixture of poly(vinyl benzyl trimethylammonium chloride) and sodium polymethacrylate

The PEG, or poly(ethylene oxide), family of crosslinkers is non-toxic, highly biocompatible, and soluble in water [119]. These crosslinkers are considered "smart," or "intelligent," when they are contained in hydrogels because they can be stimulated physically (e.g., through temperature, solvent, and/or pressure) or chemically and biologically (e.g., through pH, specific ions, and/or molecular recognition).

The crosslinked structure developed by PEG in a hydrogel corresponds to the chain-growth reaction, in which the monomers react to the active site at the end of the growing chain in the propagation stage. Some of the characteristics of the chain-growth reaction are as follows: the monomers' concentration decreases steadily over time, the velocity of the reaction depends on the concentration of the initiator, and the polymer product has a high molecular weight. Figure 21 shows the most common structural arrangements of PEG.
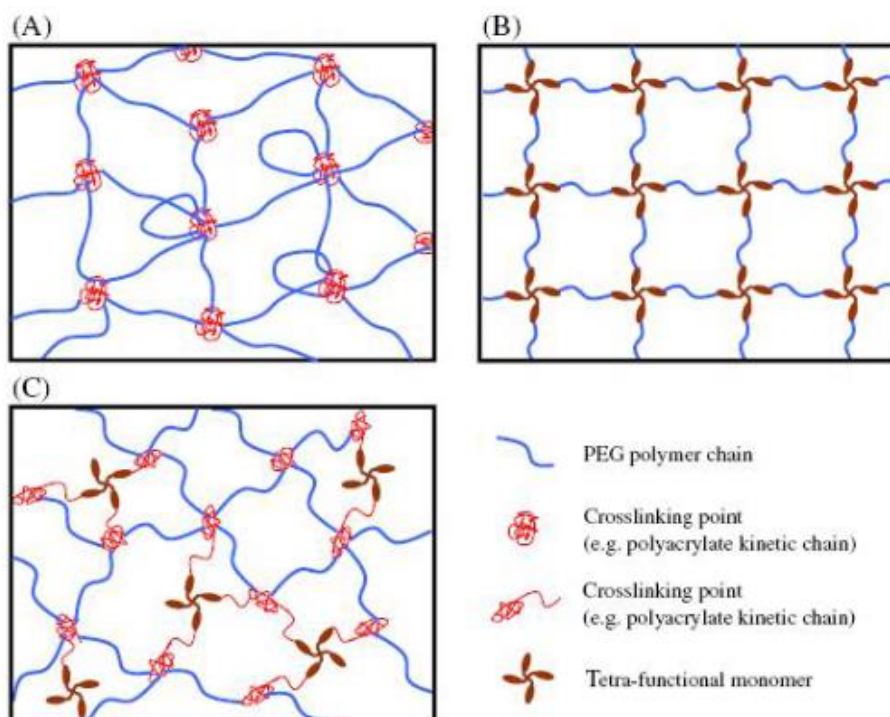
Figure 21: Common structural arrangements of PEG hydrogels formed during propagation: (A) chain-growth; (B) step-growth; and (C) mixed-mode (i.e., chain/step-growth) [119]

Graft copolymerization and crosslinking via free radical polymerization is the technique used for synthesizing the majority of cellulose-based Bio-SAPs. This method usually involves the reaction of a hydrophilic monomer and a crosslinking agent that contains one or more functional groups. PEG acrylates are commonly used as crosslinkers in bio-based polymers [120] because they contain vinyl groups and have a wide variety of average molecular weights.

Free radical graft copolymerization is triggered by an initiator, which generates the free radicals needed to propagate the reaction. Aqueous solutions ensure proximity within reactants, enhancing the reaction and controlling the heat generated during polymerization[114]. Impurities such as unreacted monomers, crosslinkers, or unwanted side products generated during the reaction are washed off the final product [121].

1.8 Crude cellulose

Although much progress has been made in research on free radical graft copolymerization, crude cellulose remains underexplored as a bio-based raw material in free radical graft copolymerization. Using crude cellulose in this way can be challenging because it requires an extended experimental design and the non-cellulose components contained in the crude cellulose can cause side reactions.

Crude cellulose can be obtained from agricultural residues, which are organic materials produced as by-products of crop harvesting and processing [122]. Agricultural residues can be categorized as primary or secondary. Primary residues are field-based residues generated during crop harvesting (e.g., maize stalks, empty coconut bunches, and paddy straw). Secondary residues, also called "processing-based residues," are generated during crop processing (e.g., maize cobs, coconut shells, coconut husks, paddy husks, sawdust, bagasse, wastewater, and black liquor).

Agricultural residues, which are widely available, are a potential source of biomass conversion to electricity, fuel, heat, and high-value chemicals. It is estimated that the amount of crop residues worldwide is 9.7 billion tonnes annually [123]. Moreover, partial removal of crop residues can positively impact soil carbon sequestration and soil maintenance [123].

1.8.1 Crude cellulose: a by-product of biomass fractionation

The goal of refinery is to separate chemical products from petroleum. In biorefinery, an analogous process, the goal is to separate chemical products from biomass. The five main components of biomass are cellulose, hemicellulose, lignin, ash, and extractives/volatiles [124]. The technologies used for processing biomass differ according to the nature of the biomass; they can be first-generation technologies (e.g., conversion of starches, sugars, and oils) or second-generation technologies (e.g., separation of lignocellulose). Usually, first-generation processing is easier than second-generation processing because the latter involves more complex biomass chemical components [125]; however, second-generation biomass is less expensive to process. The lignocellulosic processes for

conversion are classified into chemical, physical, physicochemical, and biological, and their selection depends on the desired products to be obtained from the biomass composition [126]. Lignocellulosic biomass consists of 35–50% w/w cellulose, up to 35% w/w hemicellulose, and 5–30% w/w lignin [127]. The specific valorization of these components and the inherent properties of the feedstock determine the proper process [128].

The processes most commonly applied to separate the main components of lignocellulosic biomass are hydrothermal (e.g., autohydrolysis and steam explosion), acid (e.g., H_2SO_4, HCl, HNO_3, and H_3PO_4), alkaline (e.g., $Ca(OH)_2$, NaOH, KOH, and ammonia), organosolv, and ionic liquids [129].

1.8.2   Organosolv fractionation

Organosolv fractionation, one of the processes for separating chemical products from biomass, is promising due to its low toxicity and effective lignin separation. Moreover, if the organic solvent is recycled and the lignin is recovered, organosolv fractionation could be sustainable and economically viable. However, this process has some drawbacks; for example, liquor separation, the use of high temperatures, and losses of solvent due to high solvent volatility make organosolv fractionation an expensive process [127].

The following solvents are used in organosolv fractionation: alcohols (e.g., methanol and ethanol), organic acids (e.g., acetic acid and formic acid) [130], esters, and any combination of these in the presence or absence of an acid or alkaline catalyst [131].

Organosolv fractionation is typically performed with alcohols and organic acids. In research on alcohol-based organosolv fractionation, ethanol has been the most widely investigated solvent, and the products obtained in such studies have had low lignin content [132]. In research on organic acid-based organosolv fractionation, the most studied solvents have been acetic acid and formic acid, which are attractive due to their lower boiling points and their consequent facility to be recycled during fractionation. The key characteristic of organic acid-based fractionation is the high solubilization of lignin, which increases the purity of the cellulose [133].

Organosolv fractionation has influential effects on the fractionation of non-wood feedstocks (e.g., cornstover, corn stalks, wheat straw, rice straw, and bamboo). The process involves mixing biomass feedstock with an organic aqueous solution (ranging from 40 to 80% w/w solvent concentration) at temperatures ranging from 100 to 220°C [134]. In organosolv fractionation, lignin is efficiently dissolved because a hydrolytic cleavage occurs in lignin's aryl ether bonds. During the organosolv fractionation of inter-unitary lignin bonds, more β-O-4 linkages than α-O-4 linkages are broken; generally, α-O-4 linkages require more severe conditions (e.g., elevated concentrations of acids) to be broken [131].

1.9 Identified gaps in the literature

The synthetic SAP market is expected to continue to grow throughout the 2020s. However, it has also been projected that this growth will be limited due to fossil-based raw materials' fluctuating prices and low biodegradability, both of which make these materials less attractive on the market, where consumers are leaning toward bio-based products [135]. There is an increasing demand for the production of Bio-SAPs using bio-renewable materials such as polysaccharides and proteins, which have desirable properties, such as biodegradability, non-toxicity, abundant availability, and potentially low costs. This trend is evidenced by the increasing number of Bio-SAP synthesis studies published in recent years.

Because bio-based materials (e.g., polysaccharides and proteins) are more expensive than fossil-based materials, the production of Bio-SAPs tends to be more expensive than that of fossil-based SAPs. In Bio-SAP production, to mitigate this disadvantage, crop residues can be used as a source of low-cost raw materials. Crop residues such as cornstalk are composed of approximately 20% lignin, 35% cellulose, and 35% hemicellulose [134]. If the cellulose in crop residues is cost-effectively separated and used for Bio-SAP synthesis, this will reduce Bio-SAP production costs [136]. In a recent study by our research group at Western University, organosolv fractionation using an organic solvent mixture of acetic acid–formic acid–water effectively fractionated crop residues and other lignocellulosic materials into lignin and cellulose. We used cornstalk as the feedstock,

and the yields of crude cellulose and crude lignin were 60–70% w/w and 30–40% w/w, respectively. We obtained crude cellulose with a purity of 70–80% w/w, and we determined that such crude cellulose could be used as a raw material for SAP production [134]. To the best of our knowledge, there is no published work on synthesizing Bio-SAPs using crude cellulose with the aim of attaining a high AC that is competitive with the AC of fossil-based SAPs. The present study aimed to fill this research gap.

It has been estimated that each year, the Canadian agricultural sector generates more than 30 million tonnes of crop residues, most of which are available for energy and chemical production [137]. Thus, the development of Bio-SAPs using crop residue-derived crude cellulose as a low-cost raw material would generate an additional revenue stream and create new employment opportunities, contributing to Canada's emerging bio-economy. The present study obtained a Bio-SAP by modifying pure cellulose (Cellulo-SAP) and a second Bio-SAP using crude cellulose from cornstalk (CrudeCellulo-SAP), a crop residue. The study's principal objective was to make both Bio-SAPs viable alternatives to fossil-based SAPs in agricultural applications (Figure 22).
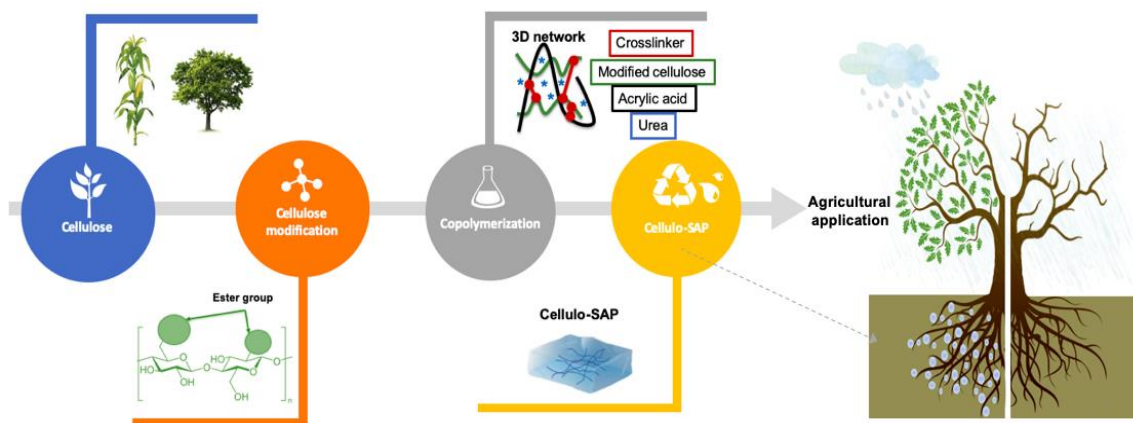
Figure 22: Bio-SAP production and application

In this dissertation, the investigation, results, and discussion of the Bio-SAP synthesis are presented as follows. Chapter 2 outlines the esterification process with two esterification agents: maleic anhydride and citric acid. Maleic anhydride was used to esterify pure cellulose, which generated optimal conditions for predicting the degree of substitution (DS) of ester groups. Citric acid was used to esterify pure cellulose and crosslink ester

groups intermolecularly, which resulted in an absorbent polymer composite; however, AC was relatively low.

Chapter 3 explicates the solubilization, copolymerization, and crosslinking of cellulose esterified using maleic anhydride (Cell-MA). These processes resulted in the optimal formulation of Cellulo-SAP, a pure cellulose-based Bio-SAP, which had a high AC. Chapter 4 describes the evaluation of Cellulo-SAP's performance. This chapter is based on our article, "Performance of a cellulose-based superabsorbent polymer (Cellulo-SAP): Absorbency, stability, reusability, and biodegradability," which was published in The Canadian Journal of Chemical Engineering.

Finally, the information obtained from pure cellulose esterification and the synthesis formulation of Cellulo-SAP was used to produce CrudeCellulo-SAP. Chapter 5 elucidates the organosolv fractionation process used to obtain crude cellulose and produce CrudeCellulo-SAP. Figure 23 shows a block diagram that illustrates how the cellulose-based SAP synthesis applied in the present study is explained, step by step, throughout this dissertation.
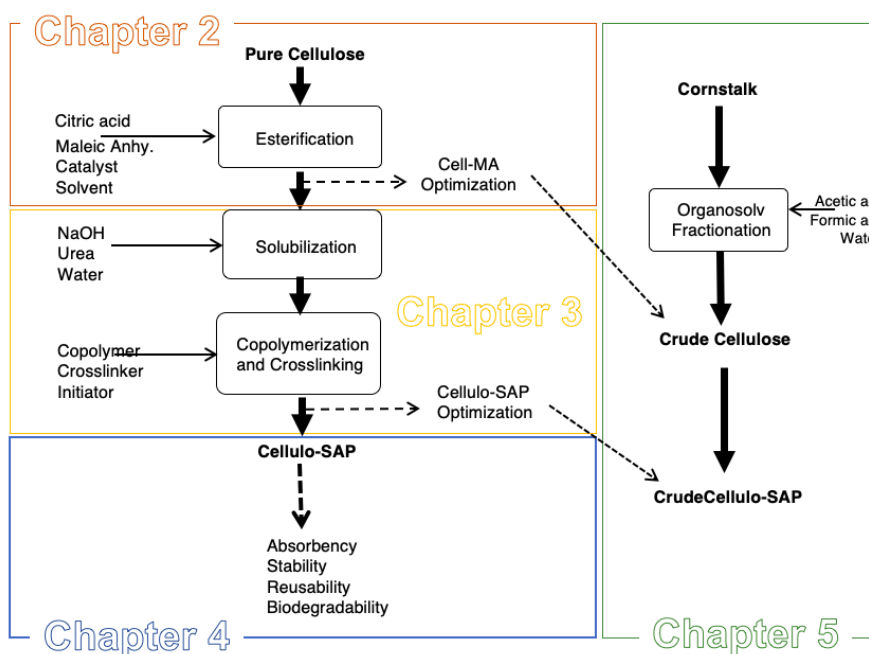
Figure 23: This dissertation's step-by-step explanation of cellulose-based SAP synthesis

1.10 Research objectives

1.10.1 General objectives

The present study aimed to develop Bio-SAPs for agricultural applications—more specifically, soil water retention—using crop residue-derived crude cellulose as a natural source. The resultant Bio-SAPs were Cellulo-SAP and CrudeCellulo-SAP. The first of these, Cellulo-SAP, was prepared using pure commercial cellulose (Sigmacell cellulose) and then synthesized in three steps: functionalization of the cellulose, copolymerization with acrylic acid, and crosslinking. CrudeCellulo-SAP was prepared using crude cellulose obtained via organosolv fractionation and then synthesized in two steps: copolymerization with acrylic acid and crosslinking.

1.10.2 Specific objectives

The present study's specific objectives were as follows:

1) To evaluate the effects of pressure, type of solvent, cellulose–maleic anhydride molar ratio, and catalyst in order to obtain a formulation for the esterification of pure commercial cellulose with maleic anhydride.

2) Method modification to obtain a Bio-SAP using pure commercial cellulose for esterification and crosslinking with citric acid.

3) Cellulo-SAP production using esterified pure cellulose, following the formulation in specific objective 1.

4) Optimization of the esterification and synthesis processes to maximize the AC of Cellulo-SAP.

5) Evaluation of Cellulo-SAP's water AC, reswelling, absorption in salt solutions, biodegradability, pH stability, and thermal stability to determine Cellulo-SAP's suitability for agricultural applications.

6) Obtainment of crude cellulose via organosolv fractionation with an acetic acid–formic acid–water mixture; CrudeCellulo-SAP production using crude cellulose, applying the synthesis method and optimal formulation used in Cellulo-SAP production.

Chapter 2

2   Cellulose modification: esterification

2.1   Introduction

Esterification is an essential process in academic and industrial chemistry [138]. Esterification occurs when an alcohol is combined with carboxylic acid to produce an ester. Commonly, Brønsted acids are employed as catalysts [138]. Esterification has been commonly used to esterify lipids [139], ethylene glycol [140,141], propylene glycol [142], glycerol[143], fuselol [144], butanol [145–147], methanol [147], etc. The esterification of alcohols results in value-added products (e.g., fuel additives) that are used in industrial applications [143].

The use of highly concentrated Brønsted acids as catalysts for esterification (e.g., H_2SO_4, p-toluenesulfonic acid) produces undesired by-products, such as acidic wastes. Therefore, to make esterification environmentally friendly, solid Lewis acids have been used as alternative catalysts. Previous studies have examined the esterification-enhancing performance of some Lewis acid catalysts, such as Fe^{+3} montmorillonite [148], acidic clay [149], ionic exchange resins [145,148], $SnCl_2$, $FeCl_3$, $ZnCl_2$, $AlCl_3$, and $NbCl_5$ [139]. In esterification, it is common to use a solvent—along with the catalyst—to facilitate contact between the alcohol, catalyst, and carboxylic acid. Previous studies have also examined the esterification-enhancing performance of some solvents, such as benzoic acid [150], toluene [138], tetrahydrofuran [138], and acetonitrile [138]. Moreover, a study by Barbosa et al. [150] proposes a solvent free methodology using a Lewis acid in a solid phase to esterify bioethanol. Lewis acids offer advantages, such as product separation and recycling, that are not offered by the conventional methods. However, Lewis acids have higher costs, longer reaction times, and lower yields of desired products [150].

Cellulose is the most abundant polymer, and its unique arrangement influences the properties and reactivity of cellulose-based materials. A cellulose molecule has five hydroxyl groups and an oxygen atom as a bridge. This configuration forms complex

structures of hydrogen bonds, which make cellulose molecules highly ordered and insoluble in water [151].

Studies on cellulose esterification have aimed to increase its reaction versatility [82]. A variety of esterification techniques have produced high added-value cellulose-based by-products, such as cellulose nitrate [152], cellulose sulfate [153], cellulose phosphates [154], and cellulose carboxylate (e.g. cellulose acetate) [155]. In particular, to obtain cellulose carboxylate, the most traditional method is called acylation, which involves esterification between cellulose and acetic acid [82].

In this chapter, maleic anhydride was used to esterify Sigmacell cellulose, a pure commercial cellulose. Subsequently, the effects of the following factors on esterification were evaluated: pressure, type of solvent, cellulose–maleic anhydride molar ratio, and catalyst. The optimal arrangement of the factors was determined using response surface methodology (RSM) with a central composite design (CCD) to produce the preferred response. In addition, citric acid was used to esterify and crosslink pure cellulose, and the effects of temperature, catalyst, and crosslinking agent were evaluated.

2.2   Materials and methods

2.2.1   Materials

All chemicals were chemical abstracts service (CAS) reagent grade, supplied by Sigma-Aldrich, and used as received (i.e., without further purification). Table 4 summarizes the chemicals' purity levels.

Table 4: Chemicals used for cellulose esterification and their purity levels

Chemical	Purity
Sigmacell cellulose	99%
starch	99%
maleic anhydride	99%

zinc chloride	≥ 98%
p-toluenesulfonic acid monohydrate	≥ 98.5%
acetonitrile	99.8%
acetone	99.5%
acetic acid	99.7%
sodium hydroxide	98%
hydrochloric acid	37%
citric acid	99%
PEG (number-average molecular weight = 400 g/mol)	≥ 99%
sodium hypophosphite	≥ 98%
ethanol	95%

2.2.2   Methods

2.2.2.1 Esterification with maleic anhydride

In these esterification experiments, preliminary tests were directed based on methodology modifications on state-of-the-art references [156–159] using cellulose or starch (pre-dried in the vacuum oven at 60°C for 2 h), maleic anhydride (cellulose–maleic anhydride molar ratio of 1:1, 1:2, or 1:3), 80 g of acetone, acetonitrile or acetic acid, and zinc chloride or p-toluenesulfonic acid monohydrate as a catalyst (2.5, 3, or 3.5% w of solids) were mixed in a 250 mL three-neck flask. The mixture was stirred for 2–8 h at a temperature chosen in accordance with the solvent type, and a nitrogen purge was used. After cooling, the resulting solid products were filtered, washed with acetone, and dried in a vacuum oven for 24 h at 70°C. Figure 24 outlines the procedure. Esterified pure

cellulose and starch samples were characterized by Fourier transformed infrared (FTIR) spectroscopy.
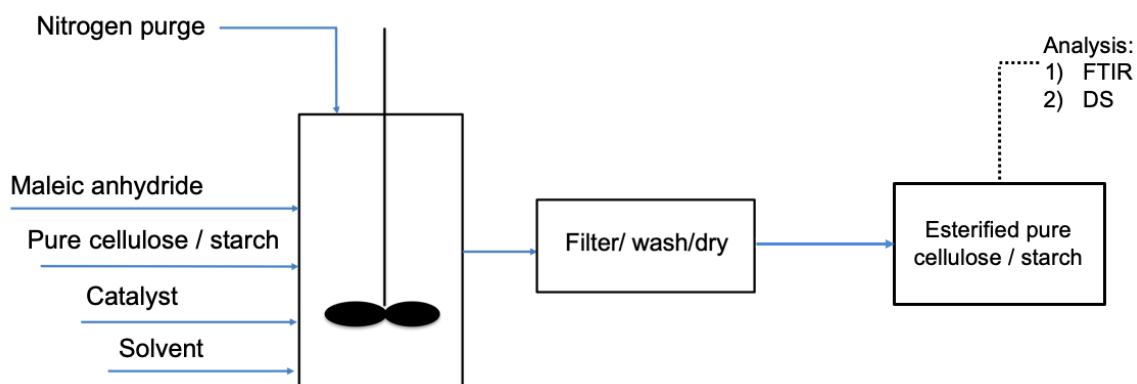
Figure 24: Cellulose/starch esterification with maleic anhydride

Figure 25 shows a Brønsted acid-based or Fischer esterification using p-toluenesulfonic acid as a catalyst. This reaction mechanism occurs due to the addition of nucleophile (cellulose) into the carboxylic acid and consists of five steps [160]. The first step is the protonation of the carboxylic acid by the p-toluenesulfonic acid catalyst. In the second step, the lone pairs of electrons from the oxygen atom located in the –OH of cellulose behave as a nucleophile, and the oxygen atom attaches to the sp^2 carbon atom and, therefore, loses a proton. The third step involves a series of equilibrium proton exchanges in the –OH of the carboxylic acid, and an ester bond is formed between the carboxylic acid carbon and the oxygen in cellulose. The fourth step is the elimination of water, and the fifth step is the regeneration of the p-toluenesulfonic acid.
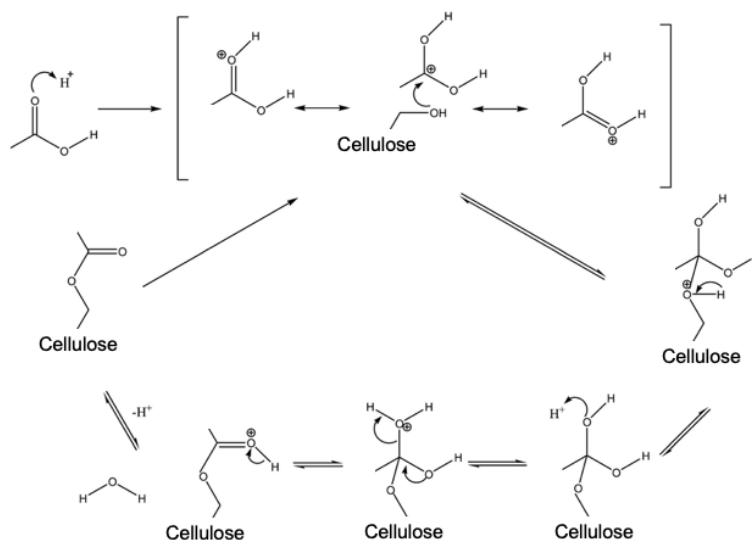
Figure 25: Brønsted acid reaction mechanism

Theoretically, the reaction mechanism of Lewis acid-based esterification is similar to that of Brønsted acid-based reactions. In the particular case of the esterification of glycerol using $ZnCl_2$, a mechanism of reaction has been proposed [160]. This mechanism describes cellulose esterification via nucleophilic addition, which occurs to the –OH group of the cellulose forming a nucleophile. The Lewis-based reaction (Figure 26) implicates a metal cation (L^+) that acts as an electrophile to aid in the interaction between the carbonyl oxygen (from the carboxylic acid) and the Lewis acid site (from the catalyst) to form a carbocation. Then, the cellulose's nucleophile attacks the carbocation to produce the esterified cellulose.

L^+ is catalyst Lewis acid site
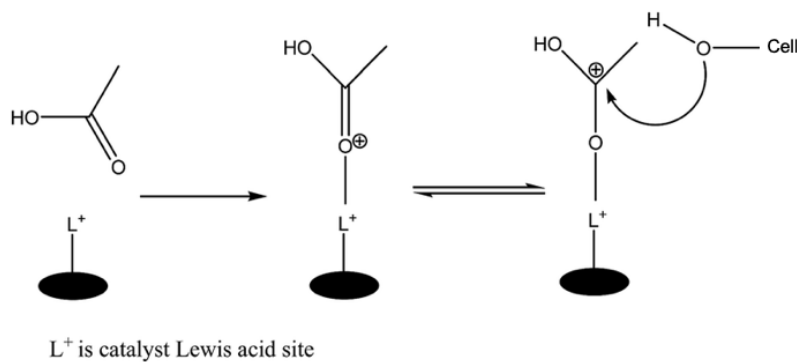
Figure 26: Lewis acid reaction mechanism

2.2.2.2 Esterification and crosslinking with citric acid

The efficacy of five methodologies for the esterification of starch using citric acid was evaluated. In these experiments, only starch was used because cellulose has low solubility in water. According to the literature, the esterification of and crosslinking within cellulose and starch occur during a curing process. In this process, crosslinking and polymerization take place, resulting in absorbent polymer production. Preliminary tests were conducted based on state-of-the-art references (Lacoste et al., 2019; Liu et al., 2013; Liu et al., 2017; Luo et al., 2011; Senna and Botaro, 2017). Five methods for gelation of the starch solution (prepared by mixing starch in deionized water at 20% w of solid content for 30 min) were evaluated. Figure 27 outlines the five methods.
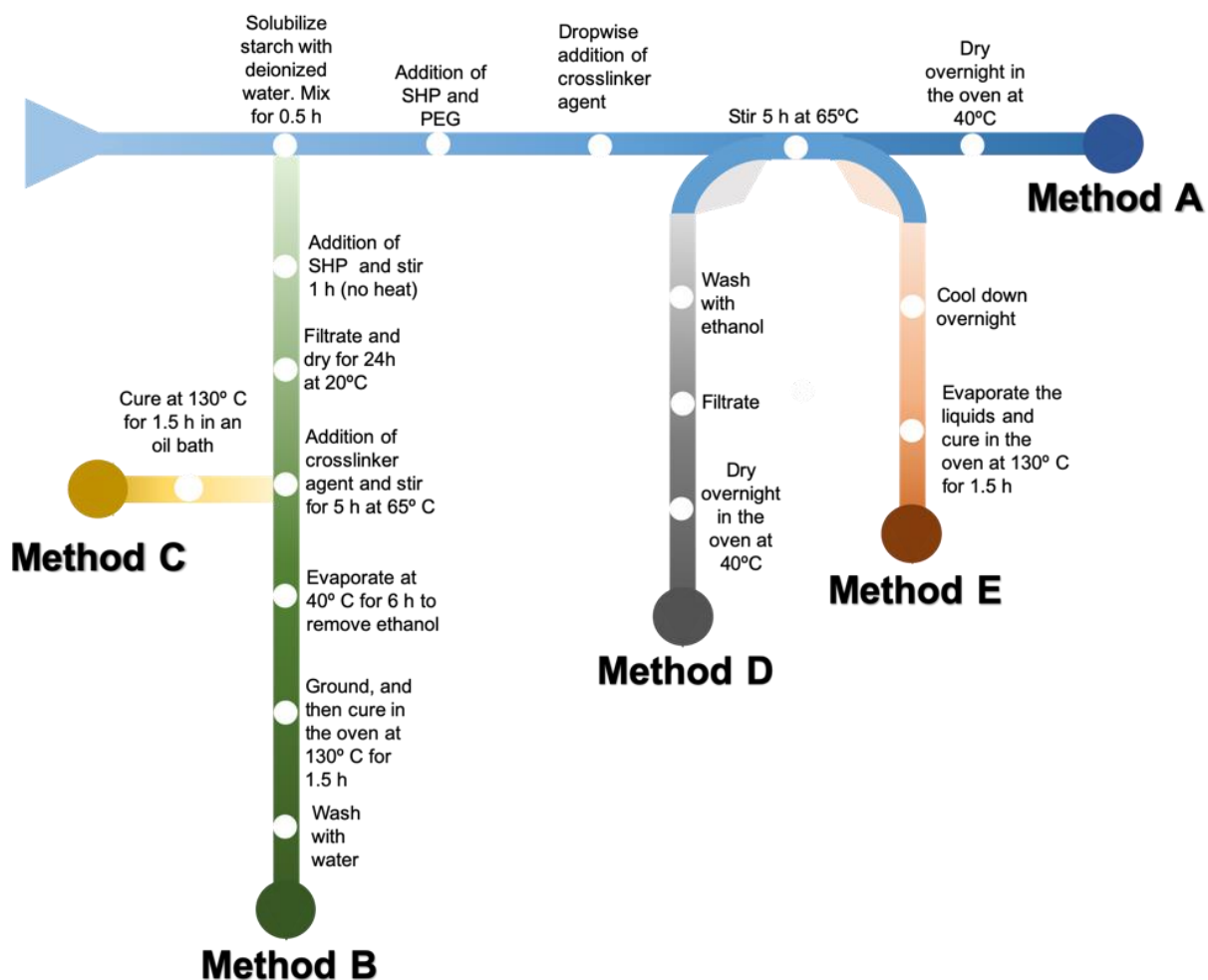
Figure 27: Method development for crosslinking of soluble starch for Bio-SAPs

- Method A: While the starch solution was being stirred in a flask, SHP and PEG were added. Then, a citric acid solution (23% w/w) was added. The stirring continued at 65°C for 5 h. The mixture was then dried in an oven at 40°C overnight.

- Method B: SHP was added to the starch solution in a flask and stirred for 1 h at room temperature. The mixture was then filtered and dried in an oven for 24 h at 40°C. A citric acid solution (23% w/w) was added, and the stirring continued at 65°C for 5 h. The mixture was dried at 40°C for 5 h in the oven. Finally, the dried sample was ground and cured in an oil bath at 130°C for 1.5 h.

- Method C: The steps of method B were followed up to the incorporation of the citric acid solution (23% w/w) and the stirring of the mixture at 65°C for 5 h. Afterward, the mixture was cured in an oil bath at 130°C for 1.5 h.

- Method D: The steps of method A were followed up to the incorporation of the citric acid solution (23% w/w) and the stirring of the mixture at 65°C for 5 h. Afterward, the mixture was washed with ethanol, filtered, and dried in the oven at 40°C overnight.

- Method E: The steps of method A were followed up to the incorporation of the solution of citric acid (23% w/w) and the stirring of the mixture at 65°C for 5 h. Afterward, the mixture cooled down; then, it was cured in an oil bath at 130°C for 1.5 h.

The SAP samples obtained via Methods A, B, C, D, and E were evaluated through analysis of each sample's AC.

2.2.2.3 AC analysis of starch esterified and crosslinked using citric acid

For this experiment, a crosslinked polymer sample was carefully dried, ground, and sieved to obtain an average particle size of 2 mm through a No. 10 standard sieve mesh (ASTM 11 standard sieve). Then, 0.05 g ($\pm$ 0.001 g) of polymer samples were immersed in 200 mL of deionized water at room temperature (23°C $\pm$ 2°C) for 24 h, during which time the samples became hydrogels. The obtained hydrogels were then removed from the solutions and filtered, and the unabsorbed aqueous solution was removed using dry tissues. The hydrogels were weighed until they reached AC equilibrium using the following equation:

$$AC = \frac{w_2 - w_1}{w_1} \quad \textbf{Equation 1}$$

where w_1 is the weight of the dry polymer sample and w_2 is the weight of the hydrogel. The entire AC analysis procedure was performed in triplicate.

2.2.2.4 Characterization of cellulose esterified with maleic anhydride

2.2.2.4.1 Infrared spectroscopy

The infrared spectrum of the samples was used to characterize the functional groups qualitatively in the modified cellulose/starch samples via FTIR spectroscopy on the spectrometer Frontier FTIR (Perkin Elmer). The infrared wavelength was 4000–550 cm^{-1} with a resolution of 4 cm^{-1}. The KBr method was used to obtain the characteristic spectra of the samples. This method involves mixing 0.0050 g of a completely dry sample with 0.1500 g of pure KBr (1:30 w/w ratio). In the present study, the pulverized mixture was used to form a transparent pellet by applying a force of approximately 8 tonnes for 2 min. The pellet was then inserted into the sample chamber to obtain the measurement.

2.2.2.4.2 X-ray diffraction analysis

X-ray diffraction analysis (XRD) was applied to the crystalline forms of the pure cellulose, maleic anhydride, and esterified pure cellulose samples on a PANalytical X'Pert PRO X-ray diffractometer using Cu Kα radiation with a wavelength of 0.1541 nm. An X-ray generator working at 30 kV and 15 mA produced an X-ray beam directed at the samples. The dissipated radiation was detected at ambient temperature over an angular area of 3 to 70°, at a rate of 10°/min, and at a step size of 0.02.

2.2.2.4.3 Scanning electron microscopy

Scanning electron microscopy (SEM) images of the cellulose before and after esterification were taken with a Zeiss/Leo 1530 field emission scanning electron microscope (FESEM) at 3 kV accelerating voltage. Prior to imaging, the samples were coated with 10 nm of osmium to improve their conductivity and avoid charging.

2.2.2.4.4 Degree of substitution of –COOH groups: back titration

The amount of –COOH grafted to the pure cellulose/starch sample after esterification was obtained through titration—specifically back titration. This method determines the –COOH concentration of the esterified pure cellulose/starch by reacting it with a known

amount of NaOH standard solution, and then this mixture is titrated with a HCl standard solution. Finally, the DS of –COOH in the esterified pure cellulose/starch was calculated using the amount of HCl standard solution needed to titrate the mixture (esterified sample-NaOH standard solution) (see Appendix A).

2.2.2.4.5 Statistical analysis of cellulose esterified with maleic anhydride

Optimization of cellulose esterification with maleic anhydride, acetic acid, using zinc chloride as a catalyst, was attained using Minitab® software. A faced centre CCD was used to study two independent variables (i.e., maleic anhydride and catalyst) with four factorial points (run order entry 2, 4, 7, and 8), four axial (star) points with an alpha value of 1.41 (run order entry 9–12), and five centre points (run order entry 1, 3, 5, 6, and 13). Table 5 presents the levels and range lists of the maleic anhydride and catalyst used in the optimization. The selection of levels was based on the results obtained in preliminary studies.

Table 5: Levels and range lists of maleic anhydride and catalyst

Levels	-1.41	-1	0	1	1.41
Maleic anhydride (molar ratio)	1.8	2	2.5	3	3.2
Catalyst (% w of solids)	1.6	2	3	4	4.4

2.2.3 Results and discussion

2.2.3.1 Effects of reaction time

The effects of the reaction time of cellulose esterification were investigated in an acetone solvent at 57°C (i.e., the boiling point) in a 250 mL three-neck glass flask reactor with a nitrogen purge. The reaction time was monitored for 6 h, and a small sample was taken to establish the effects of time on the cellulose's DS of the carboxyl group in cellulose. The cellulose–maleic anhydride molar ratio was 1:1. The zinc chloride catalyst was 2% w of

the solids. Beginning two hours after the reaction, a sample was taken every 30 min. The samples were filtered, washed with acetone, dried at 55°C in a vacuum oven for 24 h, and then analyzed via FTIR using KBr pellets. FTIR was used to characterize the presence and intensity of the –COOH groups on the cellulose/starch [164].

Figure 28 illustrates the FTIR spectra of esterified pure cellulose samples obtained after various lengths of reaction time; the main peaks were considered in the analysis, as follows:

1) The strong IR absorption at 1717 cm^{-1} can be attributed to the C=O stretch, which is the characteristic IR absorption of the functional group substituted for the cellulose's –OH group [165]. The peak at 1640 cm^{-1} corresponds to the C=C stretch introduced by the addition of the esterified agent (i.e., maleic anhydride) [166]. Therefore, the presence of these two IR peaks is evidence of the successful esterification of the cellulose.

2) The IR absorption peak at 3350 cm^{-1} can be ascribed to the –OH group's stretching band. At 3000 cm^{-1}, indicates the stretch of the C=C group vibrations. Both absorption peaks indicate the presence of cellulose [167].
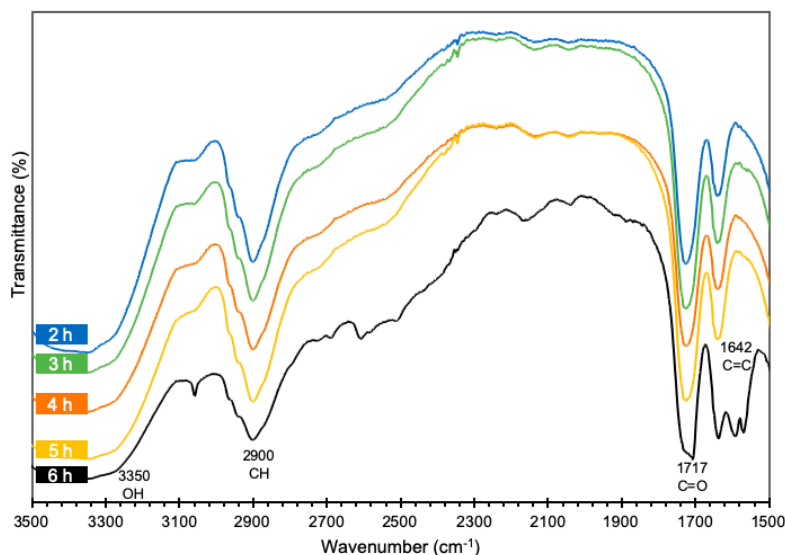
Figure 28: FTIR spectra of esterified pure cellulose samples obtained in acetone solvent at 57°C after various lengths of reaction time

The chemical kinetics of the esterification reaction between maleic anhydride and cellulose were calculated using the concentrations of maleic anhydride at 0, 2, 3, 4, 5, and 6 h after the reaction. The experimental data fit to a zero kinetic order, implying that the esterification rate did not depend on the concentration of maleic anhydride (MA); it depended exclusively on the specific rate constant at the given temperature (57°C). The zero-order kinetic equation was rearranged into the following line equation (coefficient of determination $R^2 = 0.955$):

$$[MA]_t = -kt + [A]_0 \qquad \textbf{Equation 2}$$

where [MA] is the concentration of maleic anhydride in mol/L, t is the time in h, k is the rate constant (equal to 0.0019 in mol/L h), and $[A]_0$ is the initial concentration (equal to 0.15 mol/L). The kinetics evaluation and experimental data are shown in Appendix B.

The effects of the reaction time on cellulose esterification were further investigated using acetic acid at 118°C for 2 and 8 h in a 250 mL three-neck flask reactor with a nitrogen purge. Other reaction conditions were as follows: a 1:1.5 cellulose–maleic anhydride molar ratio, zinc chloride at 2% w of the solids, and 340 revolutions per minute (rpm) stirring. Figure 29 shows the FTIR spectra of esterified pure cellulose samples obtained in an acetic acid at 118°C for 2 and 8 h. The presence of the absorption peaks at 1717 cm^{-1} and 1642 cm^{-1} indicates the stretching of C=O and C=C respectively. These two IR peaks are evidence of the successful esterification of the cellulose; the stronger intensity of the 8 h-reaction sample (DS = 1.65) indicates a higher presence of C=O and C=C than the sample that the 2 h-reaction (DS = 0.35).
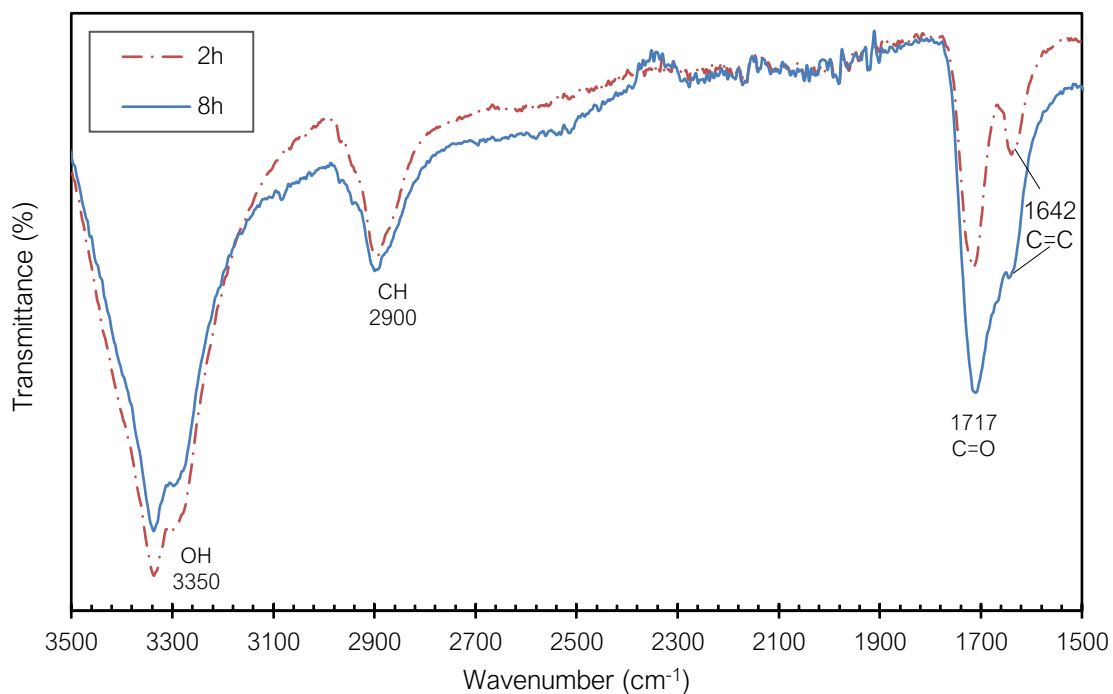
Figure 29: FTIR spectra of esterified pure cellulose samples obtained in acetic acid solvent at 118°C for 2 h and 8 h

2.2.3.2 Effects of catalyst

The effects of two catalysts—zinc chloride (Catalyst A) and p-toluenesulfonic acid (Catalyst B)—were evaluated by performing an esterification reaction in an acetic acid solvent at 118°C in a 250 mL three-neck reactor with a nitrogen purge; the catalyst (A or B) was at 2% w of the solids. The reaction conditions were as follows: a duration of 2 h, a 1:1 cellulose–maleic anhydride molar ratio, and 340 rpm stirring. As revealed in Figure 30, the esterified pure cellulose obtained using Catalyst A had stronger C=O and C=C absorption peaks than that obtained using Catalyst B, indicating that Catalyst A is more active than Catalyst B. The DS values of the esterified samples were 0.15 (zinc chloride) and 0.06 (p-toluenesulfonic acid). In this study, the DS results obtained using a Lewis acid catalyst (zinc chloride) were superior to those obtained using a Bronsted acid (p-toluenesulfonic acid). Ragab et al. [159] also performed esterification using a Lewis acid

catalyst (ferric perchlorate) and obtained cellulose acetate successfully under room temperature conditions.
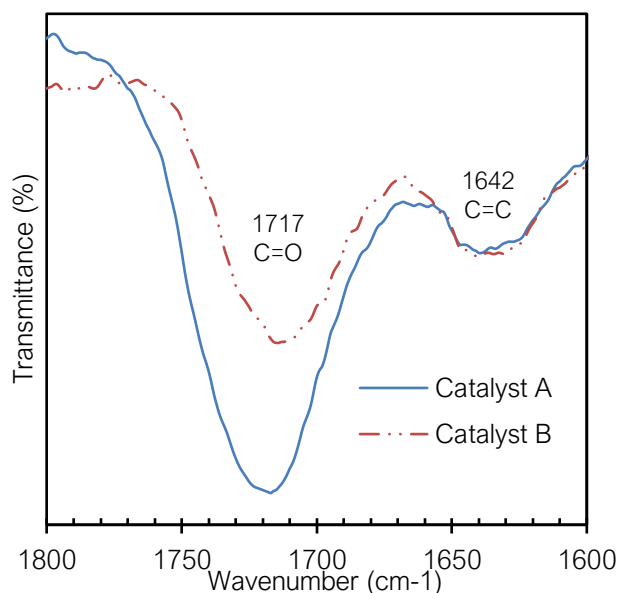
Figure 30: FTIR spectra of esterified pure cellulose samples obtained using zinc chloride (Catalyst A) and p-toluenesulfonic acid (Catalyst B)

2.2.3.3 Effects of cellulose–maleic anhydride molar ratio

The effect of the cellulose–maleic anhydride molar ratio on esterification was investigated at three different ratios: 1:1, 1:2, and 1:3 in an acetic acid solvent at 118°C (i.e., the boiling point) in a 250 mL three-neck reactor with a nitrogen purge. The other conditions were as follows: a duration of 2 h, zinc chloride at 2% w of the solids, and 340 rpm stirring. As illustrated in Figure 31, the sample with the highest concentration of maleic anhydride presented the highest characteristic peak intensity (C=O and C=C stretches), which suggests that using a higher concentration of maleic anhydride resulted in increased grafting of the –COOH group to the cellulose. The DS values of the esterified samples were 0.11 (1:1 cellulose–maleic anhydride molar ratio), 0.37 (1:2 cellulose–maleic anhydride molar ratio), and 0.9 (1:3 cellulose–maleic anhydride molar ratio).
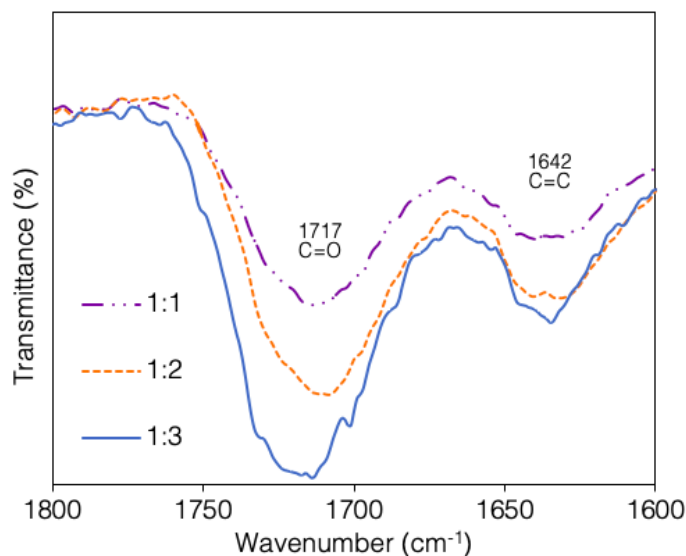
Figure 31: FTIR spectra of esterified pure cellulose samples obtained using different cellulose–maleic anhydride molar ratios

2.2.3.4 Effects of the solvent

The effects acetonitrile and acetone as solvents on the esterification reaction were investigated. These two samples were compared to a sample prepared with acetic acid to evaluate the effect on the DS of pure cellulose. The temperature conditions corresponded to each chemical's boiling point: 118°C (acetic acid), 110°C (acetonitrile), and 56°C (acetone). The esterification reaction was conducted in a 250 mL three-neck reactor with a nitrogen purge. Other reaction conditions were as follows: a duration of 2 h, a 1:1.5 cellulose–maleic anhydride molar ratio, zinc chloride at 2% w of the solids, and 340 rpm stirring.

Figure 32 shows the FTIR spectra of the esterified pure cellulose samples obtained in different solvent media. Additionally, Figure 32 shows the characteristic peaks of the – COOH groups (i.e., the C=O stretch at 1720 cm^{-1} and the C=C stretch at 1640 cm^{-1}); these peaks indicate the successful esterification of the cellulose in the three solvents. Nevertheless, the intensity of these peaks differed depending on the type of solvent. The esterified pure cellulose samples modified with acetic acid showed the highest-intensity

C=O and C=C absorption peaks; the samples modified with acetone showed the least intense absorption peaks. The DS values of the samples in the two solvents were 0.17 (acetonitrile), and 0.05 (acetone). Between these two solvents, the acetonitrile had a higher DS. Acetic acid had a DS of 0.35, which was higher than the DS of both acetonitrile and acetone, proving that acetic acid acted as a reactant and contributed to the increase of DS of pure cellulose. The resulting esterification due to the presence of acetic acid as esterification agent coincides with another study [159] in which acetic acid was used as a reagent for cellulose esterification to obtain cellulose acetate.
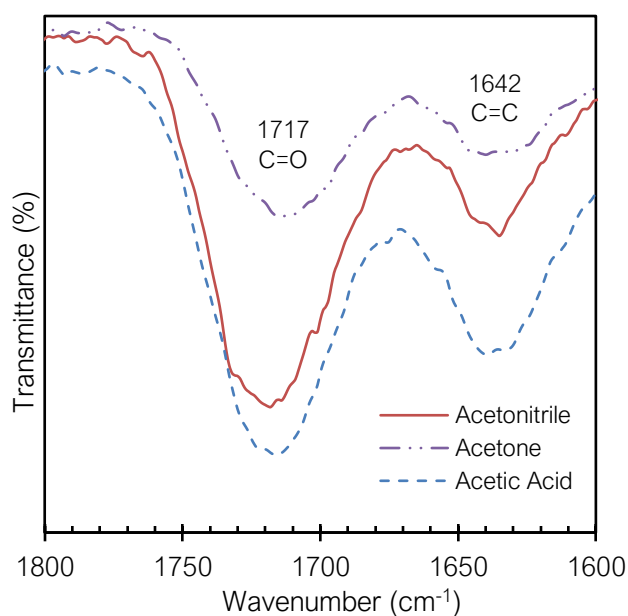
Figure 32: FTIR spectra of esterified pure cellulose samples obtained using different solvents

2.2.3.5 Effects of the substrate

The esterification reaction was performed using soluble starch as the substrate; the aim of this experiment was to compare the results with those obtained from the esterification reaction using cellulose. The reaction was conducted in a 250 mL three-neck reactor with a nitrogen purge, under the same conditions: a duration of 2 h, an acetic acid solvent at 118°C, a 1:1.5 starch–maleic anhydride molar ratio, zinc chloride at 2% w of the solids, and 340 rpm stirring. Figure 33 shows the FTIR spectrum of esterified starch obtained

under these conditions. The peaks of the –COOH groups (i.e., the C=O stretch at 1720 cm^{-1} and the C=C stretch at 1640 cm^{-1}) of the esterified starch have a higher intensity than those of the esterified pure cellulose. This result was predictable: soluble starch, which is less crystalline than cellulose, is more reactive and can therefore be grafted easily with maleic anhydride. The DS values of the esterified samples were 0.35 (cellulose) and 1.04 (starch).
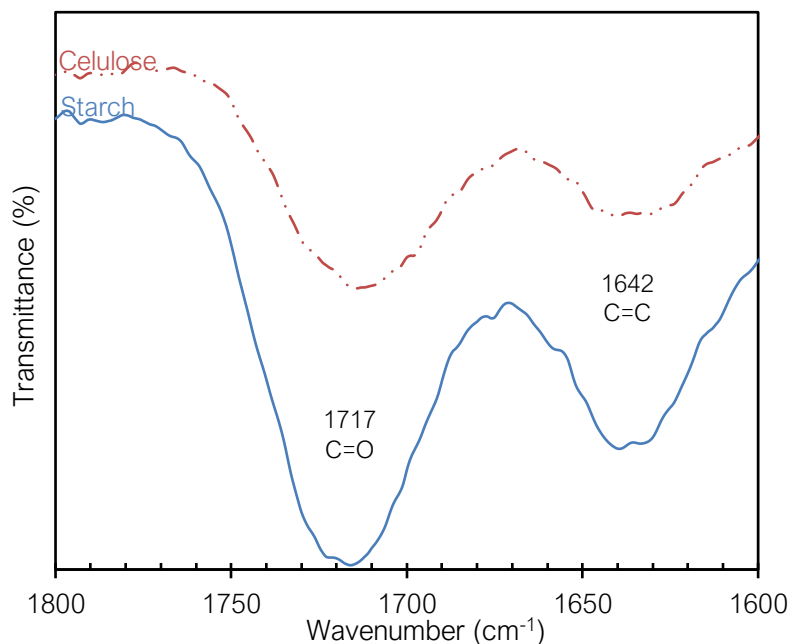
Figure 33: FTIR spectra of esterified samples—comparison of cellulose and starch

In all the above-mentioned experiments—which constitute the preliminary experiments of the present study—the DS values of the esterified pure cellulose samples were evaluated via back titration analysis. Table 6 summarizes the results of these analyses.

Table 6: Summary of DS values in preliminary experiments

Variable analyzed	Treatment	DS
Reaction time	2h	0.35
	8h	1.65
Catalyst	**Zinc chloride**	0.15

	p-toluenesulfonic acid	1.06
Cellulose–maleic anhydride molar ratio	1:1	0.11
	1:2	0.37
	1:3	0.9
Solvent	Acetonitrile	0.17
	Acetone	0.05
Substrate	**Pure cellulose**	0.35
	Starch	1.04

Based on the results of the preliminary experiments, the following variables (in boldface in Table 6) were selected for later esterification experiments: 5 h (reaction time), zinc chloride (catalyst), acetic acid, and pure cellulose (substrate). The cellulose–maleic anhydride molar ratio and the percentage weight of the catalyst were used to develop the CCD.

2.2.3.6 Statistical analysis

Table 7 shows the DS of esterified pure cellulose obtained under the following reaction conditions: a duration of 5 h; an acetic acid solvent at 118°C; zinc chloride at 1.6, 2, 3, 4, or 4.4% w of the solids; and a cellulose–maleic anhydride molar ratio of 1:1.8, 1:2, 1:2.5, 1:3, or 1:3.2. Analysis of variance (ANOVA) revealed that the "Prob > F" value for the quadratic model was < 0.05, which implies the significance of the response variables (Table 8).

Table 7: Cellulose esterification experimental design and results

Experiment ID	Level Factor A	Level Factor B	Factor A: cellulose–maleic	Factor B: zinc chloride	Response:DS

			anhydride molar ratio (cellulose = 1)	(% w of the solids)	
P1	-1	1	2	4	1.5
P2	1	-1	3	2	1.2
P3	1	1	3	4	2.3
P4	-1	-1	2	2	0.6
P5	0	0	2.5	3	1.9
P6	0	0	2.5	3	1.8
P7	0	0	2.5	3	1.4
P8	0	0	2.5	3	1.5
P9	0	0	2.5	3	1.9
P10	-1.41	0	1.8	3	0.5
P11	1.41	0	3.2	3	2.3
P12	0	-1.41	2.5	1.6	0.9
P13	0	1.41	2.5	4.4	1.9

Table 8: ANOVA for response surface quadratic model

Source of variance	Sum of squares	Degrees of freedom	Mean square	F value	p-value Prob > F
Model	3.424	2	3.403	21.90	0.0001
Factor A: cellulose–maleic anhydride molar ratio (cellulose = 1)	3.403	1	1.701	54.40	0.0001

Factor B: **zinc chloride (% w of the solids)**	1.946	1	1.946	62.22	0.0001
Square Model	0.011	2	0.006	0.18	0.8413
A²	0.006	1	0.006	0.20	0.6680
B²	0.006	1	0.006	0.20	0.6680
AB	0.010	1	0.010	0.32	0.5897
Lack of fit	0.219	3	0.069	22.99	0.006
Error	0.219	9	0.031		
Total	3.643	12			

The mechanism of esterification using maleic anhydride comprises five steps [159]. In the first step, the zinc cation acts as an electrophile, interacting with the carbonyl oxygen in the maleic anhydride. Second, the lone pair of electrons in the –OH group of the cellulose forms a bond with the carbonyl carbon, which breaks its pi bond with one of its oxygen atoms, resulting in an oxonium ion. Third, the oxonium ion transfers a proton to the –OH group, forming an activated complex. Fourth, a lone pair of oxygen atoms forms a pi bond. In the fifth and final step, the oxygen is deprotonated, resulting in an ester product. The proposed mechanism is summarized in Figure 34. Overall, in this mechanism, the cellulose–maleic anhydride ratio and catalyst are highly impactful; therefore, these two variables were selected as the key factors in optimizing esterification.
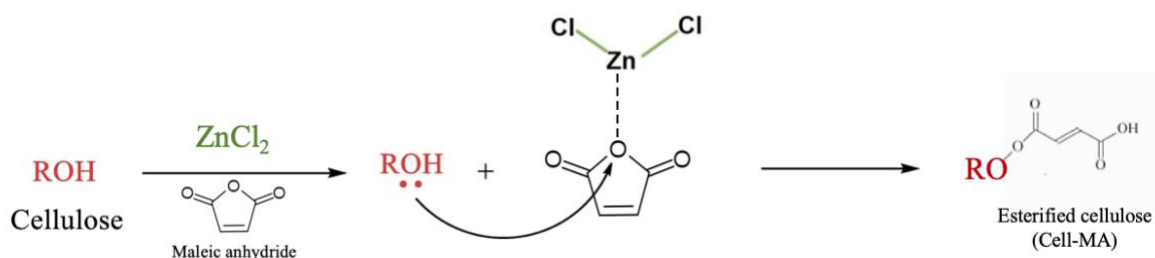
Figure 34: Cellulose esterification mechanism using maleic anhydride and zinc chloride as a catalyst

The cellulose–maleic anhydride molar ratio (factor A) was modified by adding maleic anhydride in excess. Maleic anhydride was added in excess because of the reversibility characteristic defined by Le Chatelier's principle, which states that the application of stress to the system at equilibrium shifts the position of the equilibrium in the direction that reduces stress. Therefore, an increase in maleic anhydride shifts the position of the equilibrium, increasing the ester yield. Adding a catalyst (factor B) function speeds up the reaction rate, allowing equilibrium to be reached more quickly. This is the only effect of adding a catalyst; hence, it can be inferred that maleic anhydride contributes more to the DS of cellulose than does the catalyst.

The acceptability of the quadratic model, which was obtained from the ANOVA sequential model, was verified via regression analysis. In addition, the constant values of the factor's interaction resulted in an empirical second-order polynomial equation (Equation 3) with a regression coefficient of R^2=0.93, confirming the validation of the quadratic model.

$$DS = -3.2 + 1.69A + 0.48B - 0.2A^2 - 0.05B^2 + 0.1AB \qquad \text{Equation 3}$$

2.2.4 Characterization of cellulose–maleic anhydride

2.2.4.1 Infrared analysis

The occurrence of the esterification is proved by substituting a hydroxyl group in cellulose with a carboxylic group in maleic anhydride. In the present study, FTIR

analysis demonstrated that the esterification was successful. Figure 35 shows the FTIR spectra of three Cell-MA samples with different DS values (0.6, 1.2, and 2.3) as well as the spectra of pure cellulose and pure maleic anhydride. The peaks indicating the presence of cellulose were found at 3443 cm^{-1} (–OH), 2908–2896 cm^{-1} (CH), and 1644–1642 cm^{-1} (C=C). The peaks indicating the presence of maleic anhydride were found at 1716 cm^{-1} (C=O), 1288–1274 cm^{-1} (CH), and 1054 cm^{-1} (CO). These results confirm that the cellulose esterification with maleic anhydride can be performed at different DS values by modifying the cellulose–maleic anhydride molar ratio and catalyst.
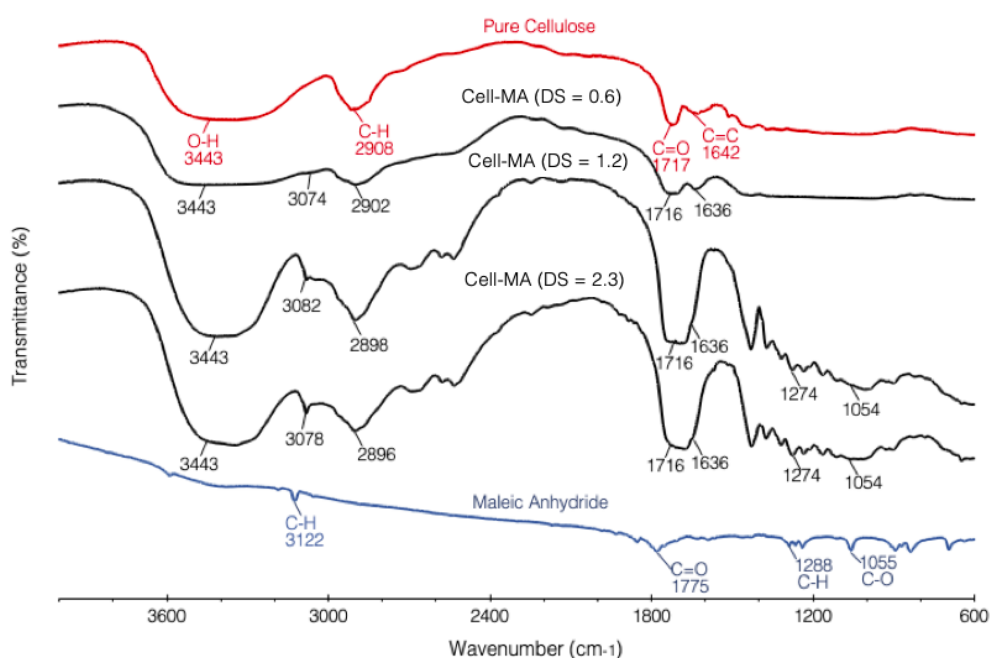
Figure 35: FTIR spectra of pure cellulose, maleic anhydride, and Cell-MA with different DS values

2.2.4.2 X-ray diffraction analysis

Cellulose crystallinity underwent changes during its modification with maleic anhydride; these changes were analyzed using powder XRD. The crystalline nature of the pure cellulose was revealed by the diffractogram, in which the pure cellulose showed peaks at 15.5° and 22.6°, corresponding to the (101) [168] and (002) planes, respectively. After esterification, the peaks shifted to 15.9° and 23.0°, respectively, which increased the d-

spacing; this increase indicated that the ester groups had grafted to the cellulose structure, which might have caused a space change between the cellulose chains while also maintaining the distinctive cellulose peaks. Moreover, the esterification increased the degree of crystallization, resulting in decreased full width at half-maximum (FWHM) values. In the diffractogram, maleic anhydride showed a characteristic peak at 30°, and Cell-MA showed a peak at 29°. Figure 36 presents the XRD patterns of maleic anhydride, pure cellulose, and Cell-MA (DS = 1.2).
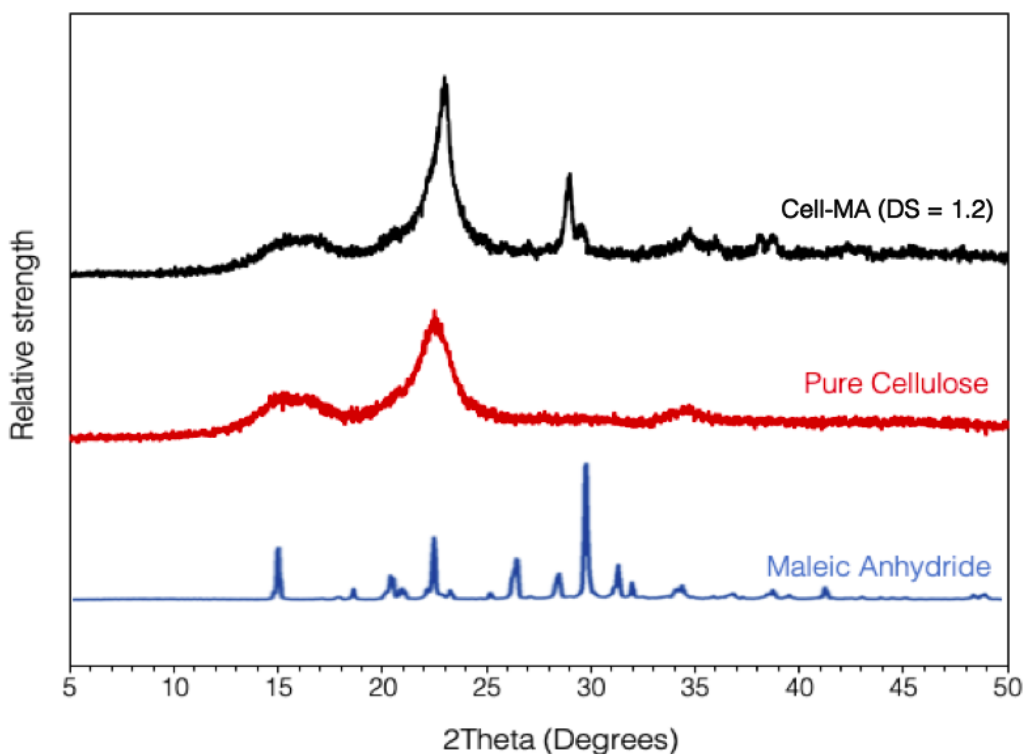
Figure 36: XRD patterns for maleic anhydride, pure cellulose, and Cell-MA (DS = 1.2)

2.2.4.3   Scanning electron microscopy analysis

SEM images (Figure 37) revealed that the pure cellulose particles had an average size of 20 mm and did not substantially change in size after modification. Nevertheless, the morphology of the pure cellulose's surface changed. Before modification, its surface looked smoother than that of Cell-MA (DS = 1.2); Cell-MA's surface had some small,

rough protuberances, which can be attributed to the chemical interaction and grafting of carboxylic groups onto the cellulose.
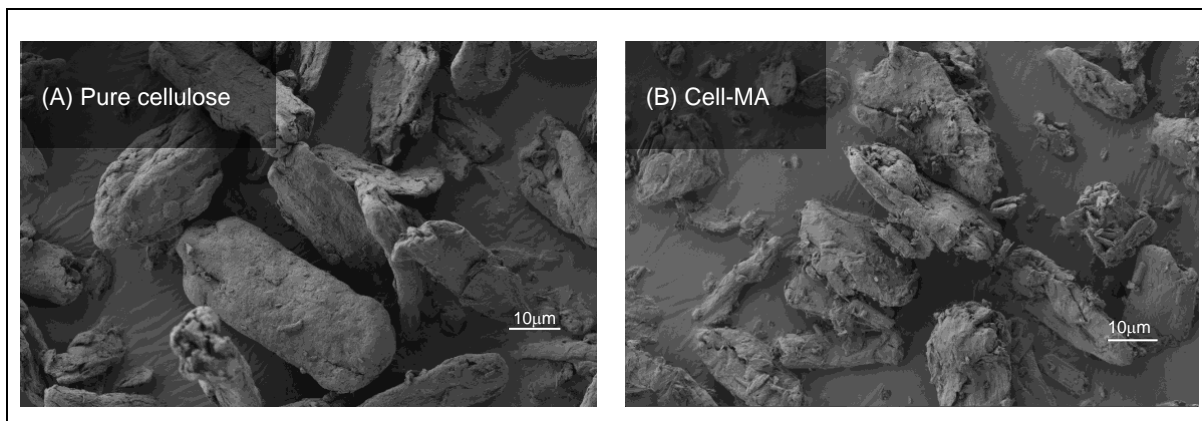
Figure 37: SEM images and size of (A) pure cellulose and (B) Cell-MA (DS = 1.2)

2.2.5 Characterization of crosslinked cellulose with citric acid

The performance of the crosslinked cellulose polymer with citric acid in the presence of SHP was evaluated by measuring the weight of the dry polymer sample after 24 h of soaking in deionized water. The appearance of the cellulose–citric acid hydrogels is shown in Figure 38, which also shows a zoom image of the superior AC sample that corresponds to method D.
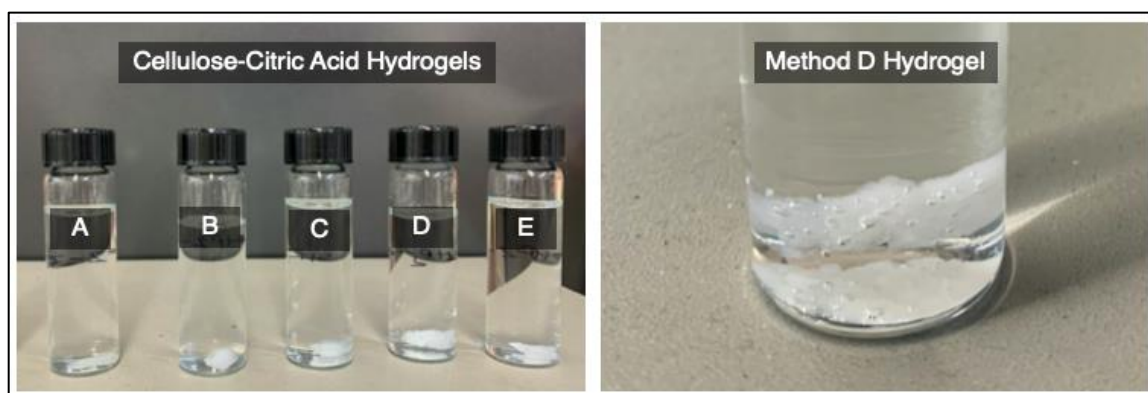
Figure 38: Hydrogels produced with cellulose–citric acid

Thus, after the samples were weighed, the AC calculations were obtained using Equation 1. Figure 39 shows the AC values of the polymers obtained using the different methodologies.
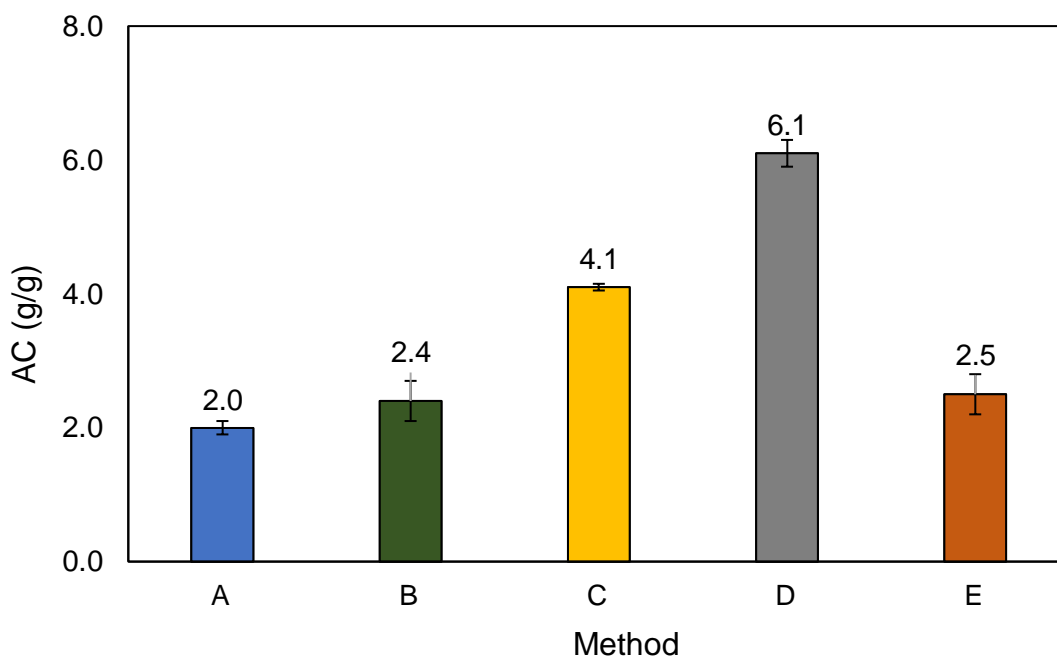
Figure 39: AC of polymers obtained with methods A, B, C, D, and E, using cellulose and citric acid

The information obtained through this evaluation indicated how much water was absorbed by each sample and which of the five methods produced the polymer with the highest AC. The AC of the samples was as follows: $D > C > E > B > A$. The method D sample had the highest AC (6.1 g/g) of all the methods; this means that, in method D, the step in which ethanol was used to wash away the residual crosslinker and SHP gave the water the freest entrance into the polymeric network. The difference between the samples obtained via method D and method C (4.1 g/g) was the presence of the step of heating and stirring for 5 h at 65°C in method D, which proved to be effective in increasing the AC by 2 g/g. The samples obtained using methods E, B, and A were not treated with a wash of ethanol, but they did go through heating and stirring for 5 h at 65°C. Methods E

(2.5 g/g) and B (2.4 g/g) had slightly different results; the only variation in these methods was that method B had a step involving the evaporation of water for 4 h at 60ºC. This step can be easily discarded, as it does not significantly improve the AC of the polymer and represents a waste of energy. Method A produced the lowest AC (2.0 g/g). In method B, the curing step of heating for 1.5 h at 150ºC helped to increase the AC.

2.3 Conclusions

Pure cellulose esterification was more difficult than soluble starch esterification due to pure cellulose's high crystallinity, which makes pure cellulose less reactive than soluble starch. Nonetheless, the use of acetic acid in pure cellulose esterification improved the esterification with maleic anhydride and resulted in a higher yield of grafted ester groups in pure cellulose samples. The DS of esterified pure cellulose was dependent on several variables, including reaction time, cellulose–maleic anhydride molar ratio, and type of catalyst. The DS values were determined via back titration and verified using FTIR spectroscopy. Regarding the citric acid used as an esterification agent, an absorbent polymer was obtained from the crosslinking of citric acid. However, this polymer was not a SAP; by definition, SAPs absorb more than 300 times their own weight. The citric acid absorbent polymer did not reach this level of absorbency. Therefore, it is unsuitable for applications that require a high AC.

Chapter 3

3   Bio-SAP synthesis and the effects of its variables

3.1   Introduction

Superabsorbent polymers (SAP) are three dimensional materials with a hydrophilic network [169]. Such characteristics make them capable of absorbing and retaining aqueous solutions. SAPs can be useful in diverse applications, such as personal care [170], agriculture [30,171], biomedicine [172], drug delivery [3], and removal of heavy metals [173].

The main groups of SAPs are the ones synthesized with acrylic acid and acrylamide [174]. SAPs are produced mainly by polymerization of a partial neutralization of acrylic acid or by suspension polymerization [175]. Additionally, a crosslinker is essential to produce SAPs that keep the polymeric network insoluble [176]. The density and the charge of the crosslinking directly impact the absorption capacity (AC) of SAPs.

Acrylic acid and acrylamide are non-renewable petroleum-based products [20]; their fossil nature makes them low biodegradable when compared to natural SAPs (Bio-SAPs) [177]. Bio-SAPs, such as cellulose-based SAPs, have higher biodegradability and lower toxicity than the majority of synthetic polymers [178].

Cellulose-based SAPs can be obtained using cellulose, synthetic polymers (e.g., polyacrylates and acrylamides [176]), and natural polymers (e.g., carboxyalkyl cellulose [179], chitosan [180], and gum [181]). Nonetheless, the maximum AC of most of the mentioned materials has been reported to be below 300 g/g, which is distant from commercial synthetic SAPs (~300–1000g/g) [177]. In recent studies, cellulose-based SAPs have been prepared using different crosslinking techniques, such as etherification with succinic anhydride [49] and dissolution of carboxymethyl cellulose and hydroxyethyl cellulose [182].

The present work addressed the challenge of increasing the AC of cellulose-based SAPs. Chapter 2 describes a procedure that was developed to esterify pure cellulose using maleic anhydride and acetic acid (Cell-MA) in order to increase cellulose reactivity. The present chapter describes how Cell-MA was solubilized using NaOH and urea to weaken the cellulose intermolecular hydrogen bonds' interactions. Therefore, the Cell-MA was grafted via free radical copolymerization with acrylic acid and crosslinked with polyethylene glycol diacrylate.

This chapter explains how the previously obtained Cell-MA was used to produce Bio-SAPs via free radical graft copolymerization with acrylic acid. RSM with a CCD was used to evaluate the effects of the factors on the AC of Bio-SAPs and to determine the factors' optimal arrangement. Statistical analysis of the experimental data based on the RSM provided an equation model to predict the optimal AC formulation.

3.2   Materials and Methods

3.2.1   Materials

The cellulose used in these experiments required a particular esterification. Therefore, the esterification conditions were determined using the response optimizer function on Minitab®, which provided the statistical analysis of the RSM.

The crosslinker PEGA500 (polyethylene glycol diacrylate, number-average molecular weight = 500 g/mol) was provided by Western Maple BioResources and was used as received. The deionized water used in these experiments was obtained from a deionization unit in the laboratory at the Institute for Chemicals and Fuels from Alternative Resources (ICFAR). Table 9 lists the other chemicals used in these experiments; all chemicals were CAS reagent grade, supplied by Sigma-Aldrich, and used as received.

Table 9: List of chemicals and their purity levels

Chemical	Purity
Sigmacell cellulose	99%

maleic anhydride	99%
zinc chloride	≥ 98%
acetone	99.5%
acetic acid	99.7%
sodium hydroxide	97%
urea	99%
ammonium persulfate	≥ 98%
acrylic acid	99%
ethanol	95%

3.2.2 Methods

3.2.2.1 Statistical analysis of graft copolymerization

The parameters for Bio-SAP synthesis via graft copolymerization of Cell-MA and acrylic acid were optimized to obtain a maximum AC using a modified synthesis methodology from previous research on synthetic and natural SAPs [20,174,178]. The experimental design was developed using the statistical software Minitab®—more specifically, faced centre CCD, a Minitab® tool. The experimental design was used to study five independent factors with their corresponding levels (Table 10). This design comprised a set of experiments that allowed for an evaluation of the factors' effects on the AC of Bio-SAPs. The factors were as follows: A) content of PEGA500, B) content of urea, C) DS of Cell-MA, D) percentage of acrylic acid's degree of neutralization (DON), and E) content of water. There were 54 experiments: 32 factorial points (P1–P32), 10 axial (star) points with an alpha value of 2.366 (P41–P50), and 12 centre points (P33–P40 and P51–P54). Table 11 presents the experimental design of graft copolymerization of Cell-MA and acrylic acid to obtain SAPs.

Table 10: Levels and factors of optimization conditions

Levels	-2.366	-1	0	1	2.366
Factor A: PEGA500 (g)	-0.07(0)	0.20	0.40	0.60	0.87
Factor B: urea (g)	-0.73 (0)	2.00	4.00	6.00	8.73
Factor C: DS	-0.22 (0)	0.60	1.20	1.80	2.61
Factor D: DON (%)	19.51	40.00	55.00	70.00	90.49
Factor E: water (g)	13.17	20.00	25.00	30.00	36.83

Table 11: Experimental design of graft copolymerization of Cell-MA and acrylic acid to obtain SAPs

Experiment ID	Factor A: PEGA500 (g)	Factor B: urea (g)	Factor C: DS	Factor D: DON (%)	Factor E: water (g)
P1	-1	-1	-1	-1	-1
P2	1	-1	-1	-1	-1
P3	-1	1	-1	-1	-1
P4	1	1	-1	-1	-1
P5	-1	-1	1	-1	-1
P6	1	-1	1	-1	-1
P7	-1	1	1	-1	-1
P8	1	1	1	-1	-1
P9	-1	-1	-1	1	-1

P10	1	-1	-1	1	-1
P11	-1	1	-1	1	-1
P12	1	1	-1	1	-1
P13	-1	-1	1	1	-1
P14	1	-1	1	1	-1
P15	-1	1	1	1	-1
P16	1	1	1	1	-1
P17	-1	-1	-1	-1	1
P18	1	-1	-1	-1	1
P19	-1	1	-1	-1	1
P20	1	1	-1	-1	1
P21	-1	-1	1	-1	1
P22	1	-1	1	-1	1
P23	-1	1	1	-1	1
P24	1	1	1	-1	1
P25	-1	-1	-1	1	1
P26	1	-1	-1	1	1
P27	-1	1	-1	1	1
P28	1	1	-1	1	1
P29	-1	-1	1	1	1
P30	1	-1	1	1	1
P31	-1	1	1	1	1
P32	1	1	1	1	1

P33	0	0	0	0	0
P34	0	0	0	0	0
P35	0	0	0	0	0
P36	0	0	0	0	0
P37	0	0	0	0	0
P38	0	0	0	0	0
P39	0	0	0	0	0
P40	0	0	0	0	0
P41	-2.366	0	0	0	0
P42	2.366	0	0	0	0
P43	0	-2.366	0	0	0
P44	0	2.366	0	0	0
P45	0	0	-2.366	0	0
P46	0	0	2.366	0	0
P47	0	0	0	-2.366	0
P48	0	0	0	2.366	0
P49	0	0	0	0	-2.366
P50	0	0	0	0	2.366
P51	0	0	0	0	0
P52	0	0	0	0	0
P53	0	0	0	0	0
P54	0	0	0	0	0

3.2.2.2 Cellulose esterification

Applying the same model that was obtained in Chapter 2 (Equation), Minitab® determined the amounts of maleic anhydride and zinc chloride needed for pure cellulose esterification at specific DS values: 0.6, 1.2, 1.8, and 2.6. The esterification statistic model's predictions had a significance $> 95\%$.

$$\mathbf{DS = -3.2 + 1.69A + 0.48B - 0.2A^2 - 0.05B^2 + 0.1AB} \qquad \textbf{Equation 4}$$

Figure 40 illustrates the Minitab® predictions regarding the amounts of zinc chloride and maleic anhydride needed to prepare the esterified pure cellulose at specific DS values; Table 12 summarizes the same information.
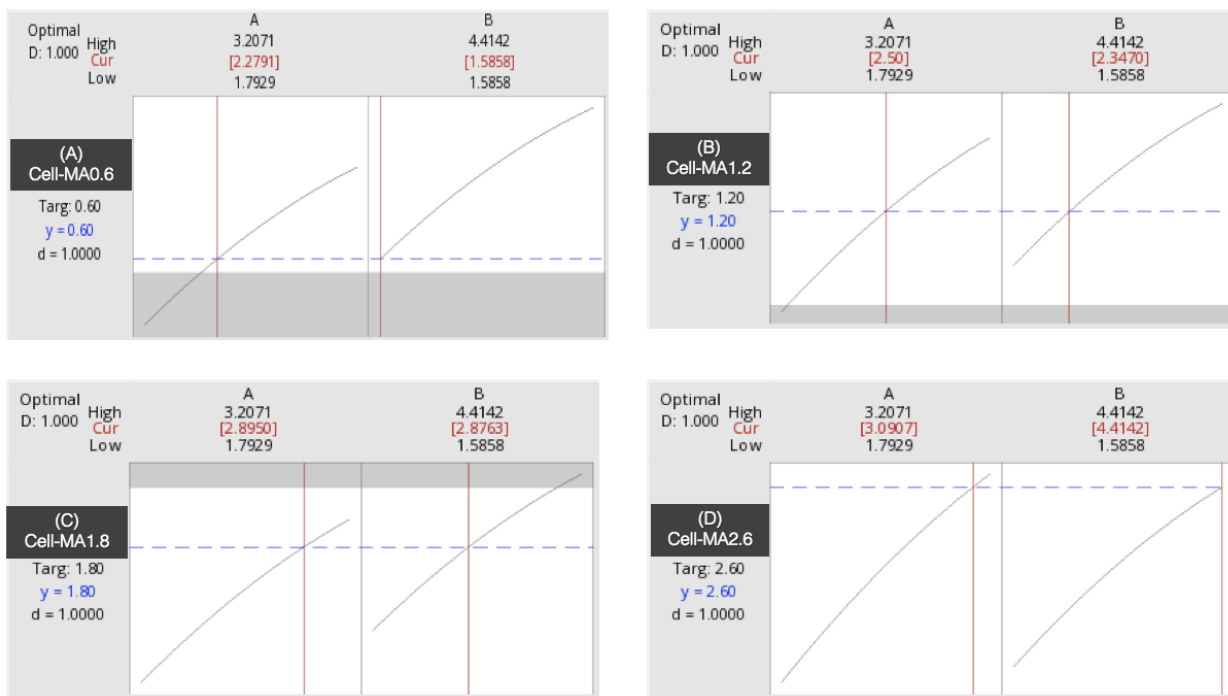
Figure 40: Plots of maleic anhydride and zinc chloride optimization for cellulose esterification targeting DS values of (A) 0.6, (B) 1.2, (C) 1.8, and (D) 2.6, where A = cellulose–maleic anhydride molar ratio and B = zinc chloride (% w of the solids) (optimal values are highlighted in red)

Table 12: Multiple response prediction for optimized cellulose esterification targeting DS values of (A) 0.6, (B) 1.2, (C) 1.8, and (D) 2.6

DS	Cellulose–maleic anhydride molar ratio	Zinc chloride (% w of the solids)
0.6	2.3	1.6
1.2	2.5	2.3
1.8	2.9	2.9
2.6	3.1	4.4

After the optimal reagent amounts were determined, esterification was performed in a 250 mL three-neck flask with the following mixture: 2 g of pure cellulose (pre-dried in a vacuum oven at 60°C for 2 h), maleic anhydride (1:2.3, 1:2.5, 1:2.9, or 1:3.1 cellulose–maleic anhydride molar ratio), 80 g of acetic acid, and zinc chloride (1.6, 2.3, 2.9, or 4.4% w of solids). The mixture was stirred for 5 h at 118°C with a nitrogen purge. After cooling, the resulting solid product was filtered, washed with acetone, and then dried in a vacuum oven for 24 h at 65°C. Figure 41 shows the esterification procedure.
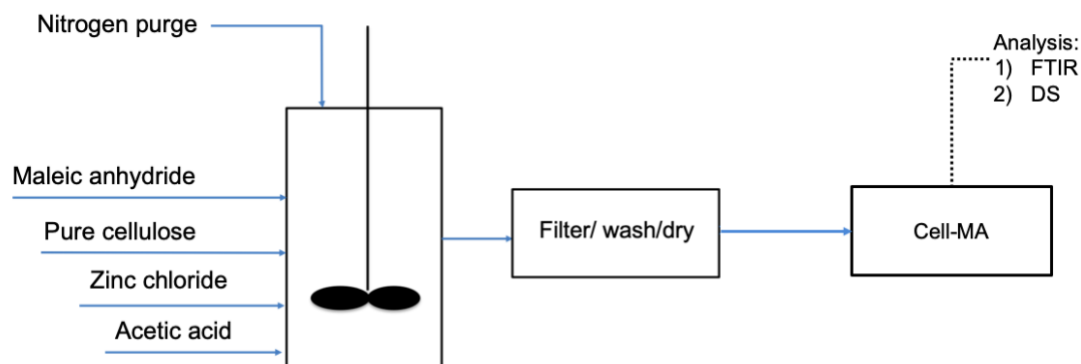
Figure 41: Pure cellulose esterification procedure

3.2.2.2.1   Characterization of Cell-MA

3.2.2.2.2   Degree of substitution of –COOH groups: back titration

The quantity of –COOH groups in the Cell-MA sample was obtained through back titration. Through this method, the –COOH concentration of Cell-MA reacted with NaOH standard solution. Then, the standard solution of HCl was used to titrate the Cell-MA–NaOH standard solution mixture. Ultimately, the DS of –COOH in Cell-MA was calculated using the volume of the HCl standard solution. The procedure is explained in Appendix A.

3.2.2.2.2.1 Infrared spectroscopy

The infrared spectrum of the pure cellulose, maleic anhydride, Cell-MA, and Cellulo-SAP samples was employed to qualitatively characterize the presence of functional groups through FTIR spectroscopy (Frontier FTIR Perkin Elmer). The infrared wavelength was set at 4000–550 cm^{-1} with 4 cm^{-1} resolution. Using KBr methodology, the characteristic spectra of the samples were evaluated. This methodology comprised the mixture of 0.0050 g of a totally dry sample with 0.1500 g of pure KBr (1:30 w/w ratio). Then, the mixture was used to form a transparent pellet under a force of 8 tonnes for 2 min. The resulting pellet was then placed inside the FTIR chamber to be measured.

3.2.2.3   Bio-based gel synthesis

Table 11 shows the experimental preparation conditions of the Bio-SAPs. The 56 samples were prepared with varying amounts (or, in the case of Cell-MA, DS values) of the following reagents: NaOH, urea, Cell-MA, deionized water, and PEGA500. At the beginning of the procedure, the following contents were mixed in a 250 mL flask: NaOH, urea, deionized water, and 2 g of pure cellulose or Cell-MA. The mixture was stirred at room temperature (23°C ± 2°C) for 30 min. Subsequently, 0.09 g of APS was added. Next, 4 g of acrylic acid was added to the mixture as the mixture was stirred; it was added dropwise to maintain a temperature below 60°C. The acrylic acid, which was stirred into the mixture for 10 min, neutralized. Finally, the PEGA500 was added to the

mixture, and the flask was transferred to a hot oil bath at 70°C, where the mixture was stirred until it became a gel. Figure 42 illustrates the entire preparation of the gel.
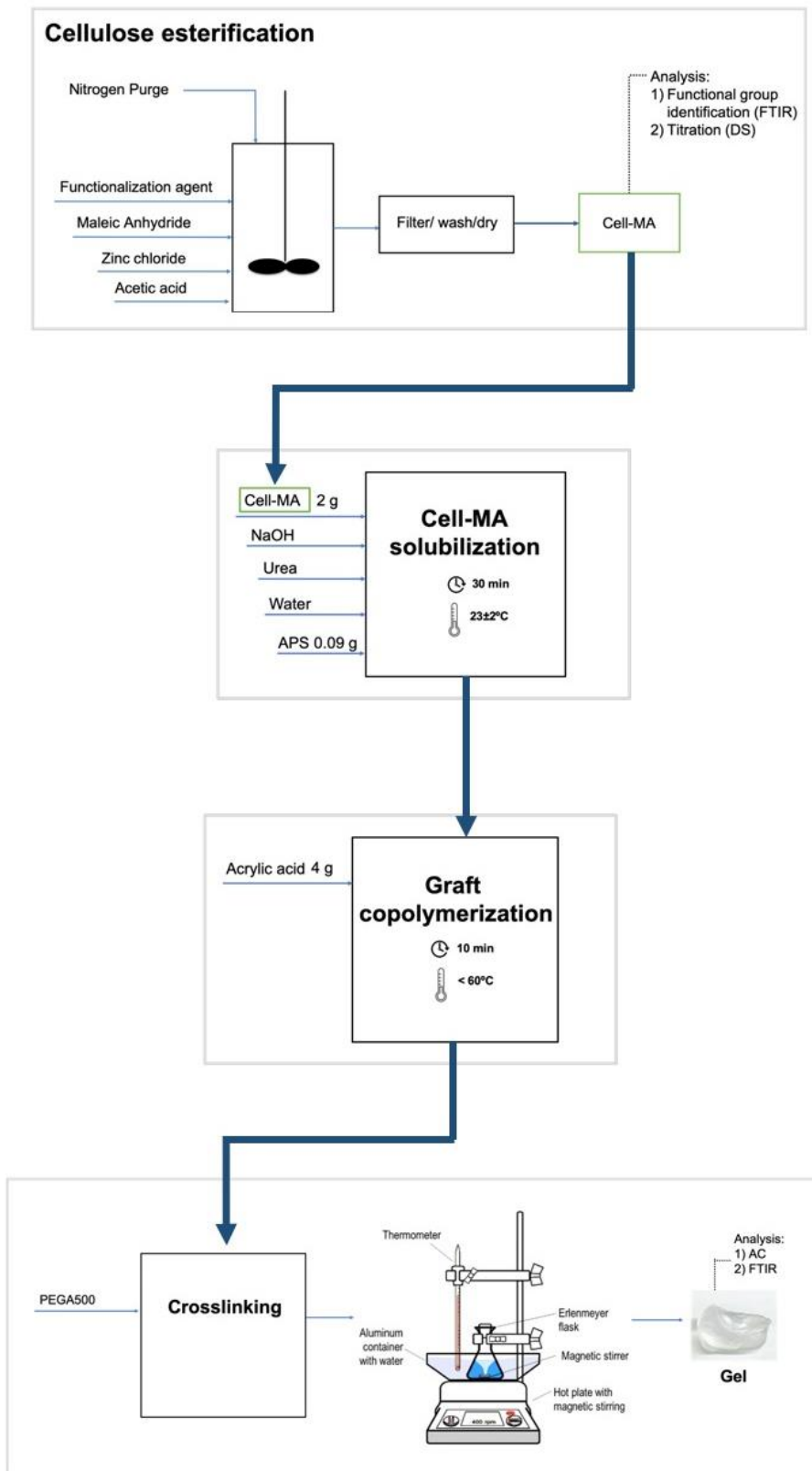
Figure 42: Preparation of the gel

3.2.2.4 Preparation of the SAP after synthesis

Following the reaction, the resultant gel was washed to remove non-reacted compounds and then dried. The washing process involved the following. The gel was transferred to a 250 mL flask containing 200 mL of 75% v/v ethanol aqueous solution and left to soak for 12 h. Then, the gel was removed from the solution and transferred to a second 250 mL flask with 200 mL of fresh 75% v/v ethanol aqueous solution and left to soak for 5 h. This process was replicated: the gel was removed from the solution and transferred to a third 250 mL flask with 200 mL of fresh 75% v/v volume ethanol aqueous solution and left to soak for 5 h. Subsequently, the gel was removed from the solution and cut into small pieces. Then, it was transferred to a flask to soak in anhydrous ethanol for 2 h. After that, the anhydrous ethanol was drained and replaced, and the gel was left to soak for another 2 h. Finally, the gel was filtered and then dried in a vacuum oven for 24 h. The SAP—which is the appropriate term for the gel in its washed and dried state—was ground and sieved to obtain an average particle size of 2 mm through a No. 10 standard sieve mesh (ASTM 11 standard sieve).

3.2.2.5 Characterization of SAPs

3.2.2.5.1 Absorption capacity of Bio-SAPs

Throughout this dissertation, AC is expressed as a weight fraction (g/g) and is used when discussing swelling behaviour in different types of solutions. It was calculated using a standard gravimetric methodology [183].

In these experiments, SAP samples were carefully dried, ground, and sieved through a No. 10 standard sieve mesh (ASTM 11 standard sieve) to obtain an average particle size of 2 mm. Then, 0.05 g ($\pm$ 0.001 g) SAP samples were soaked for 24 h in 200 mL of deionized water at room temperature (23°C $\pm$ 2°C). After this time had passed, the obtained hydrogels were then removed from the solutions and filtered. Additionally, the non-absorbed solution remaining in the hydrogel was removed using dry tissues. Finally, the hydrogel's weight was measured using the following equation:

$$AC = \frac{w_2 - w_1}{w_1} \quad \textbf{Equation 1}$$

where w_1 is the weight of the dry SAP samples and w_2 is the weight of the hydrogel. The procedure to calculate AC was performed in triplicate.

3.2.2.6 Scanning electron microscopy

Images of Cellulo-SAP were taken with a Zeiss/Leo 1530 FESEM (3 kV accelerating voltage). Before obtaining the image, the samples were treated with 10 nm of osmium to evade charging and increase their conductivity.

3.3 Results and discussion

3.3.1.1.1 Degree of substitution of –COOH groups: back titration

The quantity of –COOH groups grafted to the AGU of cellulose was verified by performing back titration (see Appendix A) on the Cell-MA samples. Each level of esterification was repeated three times to determine the average concentration of the carboxylic groups attached to the cellulose. The Cell-MA samples were mixed with ~0.100 M NaOH standard solution in the presence of phenolphthalein. Then, the solution was titrated with ~0.100 M HCl standard solution until the mixture became colourless, at which point the total volume of wasted HCl was recorded. The average moles of HCl was calculated, and the volume of HCl used to titrate the Cell-MA–NaOH was used to calculate the DS. Table 13 shows the DS results.

Table 13: DS values of Cell-MA samples

DS target	DS determined with back titration after esterification reaction
0.6	0.6 ± 0.090
1.2	1.2 ± 0.057
1.8	1.8 ± 0.012
2.4	2.4 ± 0.045

3.3.2   Infrared spectroscopy of Cell-MA

Pure cellulose, maleic anhydride, and Cell-MA samples were characterized by FTIR spectroscopy to verify the correct substitution of carboxylic groups; Figure 43 shows the FTIR spectra. In Cell-MA samples, the strong IR absorption at 1717 cm^{-1} can be attributed to the C=O stretch, which is the characteristic IR absorption of the substituted functional group [165]. The peak at 1642 cm^{-1} corresponds to the C=C stretch, which was introduced by adding the esterification agent [166]. The presence of these two IR peaks proves the successful esterification of the pure cellulose. The IR absorption peak at 3343 cm^{-1} is ascribed to the –OH stretch. At 2908 cm^{-1}, the stretching and deformation vibrations of the CH group are FTIR fingerprint peaks of cellulose in the glucose unit [167].
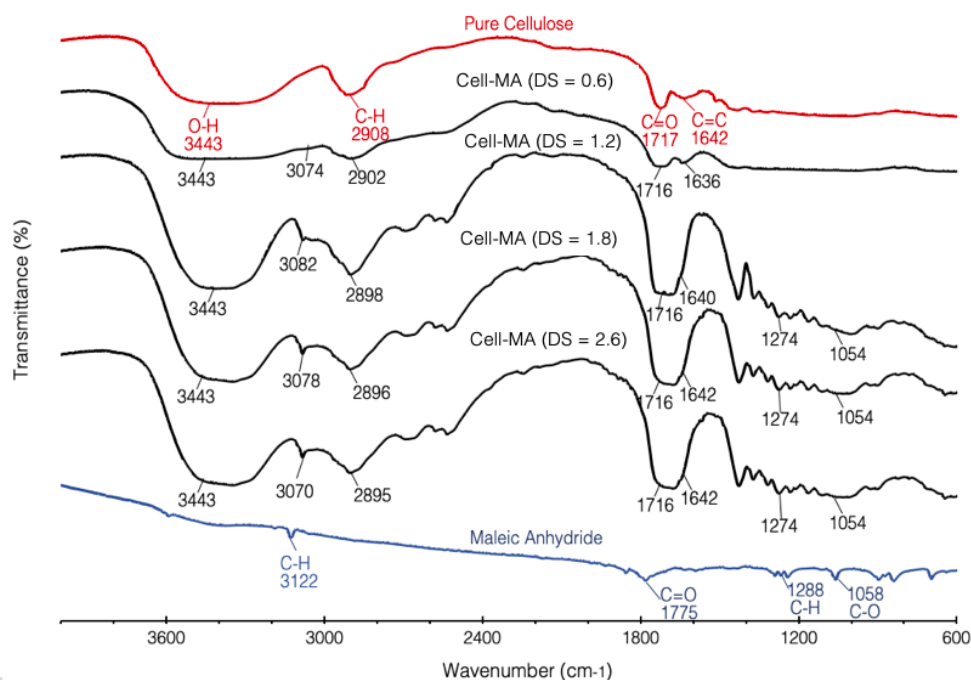
Figure 43: FTIR spectra of Cell-MA samples and their pure components, cellulose and maleic anhydride

3.3.3 Acrylic acid partial neutralization with Cell-MA–NaOH–urea–water solution

Carboxylic acid esterification was used to modify the chemical structure of cellulose. The resultant cellulose (i.e., Cell-MA) was insoluble. Therefore, before graft copolymerization, Cell-MA was solubilized in a NaOH–urea–water solution. In this solution, Cell-MA decreased in crystallinity, thereby becoming more reactive and, thus, more effective in graft copolymerization with acrylic acid.

After Cell-MA solubilization, acrylic acid was added dropwise to the Cell-MA solution while the solution was stirred. The chemical interaction between the Cell-MA–NaOH–urea solution and the acrylic acid produced an exothermic acid-base reaction with a partial neutralization of the acrylic acid. The acrylic acid was added slowly to keep the temperature below 60°C and avoid polymerization of the acrylic acid.

When the first few drops of acrylic acid were added, a coagulation formed in the mixture and developed into a weak gel. This gel stage is called micro-phase separation, and it occurred due to a separation of Cell-MA from NaOH as a result of the diffusion between the acrylic acid and the Cell-MA–NaOH–urea–water solution. The gel looked opaque, but this appearance changed when more acrylic acid was added. Then, the mixture became more homogeneous, and the gel turned from opaque to transparent while decreasing in thickness until the mixture became a solution. Figure 44 shows the neutralization between acrylic acid and NaOH, which produced sodium acrylate.
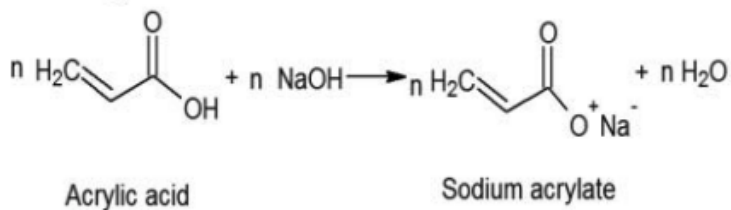
Figure 44: Neutralization between acrylic acid and NaOH, resulting in sodium acrylate

In the present study, a partial neutralization of the acrylic acid was desired, meaning that some acrylic acid was not converted into sodium acrylate. Hence, 25–70% neutralization was selected based on a previous study [114] in which the sensitivity of a polymerization solution's pH was evaluated; in this study, the pH level was controlled by increasing or decreasing the degree of neutralization (DON) of acrylic acid. In a neutralization reaction, increasing the amount of NaOH results in an increase in DON, molecular weight, and sodium acrylate production; simultaneously, in SAP synthesis, the SAP decreases in hydrophobicity and increases in AC. Conversely, decreasing the amount of NaOH results in a decrease in DON, molecular weight, and sodium acrylate production; simultaneously, in SAP synthesis, the SAP increases in hydrophobicity and decreases in AC.

In the above-mentioned study, the neutralization was performed by adding a NaOH solution to an acrylic acid solution. In the present study, the reagents were added in a different order: the acrylic acid was added to the Cell-MA–NaOH–urea–water solution. When the reagents were added in this order, the Cell–MA did not separate from the NaOH–urea–water solution. It was important to maintain the solubility of the Cell-MA and, thus, maintain a homogeneous mixture until the Cell-MA underwent graft copolymerization and crosslinking.

3.3.4   Bio-SAP synthesis

Figure 45 illustrates the chemical process of Bio-SAP synthesis. The Bio-SAP synthesis was performed after partial neutralization of the Cell-MA–NaOH–urea–water solution using acrylic acid. The graft copolymerization began when the temperature reached 70°C. In this temperature range, the APS decomposed into sulphate radical species that interacted with the –OH groups of the Cell-MA and, simultaneously, formed a radical in the C=C bond of sodium acrylate and acrylic acid monomers [184].

It is likely that after the radicals' formation, sodium acrylate and acrylic acid monomers were grafted onto the cellulose backbone. This led to the propagation phase, which involved the adjunction of many monomer units to form a macromolecule. This process was enhanced by the high temperature (70°C), which increased the molecular movement

of the monomers in the solution. At this point, graft copolymers of Cell-MA-g-poly(sodium acrylate) and Cell-MA-g-poly(acrylate) macromers were formed. Subsequently, these graft copolymers crosslinked with PEGA500 when it was added to the mixture. PEGA500 formed a bond between the –COOH units, resulting in a three-dimensional gel.
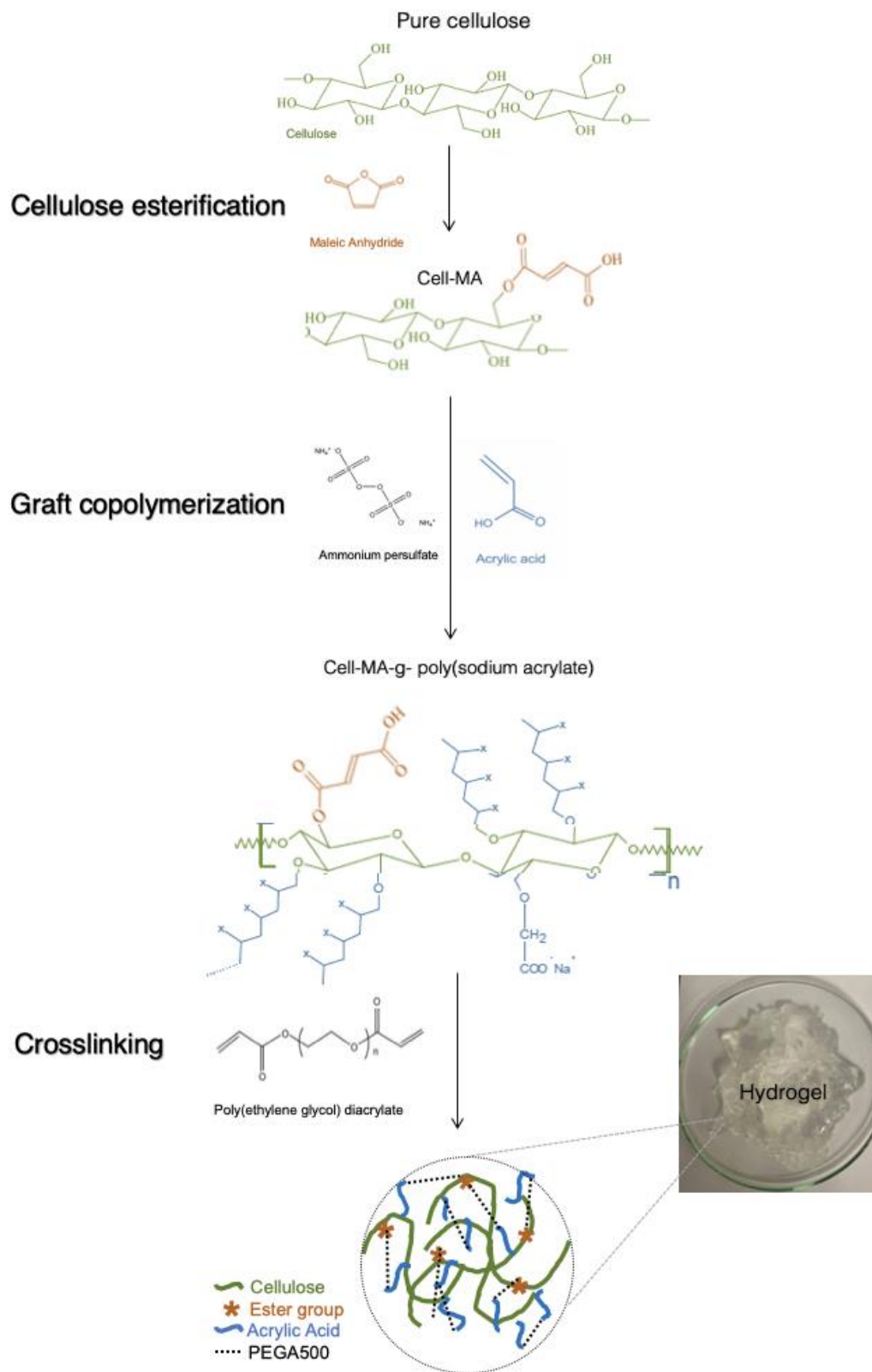
Figure 45: Chemical process of Bio-SAP synthesis

3.3.5   Statistical analysis

The statistical analysis was performed using the RSM in Minitab®, which provided an
equation with an optimal formulation for obtaining Cellulo-SAP. Using a faced centre
CCD, an experimental design was implemented to evaluate which factors were most
significant in increasing the AC of Bio-SAP samples (calculated with Equation 1). Five
factors were evaluated with the following variations: A) PEGA500 (0, 0.2, 0.4, 0.6, and
0.9 g), B) urea (0, 2, 4, 6, and 8.7 g), C) DS (0, 0.6, 1.2, 1.8, and 2.6), D) DON (19.5, 40,
55, 70, and 90.5%), and E) water (13.2, 20, 25, 30, and 36.8). Table 14 summarizes these
factors along with the software-generated experimental arrangement and the AC response
data.

Table 14: Experimental design and AC response of Bio-SAPs

Experiment ID	Factor A: PEGA500 (g)	Factor B: Urea (g)	Factor C: DS	Factor D: DON (%)	Factor E: Water (g)	Response: AC (g/g)
P1	0.2	2	0.6	40	20	**AC**
P2	0.6	2	0.6	40	20	170
P3	0.2	6	0.6	40	20	50
P4	0.6	6	0.6	40	20	495
P5	0.2	2	1.8	40	20	170
P6	0.6	2	1.8	40	20	117
P7	0.2	6	1.8	40	20	134
P8	0.6	6	1.8	40	20	200
P9	0.2	2	0.6	70	20	400
P10	0.6	2	0.6	70	20	0
P11	0.2	6	0.6	70	20	0
P12	0.6	6	0.6	70	20	0

P13	0.2	2	1.8	70	20	0
P14	0.6	2	1.8	70	20	0
P15	0.2	6	1.8	70	20	0
P16	0.6	6	1.8	70	20	0
P17	0.2	2	0.6	40	30	0
P18	0.6	2	0.6	40	30	120
P19	0.2	6	0.6	40	30	94
P20	0.6	6	0.6	40	30	435
P21	0.2	2	1.8	40	30	302
P22	0.6	2	1.8	40	30	150
P23	0.2	6	1.8	40	30	180
P24	0.6	6	1.8	40	30	400
P25	0.2	2	0.6	70	30	307
P26	0.6	2	0.6	70	30	0
P27	0.2	6	0.6	70	30	0
P28	0.6	6	0.6	70	30	0
P29	0.2	2	1.8	70	30	0
P30	0.6	2	1.8	70	30	0
P31	0.2	6	1.8	70	30	0
P32	0.6	6	1.8	70	30	0
P33	0.4	4	1.2	55	25	400
P34	0.4	4	1.2	55	25	405
P35	0.4	4	1.2	55	25	408

P36	0.4	4	1.2	55	25	405
P37	0.4	4	1.2	55	25	404
P38	0.4	4	1.2	55	25	398
P39	0.4	4	1.2	55	25	402
P40	0.4	4	1.2	55	25	396
P41	-0.0732 (0)	4	1.2	55	25	0
P42	0.8732	4	1.2	55	25	0
P43	0.4	-0.732 (0)	1.2	55	25	120
P44	0.4	8.732	1.2	55	25	180
P45	0.4	4	-0.2196 (0)	55	25	19
P46	0.4	4	2.6196	55	25	40
P47	0.4	4	1.2	19.51	25	180
P48	0.4	4	1.2	90.49	25	160
P49	0.4	4	1.2	55	13.17	0
P50	0.4	4	1.2	55	36.83	180
P51	0.4	4	1.2	55	25	400
P52	0.4	4	1.2	55	25	400
P53	0.4	4	1.2	55	25	405
P54	0.4	4	1.2	55	25	403

ANOVA revealed that the "Prob > F" values for the linear and square model were < 0.0001, which means that their response variables were significant (Table 15). The p-value of the main effects of urea and DON was < 0.05, showing the most statistically significant result of any pairing. The interactions between urea and water had a p-value < 0.05, which implied a substantial effect.

Table 15: ANOVA for the response surface model of Bio-SAP synthesis

Source of variance	Sum of squares	Degrees of freedom	Mean square	F-value	p-value Prob > F
Linear Model	431611	5	86322	12.19	0.0001
Factor A: PEGA500 (g)	639	1	639	0.09	0.7660
Factor B: Urea (g)	37229	1	37229	5.26	0.0290
Factor C: DS	3400	1	3400	0.48	0.4930
Factor D: DON (%)	389643	1	389643	55.03	0.0001
Factor E: Water (g)	700	1	700	0.10	0.755
Square Model	815509	5	163102	23.04	0.0001
A^2	227123	1	227123	32.08	0.0001
B^2	189394	1	189394	26.75	0.0001
C^2	166143	1	166143	23.46	0.0001
D^2	201590	1	201590	28.47	0.0001
E^2	189394	1	189394	26.75	0.0001
AB	120645	10	12065	1.70	0.1234
AC	1984	1	1984	0.28	0.6002
AD	17955	1	17955	2.54	0.1211
AE	6328	1	6328	0.89	0.3524
BC	1	1	1	0.00	0.9906
BD	1830	1	1830	0.26	0.6153

BE	89676	1	89676	12.67	0.0010
CD	351	1	351	0.05	0.8259
CE	84	1	84	0.01	0.9141
DE	450	1	450	0.06	0.803
Lack of fit	226402	22	10291	591.44	0.000
Error	226576	32	7081		
Total	1594405	53			

The acceptability of the quadratic model, which was obtained from the ANOVA sequential model, was verified via regression analysis. In addition, the constant values of the factors' interactions provided an empirical second-order polynomial equation (Equation 4) with a regression coefficient of $R^2 = 0.89$, validating the quadratic model.

$$\mathbf{AC} = -2507 + 795A + 231.6B + 292C + 30.12D + 114.8E - 1543A^2 - 14.09B^2 - 146.6C^2 - 0.2584D^2 - 2.254E^2 - 19.7\,AB + 197AC + 4.69AD + 0.2AE - 6.3BC - 1.765BD + 0.33BE - 0.18CD + 1.25CE - 0.105DE$$

Equation 4

The five factors and their interactions affected the AC responses of the Bio-SAPs (Figure 46). More importantly, DON had the most significant effect compared to the other factors and interactions. During the performance of the experiment to obtain the Bio-SAPs, it was observed that the DON percentage affected gel formation. Samples prepared with a DON of 70% or higher did not form a gel. Those prepared with a DON of 30% or lower formed a gel, but the gel had a low AC. Finally, those with a DON of 40% formed a gel with a high AC.

Urea was the second most significant factor in terms of the Bio-SAPs' AC. The samples' AC results showed that the presence of urea enhanced AC without affecting gel formation. DS was the third most significant factor regarding Bio-SAPs' AC. The Bio-

SAPs obtained using Cell-MA increased in their AC compared with those Bio-SAPs obtained using pure cellulose.

PEGA500 was the fourth most significant factor. The Bio-SAPs with high PEGA500 content (high crosslinking density) had low AC, whereas the Bio-SAPs with low PEGA500 content had high AC. However, the absence of PEGA500 in the formulation prevented the formation of a gel.

Water was the fifth most significant factor in terms of the Bio-SAPs' AC. An increase in the amount of water reduced the mechanical strength and increased the solubility of the resultant hydrogel. During the Bio-SAP synthesis of samples with high water content—more than 30 g—many water molecules were trapped in the three-dimensional network, creating more space between crosslinking bonds. Consequently, the gel yield decreased, and the hydrogel had high AC, low mechanical strength, and high solubility. In contrast, in samples with low water content—less than 20 g—fewer water molecules were trapped in the three-dimensional network; therefore, these samples had higher structural strength due to the reduction of space between crosslinking bonds. This resulted in an increased gel yield, and the hydrogel had low AC, high mechanical strength, and low solubility.

Figure 46 shows the Pareto chart of the interactions between the five factors that affected the Bio-SAPs' AC. The bar lengths of each term in the chart are proportional to the absolute values of the estimated effects, with a confidence level of 95%. In the chart, the red line is the Bonferroni line, which shows a statistical significance effect magnitude of 2.037. The bars that cross this line represent significant effects. DON and urea significantly affected AC: DON had a standardized value of 7.4, and urea had a standardized value of 2.24.
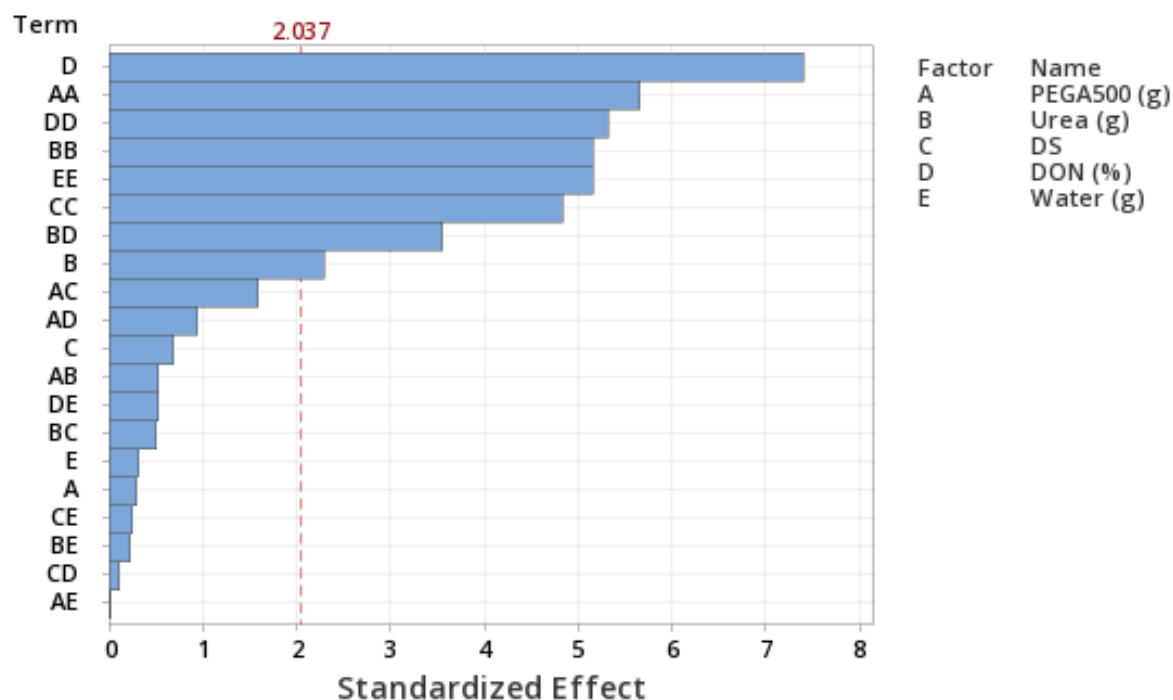
Figure 46: Pareto chart of the factors' standardized effects on AC ($\alpha = 0.05$)

3.3.5.1 Optimization for maximum AC

Using the experimental data, Minitab® revealed the optimal formulation through its optimization tool, targeting the maximum Bio-SAP AC. The Bio-SAP obtained via the optimal formulation, which had an AC of 475 g/g, was called "Cellulo-SAP." Figure 47 illustrates Minitab®'s Cellulo-SAP formulation, which is as follows: 0.87 g of PEGA500, 8.73 g of urea, Cell-MA (DS = 2.62), 90.49% DON, and 36.83 g of water.

 summarizes the same information.
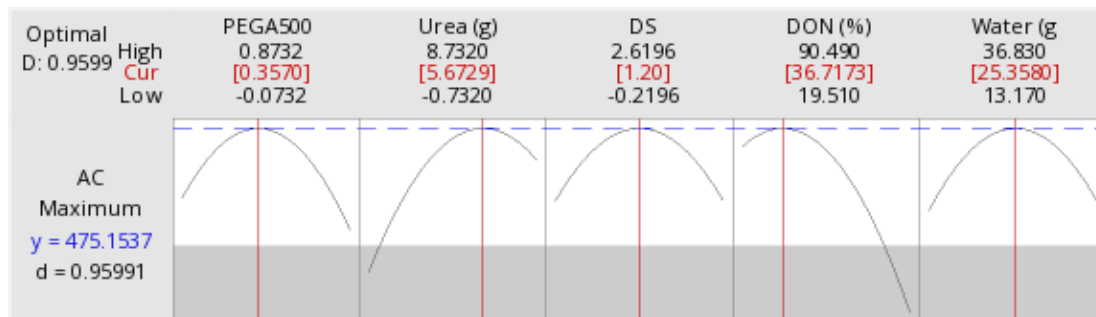
Figure 47: Minitab®'s Cellulo-SAP formulation (optimal parameters are highlighted in red)

Table 16: Cellulo-SAP formulation

Variable	Setting
PEGA500 (g)	0.4
Urea (g)	5.7
DS	1.2
DON (%)	36.7% (1.22g NaOH)
Water (g)	25.4
Response	
AC (g/g)	475.2

3.3.6   Effects of factors on Bio-SAPs' AC

As shown in Table 14, several Bio-SAPs were obtained using the same formulation (hereafter called "PA"). Samples P33–40 and P51–54 were obtained using PA: 0.4 g of PEGA500, 4 g of urea, Cell-MA (DS = 1.2), 55% DON, and 25 g of water. These Bio-SAP samples had an average AC of 400 g/g. The average AC of this formulation corresponded to the 12 centre points of the CCD (P33–40 and P51–54).

3.3.6.1 Effects of PEGA500

The crosslinking effects of PEGA500 on the Bio-SAPs were analyzed using the AC values of the following samples: P41 (0 g of PEGA500), PA (0.4 g of PEGA500), and P42 (0.87 g of PEGA500). These samples represented the different concentration levels of PEGA500 (Figure 48A) while maintaining the other four factors as follows: 4 g of urea, Cell-MA (DS = 1.2), 55% DON, and 25 g of water. P41, with zero PEGA500, did not show gel formation, whereas PA, prepared with 0.4 g of PEGA500, formed a gel whose corresponding Bio-SAP had an AC of 400 g/g. P42, prepared with 0.87 g of PEGA500, formed a weak and soluble gel. By comparing these three samples, it was observed that the amount of crosslinking determined gel formation.

PEGA500 consists of a long molecule chain with attached hydroxyl groups and a hydrophobic surface; these characteristics enhanced the solubility of Cell-MA [119]. The addition of PEGA500 in low concentrations did not provide enough crosslinker molecules to crosslink the copolymeric chains; therefore, the three-dimensional structure was not developed, and the gel was not formed. In contrast, in P42—which had a relatively high PEGA500 concentration—a non-uniform crosslinking density and a variable chain length between crosslinked molecules were produced. These crosslinking irregularities resulted in a soluble gel with low mechanical strength. In addition to gel formation, the amount of PEGA500 governed the relationship between the crosslinking density, AC, and mechanical properties of the Bio-SAP. PEGA500 played a vital role; it prevented the solubilization of Bio-SAPs by restricting the network's enlargement capacity, which increased the hydrogel's mechanical strength. As predicted by the optimization model, the optimal amount of PEGA500 was 0.4 g.
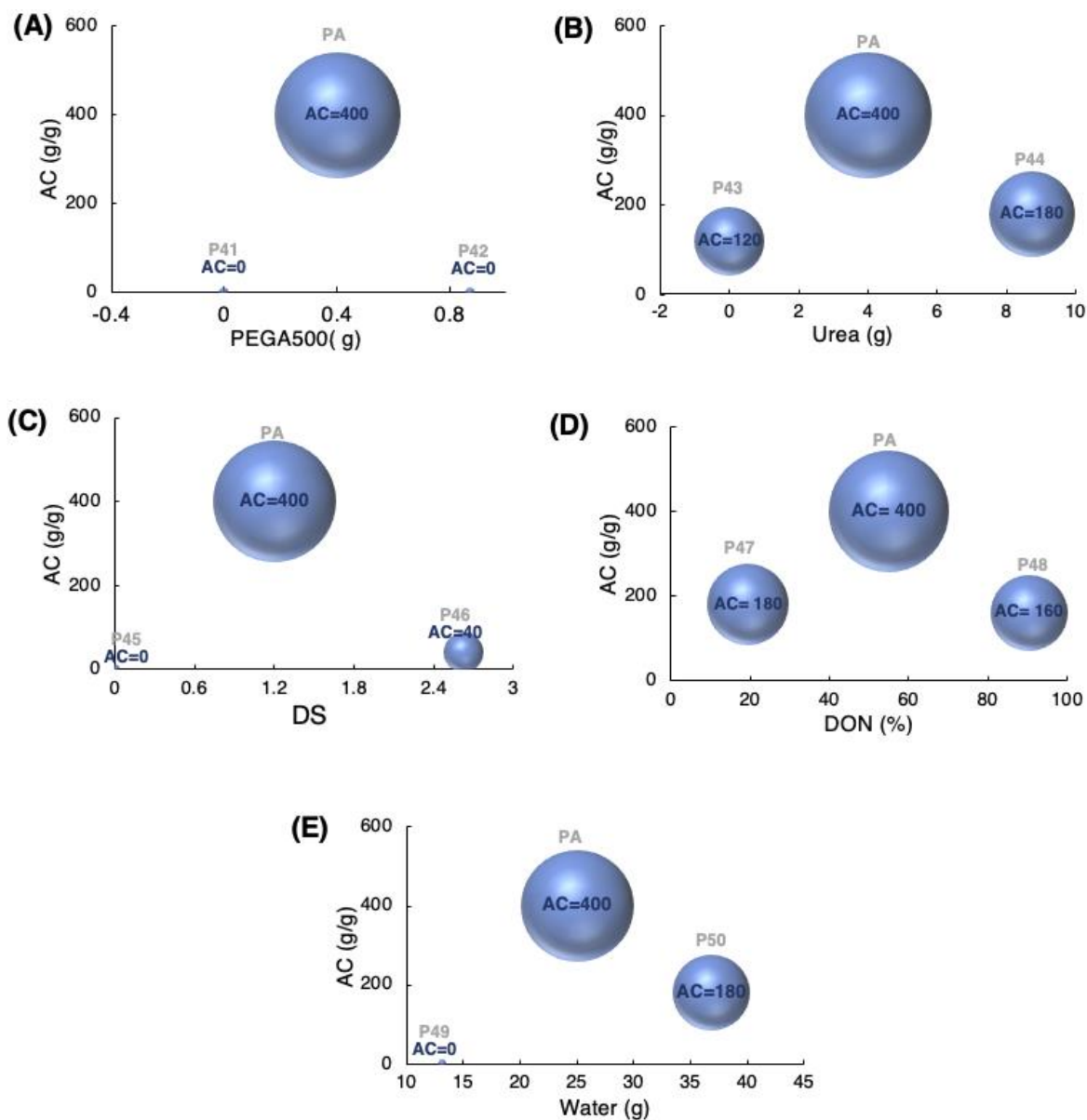
Figure 48: Effects of factors on Bio-SAPs' AC

3.3.6.2 Effects of urea

The effects of urea on the Bio-SAPs were analyzed using the AC values of the following samples: P43 (0 g of urea), PA (4 g of urea), and P44 (8.7 g of urea). These samples represented the different concentration levels of urea (Figure 48B) while maintaining the other four factors as follows: 0.4 g of PEGA500, Cell-MA (DS = 1.2), 55% DON, and 25 g of water. The three samples formed gels that were converted into Bio-SAPs. P43,

prepared with zero urea, had an AC of 120 g/g; this was less than half the AC of PA (400 g/g), prepared with 4 g of urea. P44, prepared with 8.7 g of urea, had an AC of 180 g/g. A comparison between PA and P44 showed that the increase from 4 to 8.7 g of urea reduced AC. A comparison between P43 and P44 showed that the addition of 8.7 g of urea increased AC from 120 to 180 g/g. As predicted by the optimization model, the optimal amount of urea was 5.7 g.

The degree of solubilization of Cell-MA caused by the addition of urea to the NaOH–water solution was directly related to the efficiency of the graft copolymerization and crosslinking synthesis of the Bio-SAPs; therefore, the Bio-SAPs' AC was expected to increase with the addition of urea. In a previous study, urea—in combination with non-cellulosic bio-based monomers—was used to increase Bio-SAPs' AC [161].

Urea's amphiphilic property allowed it to accumulate in Cell-MA's hydrophobic regions, thereby preventing these regions from being exposed to the NaOH–water solution [185]. Furthermore, the presence of urea allowed Cell-MA's hydroxyl groups to form hydrogen bonds with the NaOH–water solution. This occurred because the hydrogen bond interaction between water and Cell-MA's hydroxyl groups was stronger than the interaction between Cell-MA and urea. Urea prevented Cell-MA aggregation, acting as a stabilizer rather than a direct solubilizer of Cell-MA. Therefore, urea was a key factor in ensuring that Cell-MA remained soluble during Bio-SAP synthesis.

3.3.6.3 Effects of degree of substitution

The effects of Cell-MA's DS on the Bio-SAPs were analyzed using the AC values of the following samples: P45 (2 g of pure cellulose, DS = 0), PA (2 g of Cell-MA, DS = 1.2), and P46 (2 g of Cell-MA, DS = 2.6). These samples represented the different concentration levels of Cell-MA's DS (Figure 48C) while maintaining the other four factors as follows: 0.4 g of PEGA500, 4 g of urea, 55% DON, and 25 g of water. The three samples formed gels that were converted into Bio-SAPs. P45, which contained pure cellulose without esterification, had an AC of 19 g/g. The samples prepared with esterified cellulose had higher AC: the AC of PA (400 g/g) and P46 (40 g/g) were approximately 20 and two times higher than the AC of P45, respectively. These results

prove that the esterification of pure cellulose with maleic anhydride increased Bio-SAPs' AC.

Normally, when cellulose molecules are in proximity, interchain hydrogen bonds cause slippage movements [186]. However, in Cell-MA, due to the substitution of –COOH groups for –OH groups, the cellulose molecules did not slip and, therefore, did not form hydrogen bonds. This lack of hydrogen bonds reduced the mechanical deformation of Cell-MA. In the textile industry, such a low level of deformation in esterified cellulosic materials—known as "wrinkle recovery"—has been shown to enhance water retention when applied to clothes [187]. Low mechanical deformation and the associated high water retention are desirable in SAPs; these properties enhance a SAP's reusability and its mechanical resistance during absorption–desorption cycles.

In addition to the Bio-SAPs, the hydrogels (hydrated Bio-SAPs) were evaluated; 0.05 g portions of P45, PA, and P46 were placed in deionized water, and after 24 h, the resultant hydrogels were removed. Due to the different levels of cellulose esterification, the physical differences between the three hydrogels were notable. The PA and P46 hydrogels (obtained using Cell-MA) were opaquer than the P45 hydrogel (obtained with pure cellulose), which looked transparent. Figure 49 shows photographs of the three hydrogels.

The P45 hydrogel (Figure 49A) was more soluble and mechanically weaker than the PA (Figure 49B) and P46 (Figure 49C) hydrogels. This difference can be explained by the P45 hydrogel's lack of –COOH groups grafted in the cellulose chain; due to this lack, the P45 hydrogel had few crosslinking bonds, resulting in a low AC.

The PA hydrogel, prepared with Cell-MA (DS = 1.2), exhibited insolubility and a high AC, proving that the –COOH groups can increase the cellulose hydrophilic capacity within a hydrogel and, consequently, enhance that hydrogel's mechanical strength. In the P46 hydrogel, prepared with Cell-MA (DS = 2.6), the number of –COOH groups was higher than in the PA hydrogel. Compared to the PA hydrogel, the P46 hydrogel showed higher solubility, a lower AC, and less mechanical strength. These results indicate that there could be an excess of –COOH groups [188] in the P46 hydrogel, which, due to

these groups' affinity with water, allowed an excess of water to enter the network. A high number of water molecules inside the network made the network expand and weakened the crosslinks; consequently, the crosslinks failed to trap a large number of water molecules, leading to the solubilization of the hydrogel.
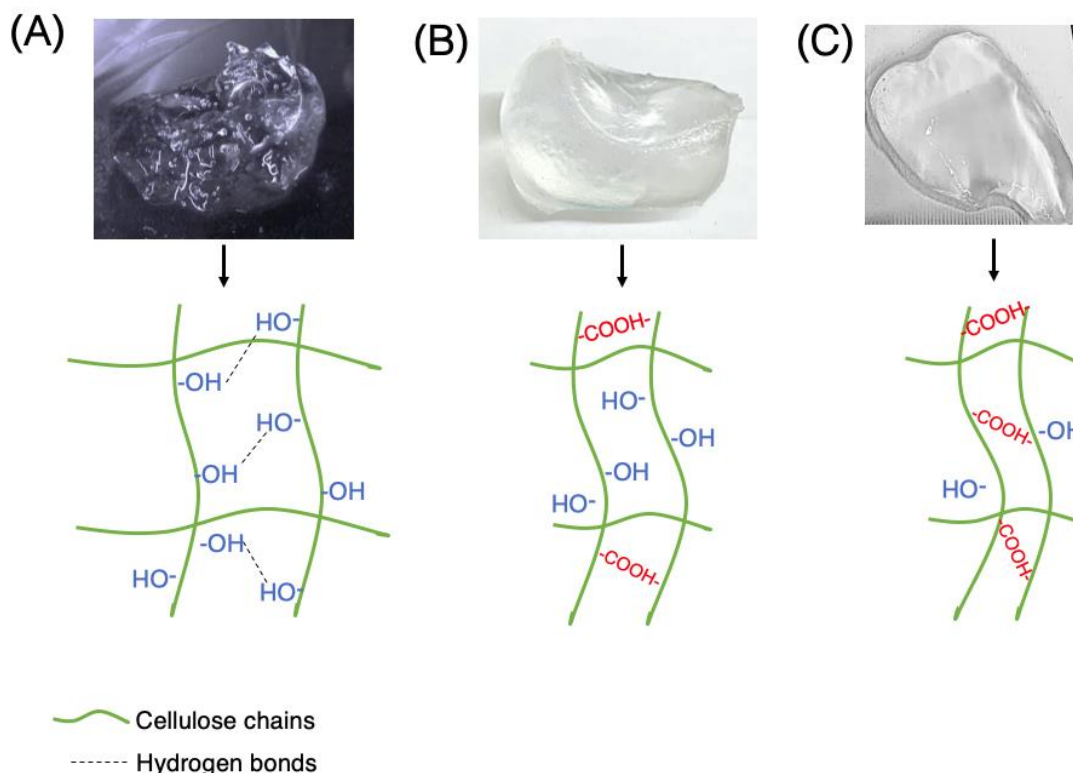
Figure 49: Bio-SAP samples in the hydrogel state (with their schematic network models): A) P45 (pure cellulose, DS = 0); B) PA (Cell-MA, DS = 1.2); and P46 (Cell-MA, DS = 2.6)

3.3.6.4 Effects of degree of neutralization

The effects of DON on the Bio-SAPs were analyzed using the AC values of the following samples: P47 (19.51% DON), PA (55% DON), and P48 (90.5% DON). These samples represented the different concentration levels of DON (Figure 48D) while maintaining the other four factors as follows: 0.4 g of PEGA500, 4 g of urea, Cell-MA (DS = 1.2), and 25 g of water. The three samples formed gels that were converted into Bio-SAPs. The DON percentage was modified in these samples by the addition of NaOH, which

partially neutralized the 4 g of acrylic acid. P47, prepared with 0.65 g of NaOH, had a 19.51% DON and an AC of 180 g/g—less than half the AC of PA (400 g/g), which was prepared with 1.83 g of NaOH and had a 55% DON. A comparison between PA and P48 showed that the increase from 1.83 to 3.02 g of NaOH reduced AC. A comparison between P47 and P48 showed that the increase in the DON from 19.5 to 90.5% reduced the AC from 180 to 160 g/g.

The NaOH had two main functions: i) solubilization of Cell-MA and ii) partial neutralization of the acrylic acid to produce certain amounts of sodium acrylate. The solubilization of Cell-MA was successful in the three samples because the NaOH–water concentration was in the range of cellulose solubilization, which was below the eutectic point (< 20% w/w of NaOH) shown in Figure 13.

The partial neutralization of the acrylic acid, up to approximately 50% DON, contributed to the increase in the Bio-SAPs' AC. Above 50% DON, the hydrogels tended to solubilize. Hydrogel P48, which had high solubility, was solubilized during the AC test.

The solubility of the hydrogels varied based on the DON, and the DON changed in accordance with the Bio-SAP's ratio between the –COOH and –COONa groups. This ratio was affected by the amount of NaOH used to neutralize the acrylic acid [161]; Figure 44 shows the neutralization reaction between NaOH and acrylic acid. Increased NaOH resulted in increased production of –COONa groups and a higher DON. Consequently, the polymeric network's osmotic pressure and electrostatic repulsion decreased, and the water absorbency equilibrium increased, allowing many water molecules to enter the polymeric network, which resulted in the solubility of the Bio-SAP.

When a Bio-SAP's DON was 35–50%, there were enough –COONa groups and, thus, Na^+ ions in the polymeric network to maintain osmotic pressure, which allowed for the absorption and retention of water. As predicted by the optimization model, the optimal DON was 36.7%.

3.3.6.5 Effects of water

The effects of water on the Bio-SAPs were analyzed using the AC values of the following samples: P49 (13.2 g of water), PA (25 g of water), and P50 (36.8 g of water). These samples represented the different concentration levels of water (Figure 48E) while maintaining the other four factors as follows: 0.4 g of PEGA500, 4 g of urea, Cell-MA (DS = 1.2), and 55% DON. P49, prepared with 13.2 g of water, formed a weak and soluble gel, whereas PA, prepared with 25 g of water, formed a gel whose corresponding Bio-SAP had an AC of 400 g/g. P50, prepared with 36.8 g of water, formed a gel whose corresponding Bio-SAP had an AC of 180 g/g. A comparison between these three samples showed that the amount of water affected gel solubility.

According to the literature, De Sterck et al. [189] studied the polymerization of acrylamide in which water plays an important role in free radical polymerization. In this study, the acrylic acid behaved similarly to acrylamides. The role of the water solution is to promote hydrogen bonding reactions that form intermediate complexes and influence the propagation phase of polymerization. A successful propagation stage results in the joining of acrylic acid monomer units to constitute the polymer.

In P49, prepared with 13.2 g of water, the formation of soluble gel showed that insufficient water leads to low propagation and, therefore, a lack of polymer formation. A comparison between P49 and PA showed that the increase in water from 13.2 to 25 g helped to produce an insoluble gel whose corresponding Bio-SAP had an AC of 400 g/g.

A comparison between P49 and P50 showed that the increase in water from 13.2 to 36.8 g produced a gel with lower solubility.

P50, which had approximately a third more water than PA, had a lower AC than PA. Probably, P50's water molecules were in excess, and its monomer molecules were dispersed, making its propagation stage less efficient.

3.3.7   Infrared analysis of Cellulo-SAP

In this study, Cellulo-SAP was compared with a SAP prepared using the same formulation as Cellulo-SAP (see Table 16) minus Cell-MA; this SAP was called "Blank." Figure 50 shows the FTIR spectra of Cellulo-SAP, Cell-MA (DS = 1.2), and Blank. The spectrum of Cell-MA (DS = 1.2) show characteristic stretching absorption peaks of –OH at 3443 cm^{-1} and –COOH at 2902 cm^{-1} [190]. Similarly, in Cellulo-SAP's spectrum, the –OH and –COOH absorption stretch peaks show at 3423 cm^{-1} and 2926 cm^{-1}, respectively, which indicates the presence of Cell-MA. Moreover, the peaks at 1698 cm^{-1} and 1716 cm^{-1} correspond to –COOH stretch. The peak at 1635 cm^{-1} corresponds to the C=C stretch.

The peak at 1045 cm^{-1}, which appeared in Cellulo-SAP and Blank, corresponds to the –CH bending mode. This peak is distinctive of acrylic polymers and corroborates a successful formation of a polyacrylane carbon backbone. More specifically, in Cellulo-SAP, this peak indicates a successful graft copolymerization of Cell-MA with acrylic acid [191].
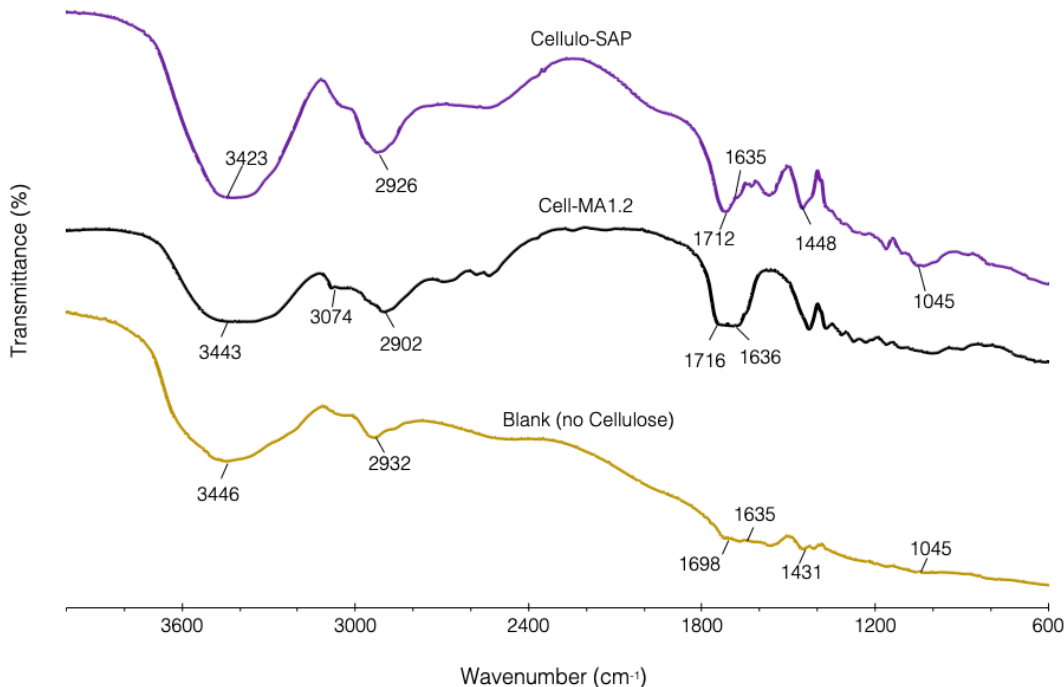
Figure 50: FTIR spectra of Cell-MA (DS = 1.2), Cellulo-SAP, and Blank

3.3.8   Scanning electron microscopy of Cellulo-SAP

SEM was used to analyze the morphology of the Cellulo-SAP samples. Photographs in Figure 51 show Cellulo-SAP's surface at a magnification of (A) 150× and (B) 500×. In the literature [191], it has been reported that SAPs have pores and spherical cracks; Cellulo-SAP possessed these characteristics and, due to the presence of Cell-MA, also had irregularly shaped cracks. Cellulo-SAP's pores ranged in diameter from 1 to 25 μm, suggesting that Cellulo-SAP has a micro- and mesoporous system, which gives it higher mechanical stability than SAPs with primarily microporous systems. In agricultural applications, SAPs typically require high mechanical stability because they are placed under loads of soil. In a previous study [191] in which SAPs performed well in agriculture applications, the mixture of micro- and mesoporous systems was present in the SAPs.
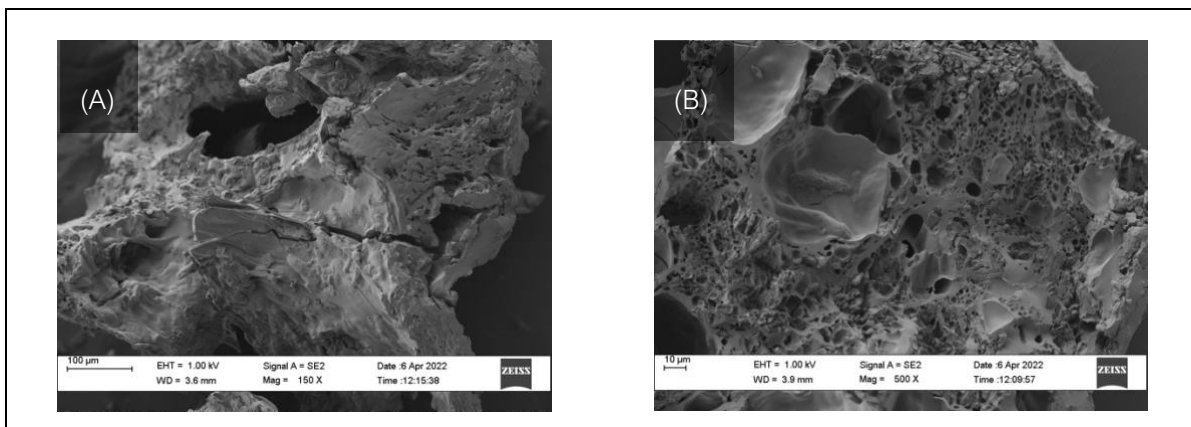
Figure 51: SEM image of Cellulo-SAP's surface at magnification of (A) 150× and (B) 500×

3.4   Conclusions

Bio-SAP synthesis via free radical graft copolymerization was conducted using Cell-MA and acrylic acid. The addition of urea enhanced Cell-MA solubility and consequently increased the AC of the Bio-SAP.

Five factors were studied. Through the application of an RSM-based experimental design, it was determined that these factors affected the AC of Bio-SAP in the following order (from strongest effect to weakest effect): acrylic acid DON percentage > urea content > DS value of Cell-MA > water content > crosslinker content. The interaction between the DON and urea had the most significant effect on AC among all the factor interactions.

A quadratic empirical model was generated via the response surface analysis of the experimental data. In this analysis, the above-mentioned factors were optimized. This equation model predicted a Bio-SAP formulation that would result in maximum AC. The formulation, which was used to synthesize a novel Bio-SAP named Cellulo-SAP, comprised the following: PEGA500 (0.36 g), urea (5.7 g), Cell-MA (DS = 1.2), DON (36.7%, corresponding to 1.22 g of NaOH), and deionized water (25 g). Cellulo-SAP had an AC of 475 g/g.

The stretch peak at 1045 cm^{-1} nm in the FTIR spectra evidenced the presence of acylane; this indicated successful graft copolymerization between Cell-MA (DS = 1.2) and acrylic acid. Additionally, SEM images displayed Cellulo-SAP's surface morphology and cross-sectional porosity distribution; a micro- and mesoporous combination was visible throughout the Cellulo-SAP. This combination indicates that Cellulo-SAP has high mechanical strength and is therefore suitable for agricultural applications.

Chapter 4

4   Performance of Cellulo-SAP: absorbency, stability, reusability, and biodegradability

With minor editorial modifications to fulfill formatting requirements, this chapter is substantially as it appears in the *Canadian Journal of Chemical Engineering* (the licence agreement is shown in Appendix C). The published paper appears with the following title:

"Performance of a novel, eco-friendly, cellulose-based superabsorbent polymer (Cellulo-SAP): Absorbency, stability, reusability, and biodegradability"

Abstract

Superabsorbent polymers (SAPs) have attracted tremendous attention recently, with researchers noting that their high water absorbability is valuable for various applications, especially in agricultural contexts. Two types of materials can be used to produce SAPs: Fossil-based (which are harmful to the environment) and bio-based (which are significantly more environmentally friendly, given their biodegradability and minimal toxic side effects). Although bio-based SAPs are preferable for environmental reasons, their synthesis tends to be time consuming and labour intensive, while their absorption capacity (AC) can be far below expectations. To address these problems, a novel, eco-friendly, cellulose-based superabsorbent polymer (Cellulo-SAP) was developed in this study through facile preparation via free radical synthesis using modified cellulose. Then, the absorbency, thermal/pH stability, reusability, and biodegradability of Cellulo-SAP were evaluated. This new polymer demonstrated reusability as a water reservoir, in addition to high thermal and pH stability. More importantly, Cellulo-SAP achieved an AC of 475 g/g and exhibited superior biodegradability compared to a commercial, fossil-

based SAP. Accordingly, these results prove that Cellulo-SAP can be used in agriculture as an effective alternative to fossil-based SAPs.

Keywords: absorption property, bio-based superabsorbent polymer, biodegradability, swelling kinetics

4.1 Introduction

A novel, eco-friendly, cellulose-based superabsorbent polymer (Cellulo-SAP) was developed in this study (Chapter 3) through facile preparation via free radical synthesis using modified cellulose. Then, the absorbency, thermal/pH stability, reusability, and biodegradability of Cellulo-SAP were evaluated. This new polymer demonstrated reusability as a water reservoir, in addition to high thermal and pH stability. More importantly, Cellulo-SAP achieved an AC of 475 g/g and exhibited superior biodegradability compared to a commercial, fossil-based SAP. Accordingly, these results prove that Cellulo-SAP can be used in agriculture as an effective alternative to fossil-based SAPs.

4.2 Materials and methods

4.2.1 Materials

Cellulo-SAP was prepared through the copolymerization of pure cellulose (Type 20, 20 µm) premodified with an anhydride in a solution of urea and acrylic acid via free radical synthesis in the presence of an initiator and a crosslinker. The preparation details are described in Chapters 2 and 3. The chemicals used in this study were CAS reagent grade purchased from Sigma-Aldrich, except for the PEGA500, which was provided by the Canadian company Western Maple BioResources Inc. All chemicals were used without any further purification.

4.2.2   Methods

4.2.2.1   Absorption capacity and swelling kinetics

Throughout this study, AC is expressed as a weight fraction (g/g) and is used when discussing swelling behaviour in different types of solutions and variations in pH. It was calculated using a standard gravimetric methodology [183].

For the experiment, Cellulo-SAP was carefully dried, ground, and sieved to obtain an average particle size of 2 mm through a No. 10 standard sieve mesh (ASTM 11 standard sieve). Then, 0.05 g ($\pm$ 0.001 g) Cellulo-SAP samples were immersed in 200 mL of deionized water $MgSO_4$ (1.0 mol/L), NaCl (1.0 mol/L), and $CaCl_2$ (1.0 mol/L) at room temperature (23°C $\pm$ 2°C) for 24 h, during which time the samples became hydrogels. The obtained hydrogels were then removed from the solutions and filtered, and the unabsorbed aqueous solution was removed using dry tissues. The hydrogels were weighed until they reached AC equilibrium using the following equation:

$$AC = \frac{w_2 - w_1}{w_1} \quad \textbf{Equation 1}$$

where w_1 is the weight of the dry Cellulo-SAP sample and w_2 is the weight of the hydrogel. The entire AC analysis procedure was performed in triplicate.

Swelling kinetics tests were conducted using the same methodology employed for the AC analysis. In this test, the Cellulo-SAP sample was placed in the solution and weighed every 30 min for 5 h. The entire procedure was performed in triplicate.

4.2.2.2   Free swelling capacity

The free swelling capacity (FSC) of Cellulo-SAP in a saline solution was determined using a gravimetric measurement in accordance with International Standard ISO 17190-5. In detail, a Cellulo-SAP sample (0.2000 g) was completely dried, placed inside a 25-µm nylon screen tea bag, immersed in a 0.9% w/w NaCl solution, and left to soak for 1 min. After the bag was removed, excess solution was left to drip away and weighed to a constant weight to determine the total amount of fluid absorbed. In the control

experiment, this process was replicated using an empty 25-µm nylon screen tea bag. Finally, the FSC was calculated using the following equation:

$$FSC = \frac{(w_w - w_b) - w_s}{w_s} \qquad \textbf{Equation 5}$$

where w_s is the weight of the dry Cellulo-SAP, w_b is the weight of the wet paper bag without Cellulo-SAP, and w_w is the weight of the wet paper bag containing the hydrogel.

4.2.2.3 Biodegradability

The biodegradability test was performed according to the norm ASTM D 5988-03 Standard Test. Three parallel experiments were performed for comparison. The first experiment was conducted using a 0.5 g sample of Cellulo-SAP, which was prehydrated with deionized water for 24 h to become a hydrogel and then mixed with 70 g of soil (commercial blend C-I-L Enriched Soil 3-in-1) presieved to a particle size of 2 mm. The second experiment was conducted using a 0.5 g sample of Sigma-Aldrich sodium polyacrylate, which underwent the same prehydration process. The third experiment was conducted using 70 g of soil in the absence of a SAP. In these experiments, the soil had a deionized water–soil weight ratio of 5:1 and a pH value of 6.8 (measured with a VWR sympHony BP10 pH meter). The moisture content of the mixture was fixed between 50% and 70% by adding deionized water. In each experiment, the samples were transferred to a biometer flask (Figure 52). Specifically, each sample was placed in the primary receptacle of biometer (A) and covered with a coated rubber stopper attached to valve (B) and filter (C), which contained 10 g of Molecular Sieve UOP Type 3Å. Then, 10 g of 0.5 Eq/L KOH solution was poured into the secondary receptacle (D). The solution was removed each week and refilled with fresh KOH solution using a syringe (E). When the solution was taken, valve (B) was opened and then closed when the secondary receptacle (D) was refilled. Each week, the removed solution was decanted into a beaker and titrated with HCl 0.05 Eq/L solution until its colour became clear (using phenolphthalein as an indicator).
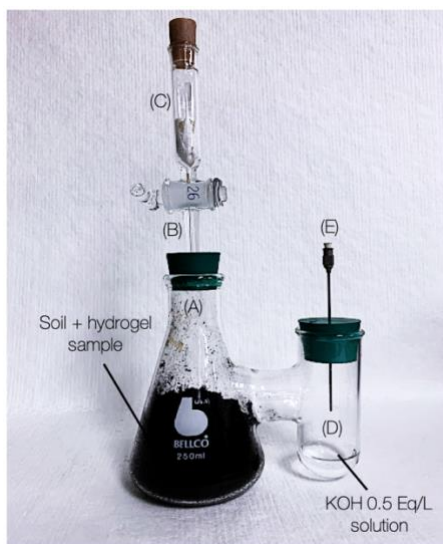
Figure 52: The setup of the biodegradation test of soil-buried Cellulo-SAP in a biometer flask: (A) primary receptacle; (B) valve; (C) filter; (D) secondary receptacle; (E) syringe

To evaluate the CO_2 produced (% w CO_2) in the biometer, the theoretical mass of each CO_2 composition sample was calculated. The theoretical quantity of C was calculated as follows:

$$w_C = \frac{\%w\ C \times S}{100} \qquad \textbf{Equation 6}$$

where w_c is the mass (mg) of the carbon charged to the biometer, % w C is the total organic carbon content of the Cellulo-SAP (42.97% C, determined by elemental analysis measured in a Vario EL III elementary analyzer using CHNS mode), and S is the mass (mg) of Cellulo-SAP.

The molecular weight (mg/mmol) of CO_2 (MW_{CO_2}) and C (MW_C) were used to calculate the theoretical yield of CO_2 (w_{CO_2}) using the following reaction and equation:

$$\textbf{C}_{(g)} + \textbf{O}_{2\ (g)} = \textbf{CO}_{2\ (g)} \qquad \textbf{Reaction 1}$$
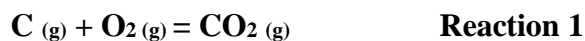
$$w_{CO_2} = \frac{w_C \times MW_{CO_2}}{MW_C} \qquad \textbf{Equation 7}$$

Therefore, the produced net CO_2 was corrected with blank titration by subtracting the amount of HCl (0.05 Eq/L solution) wasted:

$$\mathbf{V_n = V_b - V_t} \qquad\qquad \textbf{Equation 8}$$

where V_n is the volume (mL) of the HCl needed to titrate the CO_2 generated solely from the Cellulo-SAP, V_b is the volume (mL) of the HCl needed to titrate the blank with soil only, and V_t is the volume (mL) of the HCl needed to titrate the soil plus the Cellulo-SAP.

The total mass (mg) of CO_2 produced (M_{CO_2}) was determined with Equation 9 using Reaction 2, Reaction 3, and the normal concentration of the HCl solution, as follows:

$$\mathbf{2KOH_{(aq)} + CO_{2\,(g)} = K_2CO_{3\,(aq)} + H_2O_{(l)}} \qquad \textbf{Reaction 2}$$

$$\mathbf{KOH_{(aq)} + HCl_{(l)} = KCl_{(aq)} + H_2O_{(l)}} \qquad \textbf{Reaction 3}$$
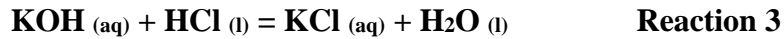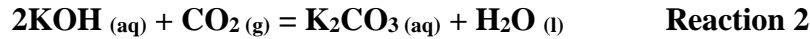
$$\mathbf{M_{CO_2} = [HCl] \times V_n \times MW_{CO_2}} \qquad \textbf{Equation 9}$$

Finally, the percentage of CO_2 evolved was calculated using the following equation:

$$\mathbf{\%wCO_2 = \frac{M_{CO_2}}{w_{CO_2}} \times 100} \qquad\qquad \textbf{Equation 10}$$

4.2.2.4 Thermal stability analysis

The thermal stability of Cellulo-SAP was analyzed using thermogravimetric analysis (TGA) in a Perkin Elmer Pyris 1 TGA unit. In this procedure, a completely dried Cellulo-SAP sample (2 mg) was heated from 33°C to 800°C at an increasing rate of 10 K/min in a nitrogen atmosphere. To analyze the effects of temperature on Cellulo-SAP in a hydrated state, a sample (0.05 g) was immersed in a 250 mL glass flask containing 200 mL of deionized water until AC equilibrium was reached. The flask was then covered with a wax film and transferred to a hot plate (95°C), where it was stirred for 2 h using a stirring bar. After this process, the final appearance of the hydrogel was observed, and the AC was calculated.

4.2.2.5 Absorption–desorption (swell–dry) cycle test

A completely dried 0.05 g Cellulo-SAP sample (particle size 2 mm) was soaked in 200 mL of deionized water for 24 h until it became a hydrogel. The hydrogel was then weighed and dried overnight in a vacuum oven at 80°C. Once dried, the sample was weighed to constant weight. This swell–dry process was repeated three times.

4.2.2.6 Effect of pH solution on hydrogel

Completely dried Cellulo-SAP samples (0.1 g) were immersed in 250 mL of deionized water until they reached AC equilibrium. The resultant hydrogels were placed in 100 mL of standard aqueous solutions (purchased from VWR International) with pH values of 1.68, 4.01, 7.01, 10.04, and 12.00 and then left at room temperature (23°C ± 2°C) for 24 h. The samples were then dried at 80°C in a vacuum oven overnight.

4.3 Results and discussion

4.3.1 Absorption capacity and swelling kinetics

The AC value is the most essential parameter when measuring the performance of SAPs. Figure 53 shows a Cellulo-SAP sample before and after reaching AC equilibrium. The initially collapsed polymeric network developed a three-dimensional appearance as it became a hydrogel through water absorption. Figure 54 portrays the swelling behaviour of Cellulo-SAP at room temperature (23°C ± 2°C), where it can be observed that the value of AC changed as a function of time when the sample was immersed in deionized water (pH 7.0, EC 0.001 Mhos/cm). First, deionized water molecules, which are smaller than those of Cellulo-SAP, enter the large polymeric molecule. This phase lasted from the beginning of absorption for approximately 30 min, during which time the Cellulo-SAP had markedly fast water uptake and reached approximately 75% of its final AC equilibrium. Second, a plasticization stage began due to internal interactions between the polymer and water, forming hydrogen bonds that increased polymer segmental flexibility in the macromolecular system[192]. This interaction resulted in a polymer volume expansion that lasted until the SAP network was saturated, and no more water could enter

the system [193]. However, due to its crosslinking density, the hydrogel did not dissolve. This second stage of AC stabilization began when the rate of water absorption slowed.
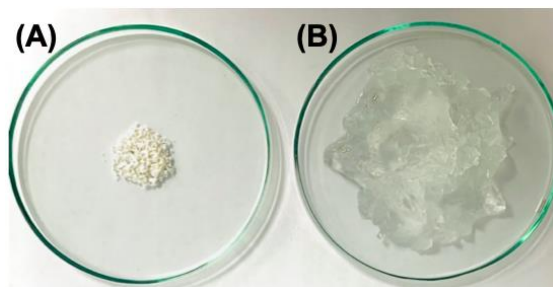
Figure 53: Physical transformation from Cellulo-SAP to hydrogel: (A) completely dried 0.5 g Cellulo-SAP sample; (B) hydrogel after reaching AC equilibrium in deionized water
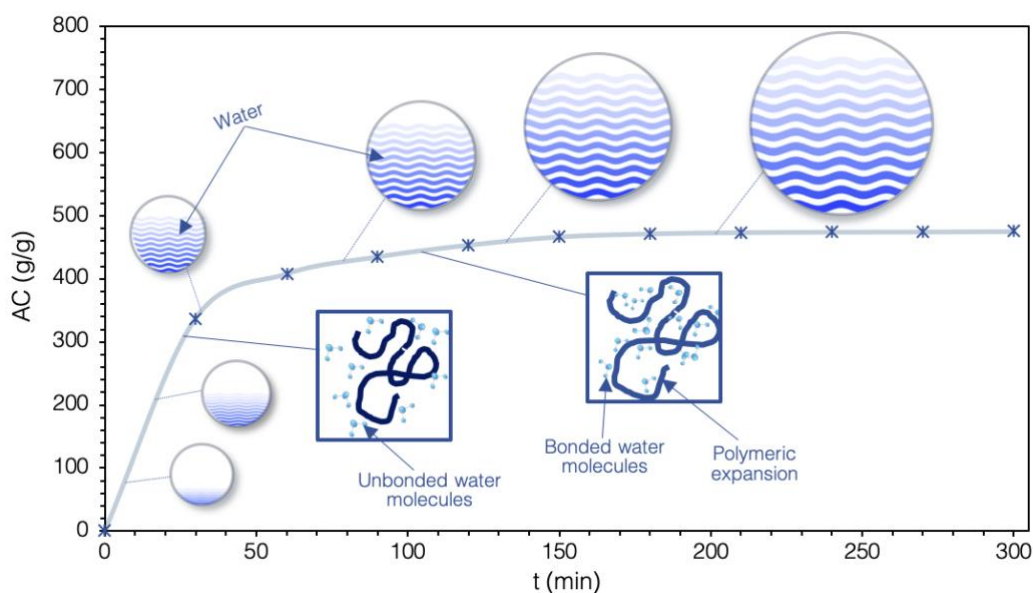
Figure 54: Cellulo-SAP's swelling behaviour and AC in deionized water versus time

To describe the time-dependent swelling kinetics, the sample was weighed at room temperature (23°C ± 2°C) to determine the amount of water absorbed. In a previous study [194], three different models were used to analyze the swelling kinetics of SAPs: a second-order equation, a power function of Fickian diffusion and Case II transport, and a Voigt-based viscoelastic model. The second-order equation model Equation accurately describes the absorption behaviour of Cellulo-SAP:

$$W_t = \frac{At}{t+B} \qquad \textbf{Equation 11}$$

where W_t (g) is the weight of the absorbed liquid at time t (min), and A (g) and B (min) are constant values (Table 17).

Following the same procedure used when investigating the swelling kinetics in deionized water, Cellulo-SAP samples (0.5 g) were immersed in 1.0 mol/L solutions of $MgSO_4$, NaCl, and $CaCl_2$ and the results were evaluated using the three models mentioned previously. Figure 55 shows the absorption rates of the samples, which were rapid during the first 30 min (in all three solutions) and then stabilized. This effect also occurred in deionized water, although the AC equilibrium values were significantly lower. The AC response decreased according to each salt solution, following the order of $CaCl_2 <$ NaCl $<$ $MgSO_4$. Furthermore, the data obtained for swelling in these solutions also fitted Equation when substituting the corresponding A and B values (Appendix D).
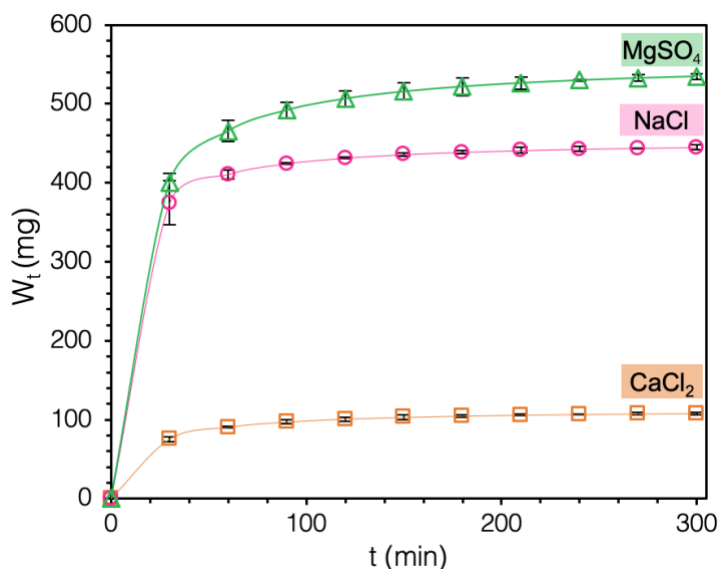
Figure 55: Weight of liquid absorbed (W_t) by Cellulo-SAP immersed in 1.0 mol/L solutions of MgSO$_4$, NaCl, and CaCl$_2$ versus time (t)

[196].

Table 17 presents Celullo-SAP's AC values at equilibrium in deionized water and other solutions. As expected, the performance of anionic Cellulo-SAP in solutions with cations

(Na^+, Mg^{+2}, and Ca^{+2}) changed, with the anions initially creating an anion–anion repulsive force. However, when deionized water entered the SAP network, the H+ protons in water formed hydrogen bonds with the polymer anions, causing the water to swell significantly.[195] In the case of solutions containing cations, the initial anion–anion repulsion was broken due to interactions between anions in the polymeric network and cations in the solution, resulting in a screening–shielding effect [36]. This caused a reduction in the osmotic pressure between the aqueous solution and the polymer. The lowest AC was achieved with $CaCl_2$ (1.5 g/g), followed by NaCl (10 g/g) and $MgSO_4$ (12 g/g). This decrease of absorption can be explained by the network occupancy of metal cations within Cellulo-SAP that restricts the water entrance. The difference between the AC behaviour of Cellulo-SAP in $CaCl_2$, NaCl and $MgSO4$ can be attributed to the atomic radius size of the metals contained in the salts, from which calcium has the biggest radius (0.197nm) followed by sodium (0.186), and then magnesium (0.160nm) [196].

Table 17: Summary of Cellulo-SAP's properties

Biodegradability CO_2 (%)[a]	FSC (g/g)[b]	Solution	AC (g/g)[d]	Constants of second-order equation kinetic model	
				A (g)	B (min)
16.7 ± 0.25	18 ± 0.39	Deionized water	475 ± 0.43	24.39	8.27
		$MgSO_4$[c]	12 ± 0.38	0.56	11.61
		NaCl[c]	10 ± 1.53	0.45	6.30
		$CaCl_2$[c]	1.5 ± 0.51	0.11	14.78

Note: The results are means of three replicates followed by ± standard deviation.

[a]After 60 days of biodegradation.

[b]NaCl 0.9% w/w solution.

[c]1.0 mol/L solution.

[d]Equilibrium conditions.

In addition, we compared the properties of Cellulo-SAP with those of similar products, both bio-based and fossil-based, reported in the literature. Notably, Cellulo-SAP has a

high AC value and high cellulose content compared to other Bio-SAPs. The full findings are summarized in the supplementary information, in Table 18.

Table 18: Comparison of Cellulo-SAP with similar products, both bio-based and fossil-based

Material	Mass ratio (cellulose–copolymer)	AC (g/g)	SAP category
Cellulose–acrylic acid [197]	1:10	16	Bio-based
Carboxymethyl cellulose–citric acid [87]	1:1	87	Bio-based
Cellulose–acrylic acid [198]	1:10	198	Bio-based
Cellulose–acrylic acid [199]	1:10	215–247	Bio-based
Hydroxyethyl cellulose–acrylic acid [78]	19:1	ca. 300	Bio-based
Cellulose–linseed gum [200]	6:4	> 300	Bio-based
Cellulose/chitosan–acrylic acid [35]	1:3.6	390	Bio-based
Cellulose–acrylic acid [201]	1:4	422	Bio-based
Cellulose–acrylic acid (Cellulo-SAP from this research)	*1:2*	*475*	*Bio-based*
Hydroxyethyl cellulose–polyacrylamide [90]	1:10	538	Bio-based

Sawdust–acrylic acid/acrylamide [202]	1:8	738	Bio-based
Carboxymethyl cellulose–acrylic acid [203]	1:5.6	750	Bio-based
Carboxymethyl cellulose–acrylic acid [204]	3.2:1	700–1000	Bio-based
Corncob cellulose–polyvinylpyrrolidone [205]	1:20	ca. 1200	Bio-based
Acrylic acid, acryl amide, and 2-acrylamido-2-methyl-propansulfonic acid [191]	Not applicable	58	Fossil-based
Acrylic acid [206]	Not applicable	417	Fossil-based
Polyvinyl alcohol, acrylic acid [207]	Not applicable	ca. 1760	Fossil-based
Acrylic acid [207]	Not applicable	ca. 2800	Fossil-based

4.3.2   Free swelling capacity

When evaluating the performance of SAPs, FSC is an absorbency property that can be used as a reference [208]. As shown in [196].

 Table 17, the FSC of Cellulo-SAP was 18 ± 0.39 g/g, meaning the hydrogel could absorb 18 times its own weight in a 0.9% w NaCl saline solution. Cellulo-SAP's FSC was 1.8 times lower than that of Sigma-Aldrich sodium polyacrylate (32 ± 0.65 g/g); nevertheless, its environmentally friendly benefits outweigh the magnitude of this difference.

4.3.3   Biodegradability

After 70 days, 16.7% of the Cellulo-SAP sample (as shown in Table 17) and 9.8% of the Sigma-Aldrich sodium polyacrylate sample were converted to CO_2, indicating that both SAPs underwent biodegradation. From the literature, another fossil-based polyacrylate SAP (from Stockhausen GmbH and Co.KG) showed a mineralization of 4.3% [72], which was almost four times lower than the degradation of Cellulo-SAP. However, there were differences in their degradation processes, which depended on their varied physicochemical and/or biological compositions. For example, fossil-based SAPs (such as Sigma-Aldrich sodium polyacrylate) decompose into small oligomeric structures and/or microplastics, which are toxic to organisms and the environment [209,210]. In contrast, Cellulo-SAP's degradation involves aerobic decomposition due to microorganisms in the soil, resulting in a microplastic-free residue process. This effect was evidenced by the Cellulo-SAP sample's high biodegradability, achieving CO_2 production that was 58.1% higher than its fossil-based counterpart. The conditions of this experiment mimicked the biodegradation of Cellulo-SAP in real environmental conditions, promoting the use of Cellulo-SAP for agricultural purposes. Compared to fossil-based SAPs, Cellulo-SAP is a green product that promotes superior waste management. More importantly, Cellulo-SAP can be part of an environmentally friendly cycle that begins with biomass (specifically cellulose) and culminates in CO_2 emissions, which plants use for growth.

4.3.4   Thermal stability analysis

4.3.4.1 Thermogravimetric analysis

The thermogravimetric analysis (TGA) provided information on the capacity of superabsorbent materials to survive high-temperature conditions. As shown in Figure 56, a 5% weight loss of organic matter occurred at 101.53°C, proving Cellulo-SAP's stability in ambient applications (< 50°C).

The first stage of decomposition (23–200°C) was associated with the loss of bound water, resulting in a 14% w reduction. In the second stage (200–344°C), there was a maximum

weight loss of 47% due the beginning of the decarboxylation of esters attached to the cellulose. At this stage, CO_2 was evolved as a result of the decarboxylation reaction and the cleavage of carboxylic groups. Thermal decarboxylation has been previously described [211–214]. In the study of Xu et al. [212], the decarboxylation of citric acid from 200–400°C was reported. Moreover, the same study showed the thermal decomposition of the crosslinker polyethylene glycol (molecular weight of 400 g/mol) starting at 300°C. These results are comparable to the present study's results; the Cellulo-SAP sample underwent a 47% weight loss between 200.41°C and 344.16°C. From a mass balance, the theoretical yield of CO_2 to be produced by the decarboxylation of carboxylic acids present in the sample should be of 58% weight. At the second stage, a partial production of theoretical yield of CO_2 was formed. In the third and final stage (344–800°C), the decarboxylation ended, resulting in a final sample weight of 24%. Following these three stages, the residual weight was 15% [36,215].
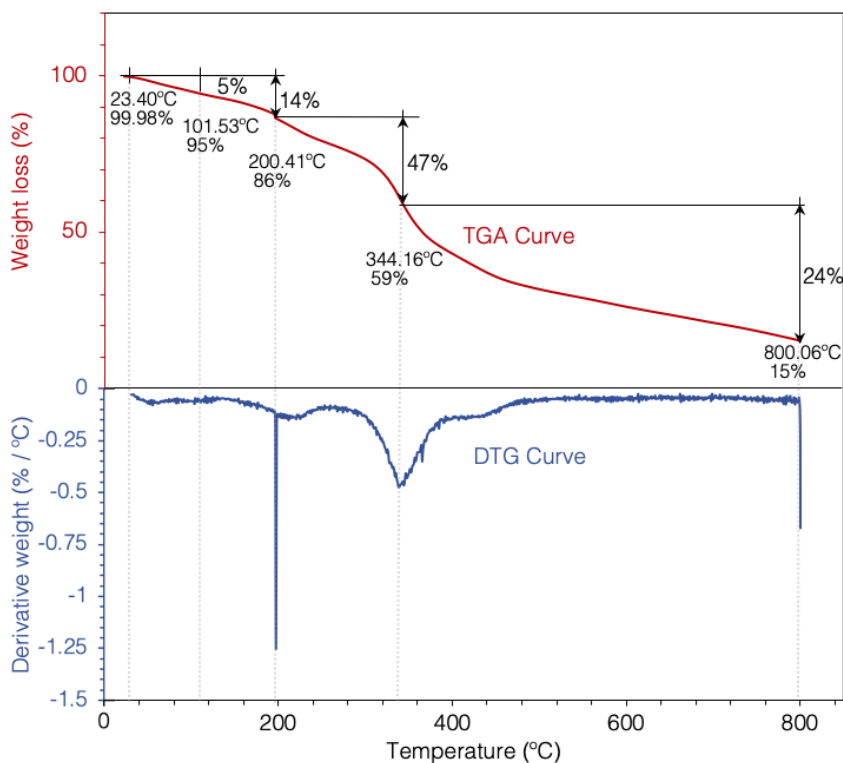
Figure 56: TGA and derivative thermogravimetry (DTG) spectra of Cellulo-SAP with indicated weight loss

4.3.5   Hydrogel thermal stability

In addition to the TGA analysis, another simple procedure was performed to evaluate the thermal stability of Cellulo-SAP under swollen conditions. The sample was quite stable after being stirred and heated, with no dissolution or decomposition. Moreover, the weight of absorbed water increased by an approximate factor of 5 (from 475 to 2248 g/g) due to polymeric chain expansion, resulting in a porous SAP network increment that allowed more water to enter the three-dimensional structure [216]. The degradation temperature of Cellulo-SAP (obtained from the TGA) also corresponded with the behaviour of the swollen hydrogel. Therefore, regardless of whether it was dry or swollen, Cellulo-SAP achieved good thermal stability and absorption performance without dissolution or decomposition, demonstrating its utility as a water reservoir.

4.3.6   Swell–dry cycle test

The reusability of Cellulo-SAP was evaluated by inducing the dry sample to swell in deionized water several times, as illustrated in Figure 57A. The sample lost weight after each swell–dry cycle (Figure 57B), maintaining 77% of its original weight after the third cycle. This weight loss occurred in nitrogen and carbon and was evaluated using elemental analyses before and after the first swell–dry cycle. The nitrogen mass content decreased from 1.44% to 1.14%, and the carbon mass content decreased from 42.74% to 41.64%.

The nitrogen in Cellulo-SAP is constitutive of urea, which can function as a fertilizer. Urea is absent from Sigma-Aldrich sodium polyacrylate and other fossil-based SAPs, which represents one of Cellulo-SAP's advantages when used in agricultural contexts. The presence of carbon in Cellulo-SAP is due to the polymeric chain, which contains cellulose. The decomposition of this polymeric chain under buried soil conditions allows carbon to mineralize to CO_2, rendering Cellulo-SAP much more environmentally friendly than fossil-based SAPs.

The AC decreased at a rate of only 6% per swell–dry cycle (Figure 57C). Moreover, the polymeric chain maintained its absorption capabilities and could withstand numerous cycles.
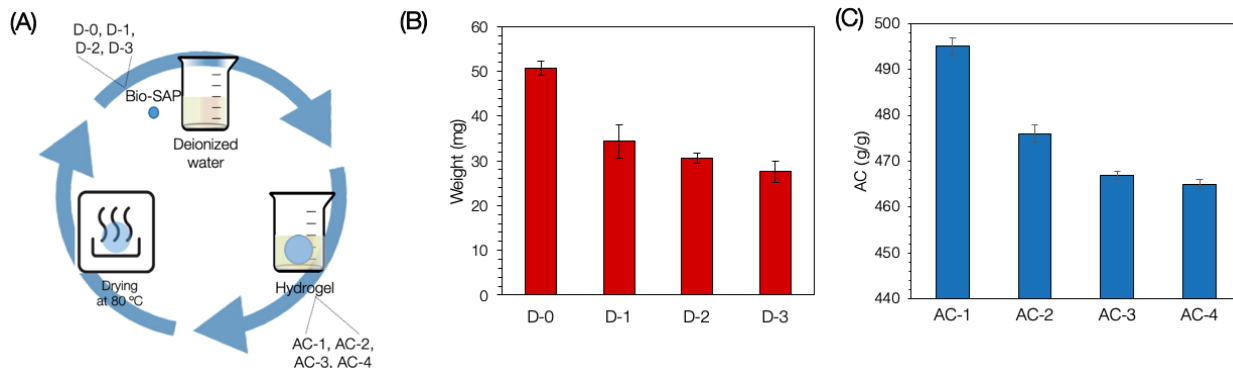
Figure 57: Absorption–desorption effects on weight and AC: (A) methodology scheme; (B) weight throughout swell–dry cycles; (C) AC throughout swell–dry cycles

4.3.7   Effects of pH solutions on hydrogels

In general, the hydrogels exhibited good chemical stability in an acid-basic pH spectrum. However, their weight decreased after exposure to external pH surroundings [217]. Figure 58 shows the effects of exposure to external pH solutions on the hydrogels' weight and volume. After soaking in pH solutions, the hydrogels' swelling varied, as shown in Figure 58A. All the hydrogels shrunk in volume (Figure 58B) and lost weight after 24 h of drying in a vacuum oven at 80°C. Specifically, the weight loss in samples exposed to acid solutions was at least twice the weight loss observed in samples exposed to solutions with pH levels of 7. In basic solutions, the weight was reduced three times less than in acid solutions. Furthermore, there was a correlation between weight loss in the Cellulo-SAP samples and contact with an external solution, whereby Cellulo-SAP improved AC performance after absorption in basic solutions compared to acid solutions. Nevertheless, the dissolution of soluble components (and consequent weight loss of Cellulo-SAP) was greater in the acid solutions. This effect can be explained by the presence of hydrogen protons in acids that interact with the anionic polymeric network bonding with anions [36,218]. Figure 58B shows how the hydrogels shrank after acidic solution exposure due

to a reversible reaction of partial acetalization, resulting in the loss of the crosslinked network [219]. These findings indicate that Cellulo-SAP is suitable for an extensive variety of application conditions, given its ability to withstand a wide range of pH values.
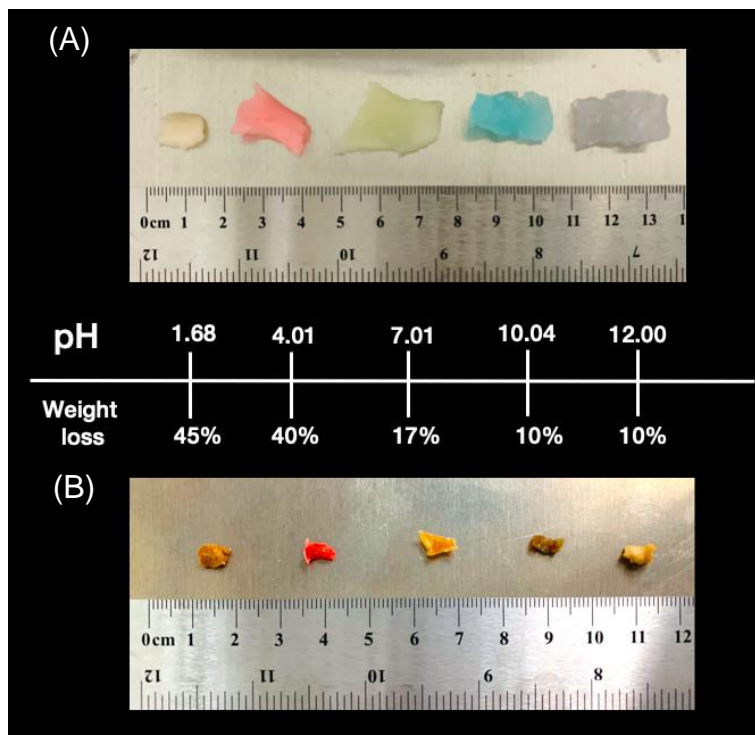
Figure 58: Weight loss of hydrogels and Cellulo-SAP: (A) hydrogels after 24 h in different pH solutions; (B) Cellulo-SAP samples vacuum oven–dried after 24 h in different pH solutions, in addition to their corresponding pH condition and weight loss percentage

4.4 Conclusions

Cellulo-SAP is an eco-friendly, cellulose-based SAP obtained through facile preparation via free radical synthesis using up to 15% w of Cell-MA. A multifaceted evaluation of Cellulo-SAP demonstrated its suitability for agricultural applications. Moreover, its AC of 475 g/g in deionized water demonstrated that it could function as a water reservoir for plants. Significantly, this AC performance was only reduced by 6% per swell–dry cycle in deionized water, which implies the reusability of Cellulo-SAP.

Cellulo-SAP's AC decreased significantly in 1.0 mol/L solutions of $MgSO_4$ (12 g/g), NaCl (10 g/g), and $CaCl_2$ (1.5 g/g), where it manifested the behaviour typical of ionic SAPs. The swelling kinetics of absorption showed a second-order behaviour in deionized water and solutions of $MgSO_4$, NaCl, and $CaCl_2$. In the biodegradability test, Cellulo-SAP achieved 16.7% mineralization, which was 58.1% higher than the mineralization of Sigma-Aldrich sodium polyacrylate, a fossil-based counterpart comparable to Cellulo-SAP. When undergoing TGA, Cellulo-SAP was stable and capable of resisting temperatures up to 101°C. Furthermore, it remained stable in its hydrogel state (without dissolution or decomposition) when immersed in boiling deionized water and stirred for 2 h. The Cellulo-SAP hydrogels withstood solutions whose pH levels ranged from 1.68 to 12.00. Moreover, these hydrogels a had higher AC in basic media than in acidic media. Cellulo-SAP exhibits the desired characteristics for use in agricultural contexts and is a promising and competitive alternative to fossil-based SAPs.

Chapter 5

5 CrudeCellulo-SAP

5.1 Introduction

Lignocellulosic materials are a natural and renewable resource that can be used as a feedstock to obtain bio-fuels and value-added chemicals [131]. The agricultural industry is a major source of lignocellulosic biomass [220], which can be fractionated into its three main components: cellulose, hemicellulose, and lignin (35–45%, 25–30%, and 15–20%, respectively) [81].

Cellulose is a homogeneous, polysaccharide long chain that forms the structure of plants and is responsible for plants' mechanical strength. Cellulose is formed by orderly arrangements of glucose monomers connected by ß-(1-4)-glycosidic bonds [98]. Cellulose can be used to make paper, chemicals, and bio-fuels.

There are several treatments to extract cellulose from the lignocellulosic biomass. The aim of such treatments is to make cellulose accessible by altering the structure of the lignocellulose material [221]. The treatments can be classified into three main groups: mechanical (e.g., chipping, milling, and grinding), chemical (e.g., acid and alkaline hydrolysis, ionic liquid, steam explosion, and organosolv), and biological (e.g., fungi and bacteria) [98].

Organosolv treatment is an attractive treatment for cellulose separation. It is considered one of the best options for obtaining high yields of cellulose due to its efficiency in removing hemicellulose and lignin [222]. The principal fundament of lignocellulosic organosolv treatment is the use of solvents (e.g., ethanol, formic acid, methanol, and glycerol) with or without a catalyst (e.g., sodium hydroxide, hydrochloric acid, and sulfuric acid) to accelerate the reaction, using temperatures between 120°C and 200°C. The reaction times can vary from 30 min to 240 min, depending on the catalyst and pH conditions of the mix [223]. During the reaction, the lignin bonds are hydrolyzed,

producing two phases: the solid phase, which contains the cellulose, and the liquid phase, which contains lignin [222].

Some of the advantages of the organosolv treatment are that the solvents are easily recovered and that it is considered environmentally friendly because it is a sulfur-free process. In contrast the disadvantages are the energy consumption for the solvent recovery and the process control associated with the management of volatile explosive solvents [224].

The cellulose obtained from this process is known as crude cellulose. It has a characteristic brown colour due to the presence of remaining lignin. Usually, bleaching processes involve the use of sodium hydroxide, sodium chlorite, sodium hypochlorite, or peroxide solutions [225].

This chapter explains how crude cellulose from agricultural lignocellulosic residues was obtained from cornstalk via organosolv fractionation with an acetic acid–formic acid–water solvent mix. Then, the obtained crude cellulose without bleaching was used as a raw material to produce CrudeCellulo-SAP by applying the methodologies and optimal formulation of Cellulo-SAP described in chapter 3.

5.2   Materials and methods

5.2.1   Materials

Table 19 lists the chemicals used in these experiments; all chemicals were CAS reagent grade, supplied by Sigma-Aldrich, and used as received.

Table 19: List of chemicals and their purity levels

Chemical	Purity
maleic anhydride	99%
zinc chloride	≥ 98%
acetone	99.5%

acetic acid	99.7%
sodium hydroxide	97%
urea	99%
ammonium persulfate	≥ 98%
acrylic acid	99%
formic acid	≥ 98%
ethanol	95%
hydrochloric acid	37%
ethyl acetate	≥ 99.9%
sodium chlorite	99%

The crosslinker PEGA500 (number-average molecular weight = 500 g/mol) was provided by Western Maple BioResources and was used as received. The deionized water used in these experiments was obtained from a deionization unit in the laboratory at ICFAR.

The crude cellulose was obtained via organosolv fractionation of cornstalk, which was provided by the Ontario Federation of Agriculture (OFA). The cornstalk was air-dried at room temperature ($23°C \pm 2°C$), ground, and sieved to obtain an average particle size of 2 mm through a No. 10 standard sieve mesh (ASTM 11 standard sieve). Table 20 presents the elemental composition and chemical components of the cornstalk.

Table 20: Cornstalk's elemental composition and chemical components

Elemental composition (% w)			
C	H	O	N
45.01	5.67	45.38	1.50

Main chemical components (% w)		
Lignin	Cellulose	Hemicellulose
18.57	35.31	32.58

5.2.2   Methods

5.2.2.1   Cornstalk organosolv fractionation

The cornstalk organosolv fractionation methodology was based on a study by Shui et al. [226]. The fractionation was conducted in a 200 mL flask glass reactor containing 5 g of oven-dried cornstalk and 50 mL of solvent (premixed HCl and acetic acid aqueous solution). The solid–solvent ratio was 1 g to 10 mL, and the catalyst was 0.4 mL of 1% w/v HCl solution. The solvent mixture comprised acetic acid, formic acid, and water (3:6:1, v/v/v). The flask was sealed and placed in a hot oil bath with a heat rate of 10°C/min up to 90°C, under atmospheric pressure; meanwhile, the mixture was stirred at 300 rpm. After 240 min, the flask was removed from the oil bath, and it cooled down to room temperature (23°C ± 2°C). Then, the mixture was transferred to a 250 mL beaker, and the reactor was rinsed with ethyl acetate. The residues from the flask and the ethyl acetate were transferred to the 250 mL beaker that contained the mixture. Fifteen minutes later, the mixture was filtered and rinsed with ethyl acetate until the filtered liquid became colourless. The solids filtered were rinsed with 300 mL of distilled water and dried at 105°C in an oven. The dried sample was designated as "crude cellulose."

The remaining liquid from the filtration was used to recover lignin. The liquid was evaporated in a rotary evaporator to remove ethyl acetate, acetic acid, and water. The solids in the flask were vacuum dried overnight at 60°C and were designated as "crude lignin." The crude cellulose and crude lignin were weighed after being dried, and their yields were calculated using the following equations:

$$\textbf{Crude cellulose yield} = \frac{W_{cc}}{W_c} \times 100\% \quad \textbf{Equation 11}$$

$$\textbf{Crude lignin yield} = \frac{W_l}{W_c} \times 100\% \quad \textbf{Equation 12}$$

where w_{cc} is the crude cellulose weight, w_c is the oven-dried cornstalk weight before fractionation, and w_l is the crude lignin weight.

5.2.2.2 Crude cellulose bleaching

Crude cellulose extracted from cornstalk was bleached using sodium chlorite. This procedure [94] was performed to compare the effects of lignin removal on Bio-SAP synthesis. In a 250 mL Erlenmeyer flask, 2.5 g of crude cellulose, 80 mL of distilled water at 50°C, 0.5 mL of acetic acid, and 1.0 g of sodium chlorite were mixed. The flask was then heated in a water bath at 70°C for 8 h while stirring. Every 60 min, an additional 0.5 mL of acetic acid and 1.0 g of sodium chlorite were incorporated into the mixture. Then, the mixture was taken out of the bath, and it cooled down to room temperature. The mixture was then filtered, and the solid residues were rinsed (with distilled water) and vacuum dried at 65°C for 24 h. The dried solid residues obtained were weighed and designated as "bleached cellulose." Finally, the bleached cellulose was ground and sieved to obtain an average particle size of 2 mm through a No. 10 standard sieve mesh (ASTM 11 standard sieve).

5.2.2.3 Characterization of crude cellulose

5.2.2.3.1 Residual lignin content and crude cellulose purity analysis

Three major components of the crude cellulose were determined according to NREL/TP-510-42618 [227]. The sulfuric acid hydrolysis method was used to calculate the residual lignin content (Klason lignin, acid insoluble). A sample of 0.3 g of crude cellulose was transferred into a glass tube ($\phi 16 \times 100$ mm); then, 4.92 g of a 72% w/v sulfuric acid solution was added to the tube. The tube was sealed and transferred to a water shaker at 30°C, and after 120 min, the mixture was transferred into a 100 mL glass pressure reactor containing 84 g of distilled water. The glass pressure reactor was sealed and placed in an oil bath at 121°C and stirred for 60 min. Subsequently, the mixture was removed from the reactor, left to cool down to room temperature (23°C ± 2°C), and then filtered. The lignin residues were rinsed with distilled water until the filtration liquids were colourless. Then,

the lignin residues were placed in the oven and dried at 105°C for 24 h. The dried product was designated as "residual lignin" and weighed. Therefore, the residual lignin content in the crude cellulose was calculated using Equation 13:

$$\textbf{Residual lignin content in crude cellulose} = {}^{\textbf{w}_{\textbf{rl}}}\!/_{\textbf{w}_{\textbf{cc}}} \textbf{ x 100\%} \qquad \textbf{Equation 13}$$

where w_{rl} is the residual lignin weight (after sulfuric acid hydrolysis), and w_{cc} is the crude cellulose weight (before hydrolysis).

In addition, a modified chlorination method was used to test cellulose purity by determining the holocellulose content. In a 250 mL Erlenmeyer flask, the following were mixed: 2.5 g of crude cellulose, 80 mL of distilled water at 50°C, 0.5 mL of acetic acid, and 1.0 g of sodium chlorite. The flask was sealed and heated in a water bath at 70°C for 32 h while stirring. Every 60 min for the first 8 h, an additional 0.5 mL of acetic acid and 1.0 g of sodium chlorite were incorporated into the mixture. Then, the flask was left in the water bath for the remaining 24 h. The flask was then removed and left to cool down; the mixture was filtered, and the solids were rinsed with acetone. The holocellulose residues were vacuum dried at 65°C for 24 h and weighed. Finally, crude cellulose purity was calculated using Equation 14:

$$\textbf{Crude cellulose purity} = {}^{\textbf{w}_{\textbf{h}}}\!/_{\textbf{w}_{\textbf{cc}}} \textbf{ x 100\%} \qquad \textbf{Equation 14}$$

where w_h is the dried holocellulose weight, and w_{cc} is the weight of crude cellulose used in the chlorination method.

Likewise, the α-cellulose and hemicellulose content in the crude cellulose was calculated by testing the previously obtained holocellulose. In a 200 mL glass flask reactor, 2.0 g of dried holocellulose and 30 mL of 17.5% w/w NaOH solution were mixed for 5 min. Then, 15 mL of 17.5% w/w NaOH solution was added and stirred. After 40 min (23°C ± 2°C), 99 mL of distilled water was added, and stirring continued for an additional 60 min. The mixture was then filtered, and the solid residues were transferred to a 250 mL beaker, rinsed with 8.3% w/w NaOH solution at room temperature (23°C ± 2°C), and filtered. Then, the solids were washed three times with distilled water. Subsequently,

filtration was performed; the first 15 mL of 10% w/v acetic acid solution was added to the solids, and then the solids were filtered and rinsed with distilled water until the acetic acid was entirely removed, which was confirmed using a pH meter. Finally, the solids were dried at 105°C for 24 h, weighed, and designated as "α-cellulose." The contents of cellulose and hemicellulose were calculated using Equation 21 and 22, respectively:

$$\boldsymbol{\alpha - \textbf{cellulose content} = \frac{\textbf{w}_\alpha \times \textbf{cellulose purity}}{\textbf{w}_{ho}} \times \textbf{100\%}} \qquad \textbf{Equation 15}$$

$$\textbf{Hemicellulose content} = \frac{(\textbf{w}_{ho} - \textbf{w}_\alpha) \times \textbf{cellulose purity}}{\textbf{w}_{ho}} \times \textbf{100\%} \qquad \textbf{Equation 16}$$

where w_α is the weight of α-cellulose in holocellulose, and w_{ho} is the weight of the holocellulose used in the α-cellulose and hemicellulose content test.

5.2.2.3.1.1 Infrared spectroscopy

Cornstalk, crude cellulose, and CrudeCellulo-SAP samples were characterized by quantifying functional groups via FTIR spectroscopy (spectrometer Frontier FTIR Perkin Elmer). The wavelength of the infrared was 4000–550 cm^{-1} with a resolution of 4 cm^{-1}. The KBr method was used to obtain the characteristic spectra of the samples; in this method, 0.0050 g of a completely dry sample was added to 0.1500 g of pure KBr (1:30 w/w ratio) and mixed. Then, the pulverized mixture was compacted, applying a force of around 8 tonnes for 2 min, forming a pellet. The pellet was then placed into the sample chamber to perform the measurement.

5.2.2.3.2   X-ray diffraction analysis

XRD was applied to the crystalline forms of the pure cornstalk, crude cellulose, and pure cellulose samples using Cu Kα radiation with a wavelength of 0.1541 nm on a diffractometer (PANalytical X'Pert PRO X-ray). An X-ray beam was generated (at 30 kV and 15 mA) and directed at the samples. The detection of the dissipated radiation was detected over an angular area of 3 to 70°, at a step size of 0.02, at ambient temperature and rate of 10°/min.

5.2.2.3.3   Scanning electron microscopy

SEM images of crude cellulose were taken with a Zeiss/Leo 1530 FESEM (3 kV accelerating voltage). Before the image was obtained, the samples were coated with 10 nm of osmium to improve their conductivity and avoid charging.

5.2.2.3.4   Degree of substitution of –COOH groups: back titration

The amount of –COOH groups in a crude cellulose sample was determined using back titration. The crude cellulose was mixed with a NaOH standard solution; then, this mixture (crude cellulose–NaOH standard solution) was titrated with a HCl standard solution. The volume of HCl standard solution was used to calculate the DS of –COOH in crude cellulose. This methodology is explained in Appendix A.

5.2.2.4 Crude cellulose gel synthesis

Table 21 shows the experimental preparation formulations for Cellulo-SAP and CrudeCellulo-SAP.

Table 21: Formulations for Cellulo-SAP and CrudeCellulo-SAP

Cellulo-SAP	Mass (g)	CrudeCellulo-SAP
Cell-MA (DS=1.2)	2.0	*crude cellulose*
acrylic acid	4.0	acrylic acid
ammonium persulfate	0.09	ammonium persulfate
PEGA500	0.4	PEGA500
urea	5.7	urea
DON (36.7%)	1.2 (NaOH)	DON (36.7%)
water	25.4	water

A CrudeCellulo-SAP sample was prepared with the following reagents: NaOH, urea, crude cellulose, deionized water, APS, acrylic acid, and PEGA500. At the beginning of the procedure, the following contents were mixed in a 250 mL flask: 1.2 g of NaOH, 4 g of urea, 30 g of deionized water, and 2 g of crude cellulose. The mixture was stirred at room temperature (23°C ± 2°C) for 30 min. Subsequently, 0.09 g of APS was added. Next, 4 g of acrylic acid was added to the mixture as the mixture was stirred; it was added dropwise to maintain a temperature below 60°C. The acrylic acid, which was stirred into the mixture for 10 min, neutralized. Finally, the PEGA500 was added to the mixture, and the flask was transferred to a hot oil bath at 70°C, where the mixture was stirred until it became a gel.

5.2.2.5 Preparation of CrudeCellulo-SAP after synthesis

Following the synthesis reaction, the gel was washed to remove non-reacted compounds and dried, becoming a SAP. The washing process involved the following. The gel was transferred to a 250 mL flask containing 200 mL of 75% v/v ethanol aqueous solution and left to soak for 12 h. Then, the gel was removed from the solution, transferred to another flask with 200 mL of fresh 75% v/v ethanol aqueous solution, and left to soak for 5 h. Next, the process was replicated: the ethanol solution was replaced by a fresh solution, and the gel was left to soak for another 5 h. Subsequently, the gel was removed from the solution and cut into small pieces. Then, it was transferred to a flask to soak with anhydrous ethanol for 2 h. Subsequently, the anhydrous ethanol was removed from the gel, and the solution was replaced by fresh anhydrous ethanol and left to soak for another 2 h. Finally, the gel was filtered and then dried in a vacuum oven for 24 h; in its non-swollen, dried state, the gel had become a SAP. The SAP was ground and sieved to obtain an average particle size of 2 mm through a No. 10 standard sieve mesh (ASTM 11 standard sieve).

5.2.2.5.1 Absorption capacity of Cellulo-SAP

In this dissertation, AC is a weight fraction (g/g) and a parameter used to discuss swelling performance. AC was calculated following a standard gravimetric methodology [183]. CrudeCellulo-SAP samples were meticulously dried, ground, and sieved (No. 10 standard

sieve mesh, ASTM 11 standard sieve) to achieve an average particle size of 2 mm. Next, 0.05 g (± 0.001 g) CrudeCellulo-SAP samples were immersed in 200 mL of deionized water at 23°C ± 2°C for one day, during which time the samples developed into hydrogels. The obtained hydrogels were then removed from the liquid and filtered, and the remaining liquid was removed using dry tissues. The hydrogels were weighed, and the AC was calculated using Equation 1:

$$AC = \frac{w_2 - w_1}{w_1} \quad \textbf{Equation 1}$$

where w_1 is the weight of the dry CrudeCellulo-SAP samples, and w_2 is the weight of the hydrogel. The complete AC analysis method was performed three times.

5.3 Results and discussion

5.3.1 Characterization of cornstalk and crude cellulose

In this study, organosolv fractionation was used to extract crude cellulose from cornstalk. The characterization of the crude cellulose revealed its chemical composition. Consequently, the discoveries of Chapters 2 and 3 were applied to the development of Cellulo-SAP. The crude cellulose's chemical composition (Table 22) was analyzed using techniques such as hydrolysis with sulfuric acid and alkali chlorination.

Table 22: Chemical composition of crude cellulose from cornstalk fractionation

Chemical composition of cornstalk crude cellulose (% w)	
Residual lignin content	13.87
Hemicellulose	27.58
α-cellulose	57.46
Cellulose purity	90.64
Crude cellulose yield	45.15

Crude cellulose was compared with cornstalk; crude cellulose's α-cellulose content (57.46% w) was higher than cornstalk's α-cellulose content (35.31% w), but crude cellulose's hemicellulose (27.58% w) and lignin (9.87% w) contents were lower than cornstalk's hemicellulose (32.58% w) and lignin (15.57% w) contents. These values suggest a successful cellulose extraction from the cornstalk during the organosolv fractionation. The cornstalk and the crude cellulose extracted were photographed (Figure 59). Figure 59A shows the cornstalk before organosolv fractionation, and Figure 59B shows the crude cellulose obtained via organosolv fractionation.
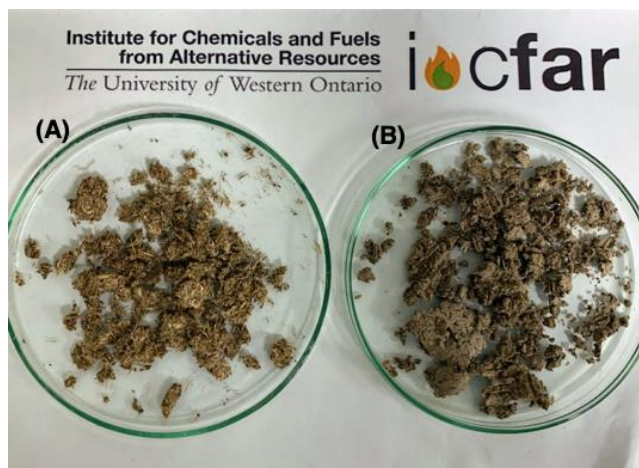
Figure 59: (A) cornstalk and (B) crude cellulose extracted from cornstalk

5.3.1.1   Scanning electron microscopy analysis

Figure 60 shows scanning electron micrographs of the surface of cornstalk, and Figure 61 shows micrographs of the extracted crude cellulose. The cornstalk fibres seemed to be formed by microfibrils that integrated in a matrix composed of individual cells corresponding to cellulose bundles, hemicellulose, and lignin [228]. After the organosolv fractionation, the hemicellulose and lining were partially removed, and the microfibrils of the cellulose bundle were separated from each other, producing fibrils [229]. Moreover, after modification, the cornstalk fibres, with a ribbon shape, appeared to have larger diameters than the crude cellulose fibrils.
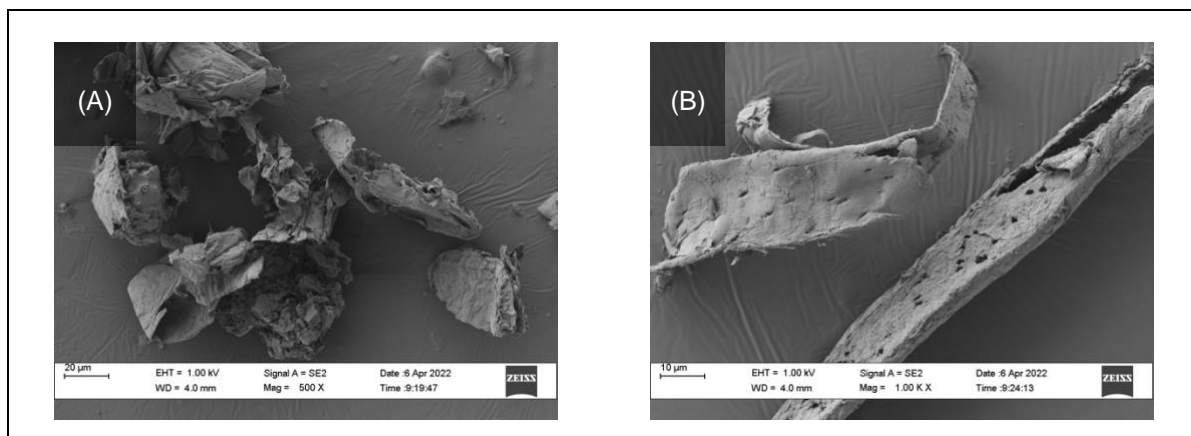
Figure 60: SEM images of the surface of cornstalk at (A) 500× and (B) 1000× magnification
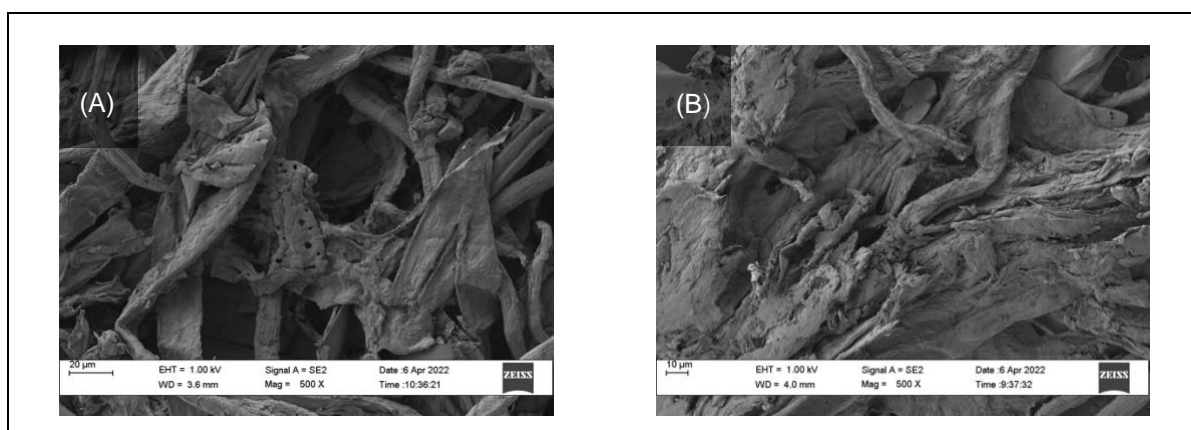
Figure 61: SEM images of crude cellulose obtained via organosolv fractionation of cornstalk: (A) cross section and (B) surface

5.3.1.2 Infrared spectroscopy of crude cellulose and cornstalk

Figure 62 shows the FTIR spectrum of cornstalk. The results showed cellulose's typical broad peak at 3423 cm^{-1}, which corresponds to the –OH stretch, and at 2898 cm^{-1}, which corresponds to the CH stretch [229]. Also, the C=O stretch was observed in the absorption bands at 1732 cm^{-1} and 1238 cm^{-1}, representing the hemicellulose's acetyl group [230]. At 1604 cm^{-1}, the stretch corresponds to the C=C ring, and at 1516 cm^{-1}, the CH stretch of the methyl, methylene, and methoxyl groups indicated the presence of lignin [231]. Interestingly, these peaks were not observed in the crude cellulose, which revealed that hemicellulose and lignin were extracted during the organosolv fractionation.

Nonetheless, it was also observed that slight esterification occurred during the organosolv fractionation. In the spectrum of crude cellulose, this effect was observed and possibly was due to the ester band stretch C=O at 1726 cm^{-1} [231].
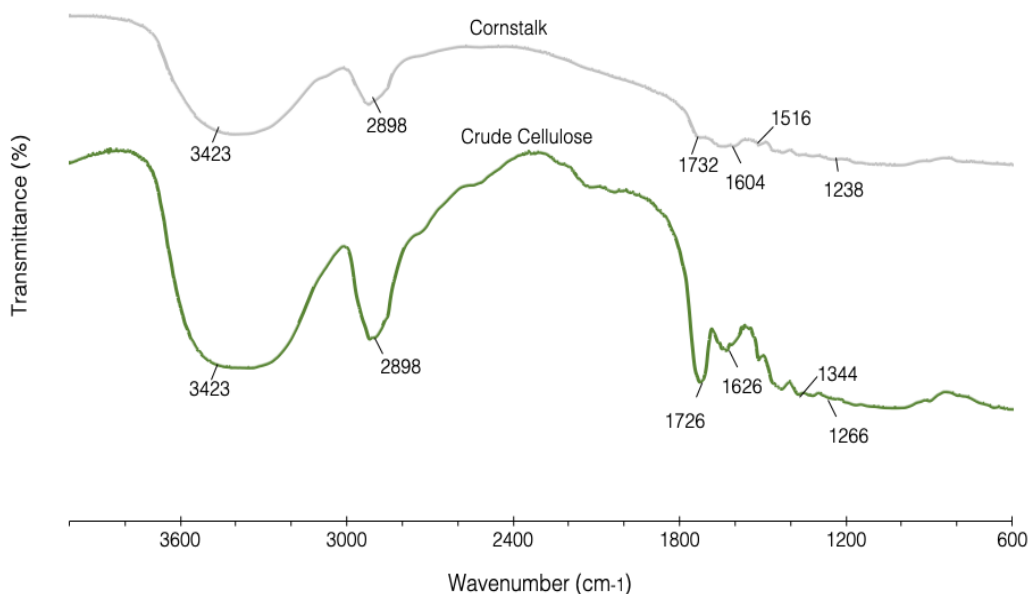
Figure 62: FTIR spectra of cornstalk and crude cellulose

5.3.1.2.1 Degree of substitution of –COOH groups: back titration

The back titration method showed a DS value of 0.41 in crude cellulose. This result indicated that during the organosolv fractionation, a simultaneous separation and esterification of cellulose occurred. Therefore, three 0.25 g samples of crude cellulose were placed in a flask and mixed with ~0.100 M NaOH standard solution. Then, the mixture, which had a brownish colour, was titrated with ~0.100 M HCl standard solution until the pH meter indicated 8.6. The volume of wasted HCl was recorded for each sample, and this data was used to calculate the average. Then, the crude cellulose resulted in the following DS: 0.41 ± 0.36. This result verified the observations made on the FTIR spectrum regarding the crude cellulose's ester group presence. It is likely that during the cellulose fractionation with the acetic acid–formic acid–water solvent mix, simultaneous separation and esterification occurred.

5.3.1.3 X-ray diffraction analysis

Cornstalk and crude cellulose crystallinity were analyzed using powder XRD. The distinctive peaks of the cellulose pattern were revealed by the diffractogram, in which the cornstalk and crude cellulose showed peaks at 15.5° and 16.2°, corresponding to the (101) [168] and (002) planes [232], respectively. The cornstalk and crude cellulose peaks showed higher FWHM values compared to the pure cellulose peaks. Higher FWHM values indicate a lower crystallinity, meaning that cornstalk and crude cellulose have a less orderly structure and are more amorphous than pure cellulose [233].

Moreover, the organosolv fractionation could have degraded the cornstalk and simultaneously modified the crude cellulose. In the diffractogram, the peak at 27.9° was only present in the crude cellulose sample. Likewise, a distinctive peak was identified at 30°, indicating the presence of a –COOH group in crude cellulose. Its presence corroborates that the esterification of crude cellulose occurred due to the use of acetic acid in the organosolv fractionation. Acetic acid can form esters at 50–70°C and under acidic conditions. In this study, the organosolv fractionation was run at 90°C using a strong acid (HCl) as a catalyst, which provided a high temperature and acidic conditions. Additionally, the crude cellulose's esterification might have occurred in its crystalline region [234].

In the amorphous region of cellulose at 18°, the diffraction intensity was higher in the crude cellulose than in the pure cellulose, due to crude cellulose's less orderly region of cellulose chains [235]. The crystalline structure of pure cellulose makes the functionalization of its –OH groups difficult. This difficulty can be resolved by reducing cellulose's crystallinity, causing an increase in amorphous areas, which can be accessed by functional agents [236]. In the case of cornstalk, a naturally amorphous raw material, esterification is easier; it can take place at the same time as the disintegration of its components [237]. Figure 63 presents the XRD patterns of cornstalk, crude cellulose, and pure cellulose.
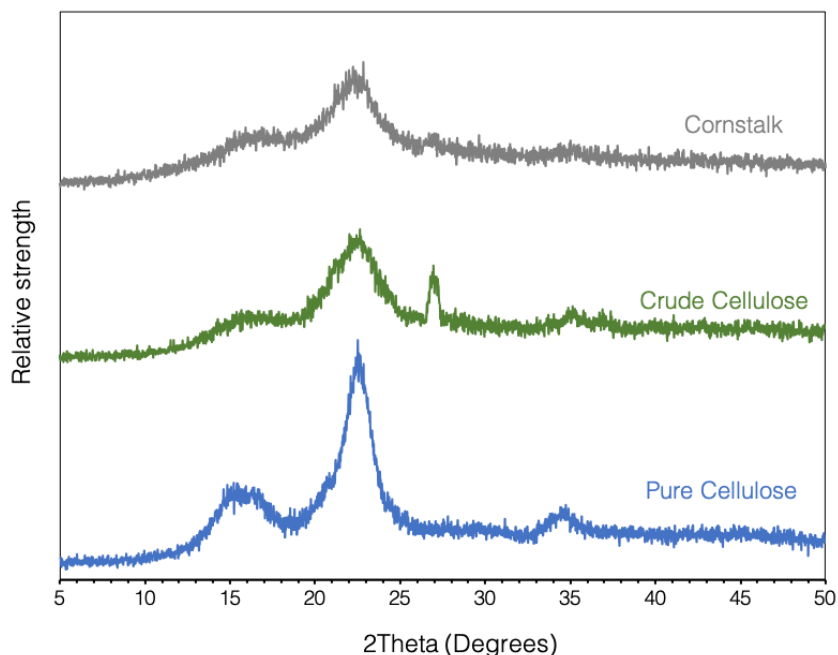
Figure 63: XRD patterns of cornstalk, pure cellulose, and crude cellulose

5.3.2   Absorption capacity of CrudeCellulo-SAP

The AC value is the most crucial parameter when measuring the performance of SAPs. Figure 64 shows a CrudeCellulo-SAP sample before and after reaching AC equilibrium. Initially, the polymeric network had a collapsed appearance and was brown, which is characteristic of lignin presence in the crude cellulose. When the CrudeCellulo-SAP was hydrated, it developed a three-dimensional appearance and became more transparent than brown. CrudeCellulo-SAP absorbed up to 369 ± 0.81 g/g of deionized water. The AC of CrudeCellulo-SAP was lower than the AC of other Bio-SAPs, such as sawdust–acrylic acid/acrylamide (738 g/g) [202] and corncob cellulose–polyvinylpyrrolidone (ca. 1200 g/g) [205]. However, CrudeCellulo-SAP's mass ratio of cellulose–copolymer is 1:2, substantially smaller than that of sawdust–acrylic acid/acrylamide (1:8) and that of corncob cellulose–polyvinylpyrrolidone (1:20); this difference is due to CrudeCellulo-SAP's higher mass content of crude cellulose.
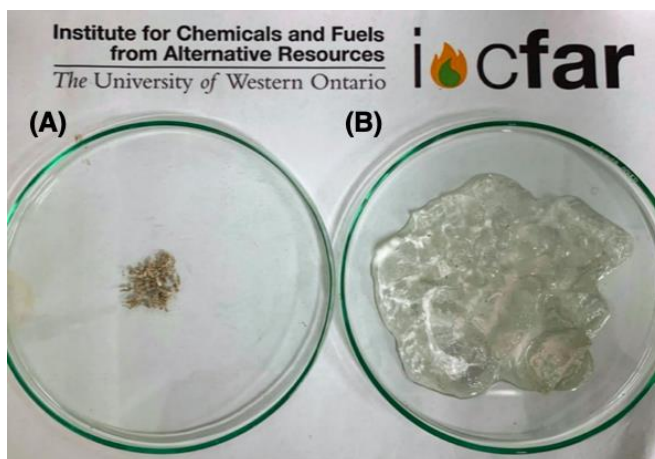
Figure 64: Physical transformation from CrudeCellulo-SAP to hydrogel: (A) completely dried 0.5 g CrudeCellulo-SAP sample; (B) hydrogel after reaching AC equilibrium in deionized water

Figure 65 presents the AC values of Cellulo-SAP and CrudeCellulo-SAP at equilibrium in deionized water as well as the percentage of each component. The reagents in the formulation had the same weight composition. For Cellulo-SAP, pure cellulose was used for esterification and then synthesis; for CrudeCellulo-SAP, crude cellulose underwent synthesis without esterification.
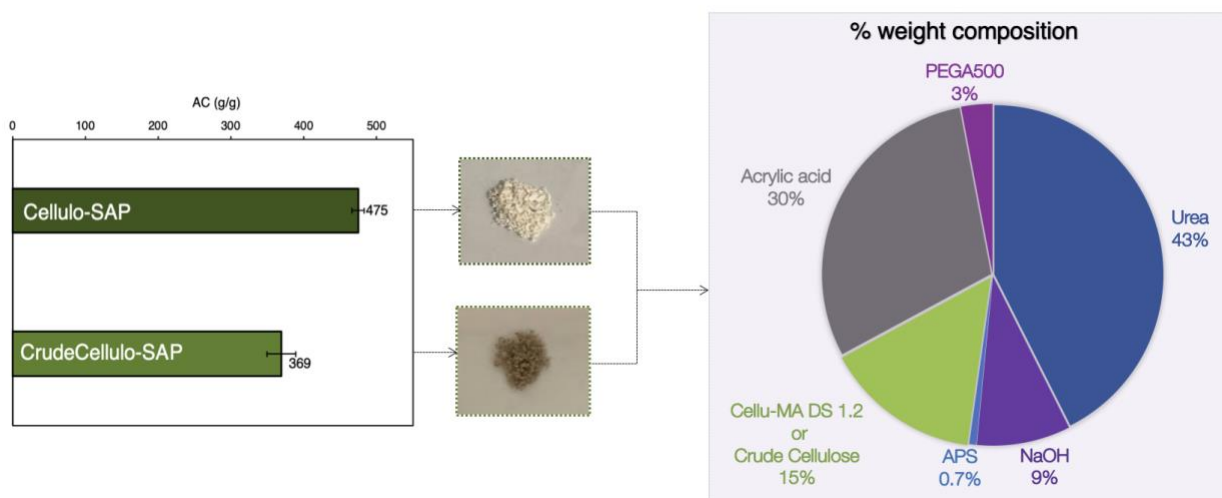
Figure 65: Cellulo-SAP's and CrudeCellulo-SAP's AC and their reagents' % weight compositions

Both samples were prepared with a mass ratio of bio-based component (cellulose) to copolymer (acrylic acid) of 1:2. Moreover, the 15% w of cellulose was preserved since the other components of both Bio-SAPs maintained the same mass composition. Therefore, any change in the AC response can be attributed to the type of cellulose added. CrudeCellulo-SAP's AC was lower than Cellulo-SAP's AC (369 ± 0.81 g/g vs. 475 ± 0.43 g/g). Importantly, the crude cellulose in CrudeCellulo-SAP was used without modification, whereas in Cellulo-SAP, the pure cellulose underwent esterification. To obtain the pure cellulose used in Cellulo-SAP, cellulosic material had to undergo processes such as separation and purification. Overall, more processes are involved in obtaining pure cellulose than in obtaining crude cellulose.

Cell-MA's DS was 1.2, whereas crude cellulose's DS was only 0.41 ± 0.36. Crude cellulose's lower DS could explain CrudeCellulo-SAP's lower AC; however, it is worth mentioning that no other treatment was given to the crude cellulose. The crude cellulose was esterified during fractionation; therefore, its processing was more efficient than that of pure cellulose.

Crude cellulose might be more susceptible to reaction because it has a less orderly structure than pure cellulose; therefore, the dissolution with NaOH–urea solution and synthesis were more efficient with crude cellulose than with pure cellulose. In the experiments performed with pure cellulose in Chapters 2 and 3, the main challenges to using cellulose and obtaining a Bio-SAP with the desired properties were the esterification and dissolution. Therefore, crude cellulose's conditions—in terms of its esterification and amorphous structure—are advantages when it is used as a raw material for Bio-SAP production.

5.3.3   FTIR analysis of CrudeCellulo-SAP

Blank was obtained following the formulation (Table 21) and methodology used to obtain Cellulo-SAP. However, Blank was prepared without cellulose. The FTIR spectrum of Blank were collected in Figure 66 and reported with the crude cellulose FTIR spectrum of CrudeCellulo-SAP and crude cellulose. The spectrum results showed that CrudeCellulo-SAP had characteristic peaks at 3423 cm^{-1} and 2926 cm^{-1}—similar to crude

cellulose's peaks at 3423 cm^{-1} and 2898 cm^{-1} [190], which correspond to the –OH and CH stretches, respectively. Moreover, the peaks at 1698 cm^{-1} and 1726 cm^{-1} correspond to –COOH stretch. Blank showed a peak at 1635 cm^{-1} that corresponds to C=C stretch. In addition, the peak found at 1045 cm^{-1} in Cellulo-SAP and Blank corresponds to the CH$_2$ bend. In the Blank spectrum, this peak is distinctive of acrylic polymers and corroborates a successful formation of polyacrylane carbon. CrudeCellulo-SAP's spectrum showed representative acrylane groups, which indicated a successful graft copolymerization of crude cellulose with acrylic acid [191].
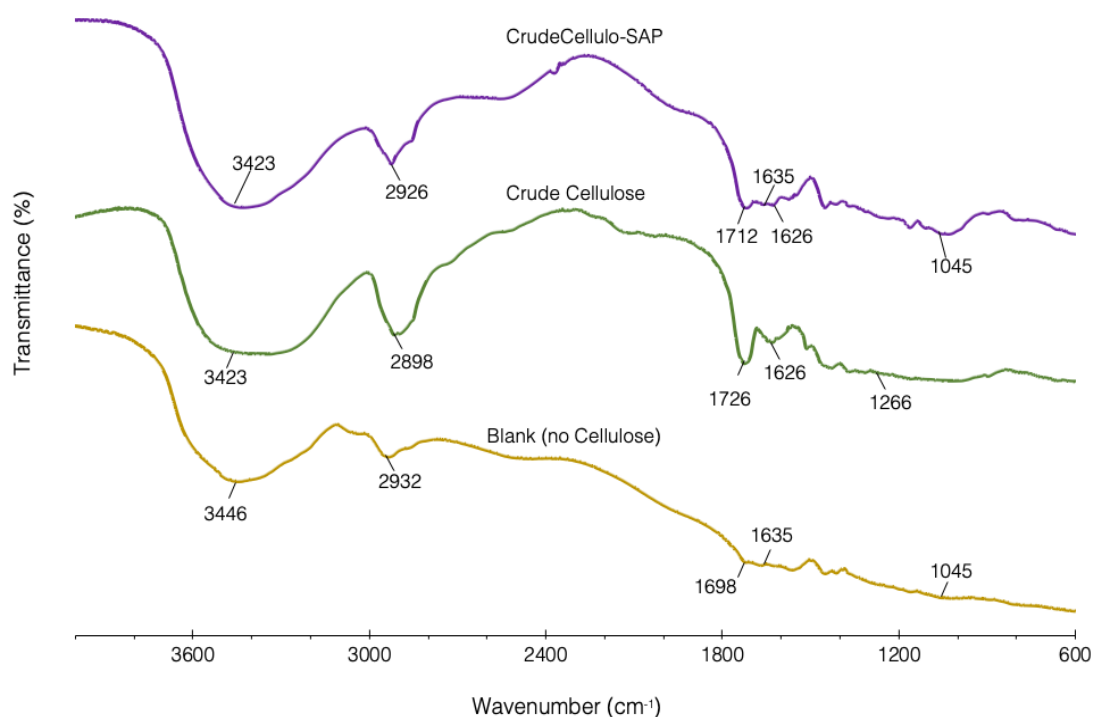
Figure 66: FTIR spectra of crude cellulose, CrudeCellulo-SAP, and Blank

5.3.4   Scanning electron microscopy

SEM was used to analyze the morphology of the synthesized CrudeCellulo-SAP sample. Photographs in Figure 67 show the surface of CrudeCellulo-SAP at a magnification of (A) 500× and (B) 1000×. The sample showed a dense SAP network formed by irregular ribbon-shaped fibres whose diameters ranged from 2 μm to 20 μm. The surface micrograph revealed that graft copolymerization with acrylic acid significantly altered the

crude cellulose fibrils, creating a more compact structure with irregular unions between these fibrils. The space between these fibrils probably created irregular, interconnected pores, which would account for CrudeCellulo-SAP's high AC. The pores were elongated and extended throughout the sample, creating long channels that probably had flexible lattices. In a SAP, such lattices allow liquids to expand the pores and thereby enhance the SAP's swelling capacity.
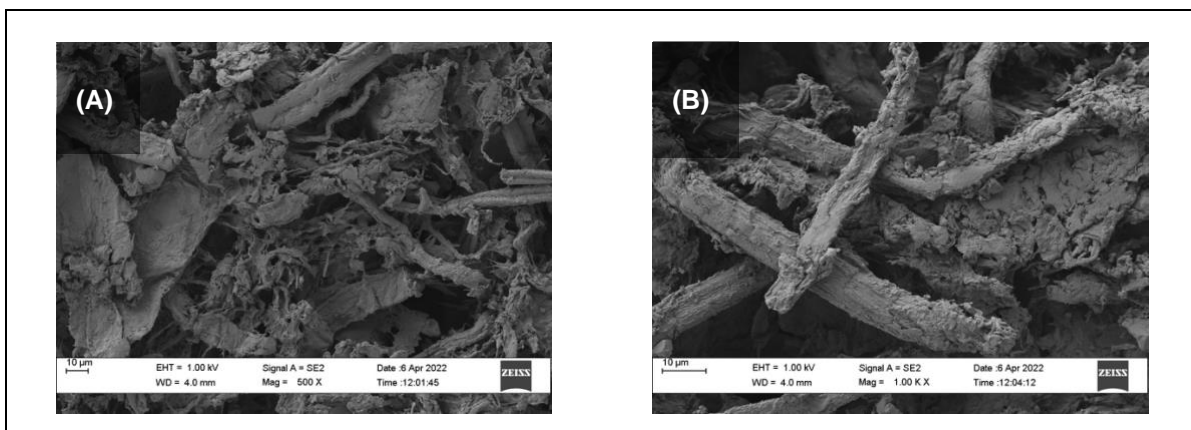
Figure 67: SEM images of the CrudeCellulo-SAP surface at (A) 500× and (B) 1000× magnification

5.4   Conclusions

Crude cellulose was obtained via organosolv fractionation using biomass from cornstalk residues and an acetic acid–formic acid–water mix. Crude cellulose comprised a composition of 13.87% lignin, 27.58% hemicellulose, and 57.46% α-cellulose. It had a DS of 0.41 after fractionation. Through the application of the methodology developed for Cellulo-SAP synthesis, crude cellulose was used as a raw material to obtain CrudeCellulo-SAP, which had an AC of 369 g/g.

Chapter 6

6   Conclusions

6.1   Contributions

Cellulose, a major component of plants, is the most abundant natural organic polymer. It is a glucose polymer that gives plant cells rigidity. Crop residues—such as cornstalk—which contain 30–50% cellulose, constitute an immense source of cellulose worldwide. For example, the annual production of crop residues amounts to more than 30 million tonnes in Canada, more than 700 million tonnes in China, and more than 1.3 billion tonnes in the United States. Currently, agricultural residues are mainly used as livestock bedding on farms and as solid fuels for heat/power generation; alternatively, in some Asian countries (e.g., China and India), they are disposed of via open-field burning, which generates severe environmental emissions. Therefore, the development of transformative technologies for the valorization of crop residues is urgently needed. The present study produced high-value bioproducts: Cellulo-SAP and CrudeCellulo-SAP. The latter is particularly significant due to its environmental and economic benefits, which arise from its use of crude cellulose derived from crop residues.

Pure cellulose and crude cellulose can be used to produce high-AC Bio-SAPs. However, cellulose-based SAP synthesis presents technical challenges due to the high crystallinity of cellulose, which makes it low in reactivity. In the present study, these challenges were addressed through pure cellulose esterification, which enhanced the reactivity of pure cellulose. Moreover, the crude cellulose obtained via organosolv fractionation using an acetic acid–formic acid–water solvent mix was sufficiently esterified; therefore, the crude cellulose's reactivity was also enhanced. Both types of cellulose were used to obtain SAPs via free radical graft copolymerization with acrylic acid. The obtained cellulose-based SAPs had high AC values and, therefore, could replace fossil-based SAPs in agricultural contexts. Cellulose-based SAPs could be used as biodegradable soil water retainers.

This dissertation has contributed to scientific knowledge by presenting an alternative cellulose-based SAP. It has proved that modifying pure cellulose via esterification with maleic anhydride and acetic acid can enhance SAPs' absorption properties. Additionally, this work has provided an optimal formulation for obtaining a pure cellulose-based SAP (Cellulo-SAP) and a crude cellulose-based SAP (CrudeCellulo-SAP). This formulation has a cellulose–copolymer mass ratio of 1:2 and, therefore, has a higher content of cellulose than the formulations used to produce other state-of-the-art cellulose-based SAPs. Furthermore, the environmentally friendly SAPs presented in this dissertation, when compared to commercial fossil-based SAPs, had comparable AC values and higher biodegradability.

This dissertation proved to be successful in the use of lignocellulosic residue biomass to obtain a Bio-SAP. The proposed formulation involved fractionating crude cellulose and using it without bleaching treatment. The cellulose fractionation selected was an organosolv method. By using organic solvents, including acetic acid, the following objectives were attained: i) obtaining crude cellulose and ii) esterifying the crude cellulose to increase the AC of Bio-SAPs.

6.2 Conclusions

Cellulose-based SAPs with high AC were obtained via two main steps: pure cellulose esterification and free radical graft copolymerization with acrylic acid. The esterification substantially improved the absorption properties of the SAPs. Subsequently, this methodology was used to produce crude cellulose-based SAPs. The crude cellulose was obtained via organosolv fractionation using cornstalk and an acetic acid–formic acid– water solvent mix; importantly, the obtained crude cellulose was sufficiently esterified; therefore, additional esterification was not performed. The free radical graft copolymerization with acrylic acid was conducted using the same formulation and under the same conditions for both Cellulo-SAP and CrudeCellulo-SAP.

6.3 Recommendations

- This research can serve as a foundation for studying the effects of esterification on crude cellulose. In the present study, the separation of crude cellulose from biomass and esterification were conducted simultaneously during organosolv fractionation, but this simultaneous process requires further investigation.

- The optimal degree of esterification and conditions during organosolv fractionation in cellulose-based SAP production should be further investigated with the aim of improving AC.

- The absorbency, stability, reusability, and biodegradability of CrudeCellulo-SAP should be evaluated.

- The efficacy of Cellulo-SAP and CrudeCellulo-SAP as substitutes for fossil-based SAPs in food packaging and hygiene domains should be evaluated.

- The effects and cost benefits of applying Cellulo-SAP and CrudeCellulo-SAP in a greenhouse or agricultural field should be evaluated.

References

[1]   Laftah WA, Hashim S, Ibrahim AN. Polymer hydrogels: A review. Polym - Plast Technol Eng 2011;50:1475–86. doi:10.1080/03602559.2011.593082.

[2]   Zohuriaan-Mehr M, Journal KK-I polymer, 2008 U. Superabsorbent polymer materials: a review. ResearchgateNet n.d.;17.

[3]   Ottenbrite RM, Park K, Okano T. Biomedical Applications of Hydrogels Handbook. Biomed. Appl. Hydrogels Handb., 2010. doi:10.1007/978-1-4419-5919-5.

[4]   Bakass M, Mokhlisse A, Lallemant M. Absorption and desorption of liquid water by a superabsorbent polymer: Effect of polymer in the drying of the soil and the quality of certain plants. J Appl Polym Sci 2002;83:234–43. doi:10.1002/app.2239.

[5]   Ma CJ, Kasahara M, Tohno S. Application of polymeric water absorbent film to the study of drop size-resolved fog samples. Atmos Environ 2003;37:3749–56. doi:10.1016/S1352-2310(03)00318-2.

[6]   Tanan W, Panichpakdee J, Saengsuwan S. Novel biodegradable hydrogel based on natural polymers: Synthesis, characterization, swelling/reswelling and biodegradability. Elsevier Ltd; 2018. doi:10.1016/j.eurpolymj.2018.10.033.

[7]   Chen J, Park H, Park K. Synthesis of superporous hydrogels: Hydrogels with fast swelling and superabsorbent properties. J Biomed Mater Res 1999;44:53–62. doi:10.1002/(SICI)1097-4636(199901)44:1<53::AID-JBM6>3.0.CO;2-W.

[8]   Borchard W, Jablonski P. The thermodynamic water retention capacity of solutions and gels. Water Res 2003;37:386–92. doi:10.1016/S0043-1354(02)00277-4.

[9]   Henry CJ, Brant JA, Kelleners TJ. Water transport mechanisms for salt-rejecting membranes driven by soil-water potentials. J Memb Sci 2018;563:107–14. doi:10.1016/j.memsci.2018.05.041.

[10]   Bao Y, Ma J, Li N. Synthesis and swelling behaviors of sodium carboxymethyl cellulose-g-poly(AA-co-AM-co-AMPS)/MMT superabsorbent hydrogel. Carbohydr Polym 2011;84:76–82. doi:10.1016/j.carbpol.2010.10.061.

[11]   Ahmed EM. Hydrogel: Preparation, characterization, and applications: A review. J Adv Res 2015;6:105–21. doi:10.1016/j.jare.2013.07.006.

[12]   Oyen ML. Mechanical characterisation of hydrogel materials. Int Mater Rev 2013;59:44–59. doi:10.1179/1743280413y.0000000022.

[13]   Khan S, Ullah A, Ullah K, Rehman NU. Insight into hydrogels. Des Monomers Polym 2016;19:456–78. doi:10.1080/15685551.2016.1169380.

[14]   Bannai M, Ichikawa M, Nishimura F, Nishihara M, Takahashi M. Water-absorbent polymer as a carrier for a discrete deposit of antisense oligodeoxynucleotides in the central nervous system. Brain Res Protoc 1998;3:83–7. doi:10.1016/S1385-299X(98)00027-0.

[15]   Andrade JD. Hydrogels for Medical and Related Applications. vol. 31. 1976. doi:10.1021/bk-1976-0031.

[16]   Li J, Mooney DJ. Designing hydrogels for controlled drug delivery. Nat Rev Mater 2016;1. doi:10.1038/natrevmats.2016.71.

[17]   Zhao W, Jin X, Cong Y, Liu Y, Fu J. Degradable natural polymer hydrogels for articular cartilage tissue engineering. J Chem Technol Biotechnol 2013;88:327–39. doi:10.1002/jctb.3970.

[18]   Senna AM, Botaro VR. Biodegradable hydrogel derived from cellulose acetate and EDTA as a reduction substrate of leaching NPK compound fertilizer and water retention in soil. J Control Release 2017;260:194–201. doi:10.1016/j.jconrel.2017.06.009.

[19]   Roshanizarmehri M, Fotovat A, Emami H, Kehl M, Hirmas DR, Hosseinalizadeh M, et al. Combined effects of polyacrylamide and nanomagnetite amendment on

soil and water quality, Khorasan Razavi, Iran. J Environ Manage 2018;223:703–12. doi:10.1016/j.jenvman.2018.06.061.

[20] Thombare N, Mishra S, Siddiqui MZ, Jha U, Singh D, Mahajan GR. Design and development of guar gum based novel, superabsorbent and moisture retaining hydrogels for agricultural applications. Carbohydr Polym 2018;185:169–78. doi:https://doi.org/10.1016/j.carbpol.2018.01.018.

[21] Fan R, Luo J, Yan S, Zhou Y, Zhang Z. Effects of Biochar and Super Absorbent Polymer on Substrate Properties and Water Spinach Growth. Pedosphere 2015;25:737–48. doi:10.1016/S1002-0160(15)30055-2.

[22] Chen Z, Wang R, Han P, Sun H, Sun H, Li C, et al. Soil water repellency of the artificial soil and natural soil in rocky slopes as affected by the drought stress and polyacrylamide. Sci Total Environ 2018;619–620:401–9. doi:10.1016/j.scitotenv.2017.11.146.

[23] Egrinya Eneji A, Islam R, An P, Amalu UC. Nitrate retention and physiological adjustment of maize to soil amendment with superabsorbent polymers. J Clean Prod 2013;52:474–80. doi:https://doi.org/10.1016/j.jclepro.2013.02.027.

[24] Hüttermann A, Orikiriza LJB, Agaba H. Application of superabsorbent polymers for improving the ecological chemistry of degraded or polluted lands. Clean - Soil, Air, Water 2009;37:517–26. doi:10.1002/clen.200900048.

[25] Qiao D, Liu H, Yu L, Bao X, Simon GP, Petinakis E, et al. Preparation and characterization of slow-release fertilizer encapsulated by starch-based superabsorbent polymer. Carbohydr Polym 2016;147:146–54. doi:10.1016/j.carbpol.2016.04.010.

[26] Ghazali S, Jamar S, Noordin N, Tan KM. Properties of Controlled-Release-Water-Retention Fertilizer Coated with Carbonaceous-g-Poly(acrylic acid-co-acrylamide)Superabsorbent Polymer. Int J Chem Eng Appl 2017;8:141–7. doi:10.18178/ijcea.2017.8.2.646.

[27]   Guilherme MR, Aouada FA, Fajardo AR, Martins AF, Paulino AT, Davi MFT, et al. Superabsorbent hydrogels based on polysaccharides for application in agriculture as soil conditioner and nutrient carrier: A review. Eur Polym J 2015;72:365–85. doi:10.1016/j.eurpolymj.2015.04.017.

[28]   Narjary B, Aggarwal P, Singh A, Chakraborty D, Singh R. Water availability in different soils in relation to hydrogel application. Geoderma 2012;187–188:94–101. doi:10.1016/j.geoderma.2012.03.002.

[29]   Yang L, Yang Y, Chen Z, Guo C, Li S. Influence of super absorbent polymer on soil water retention, seed germination and plant survivals for rocky slopes eco-engineering. Ecol Eng 2014;62:27–32. doi:10.1016/j.ecoleng.2013.10.019.

[30]   Cannazza G, Cataldo A, de Benedetto E, Demitri C, Madaghiele M, Sannino A. Experimental assessment of the use of a novel superabsorbent polymer (SAP) for the optimization of water consumption in agricultural irrigation process. Water (Switzerland) 2014;6:2056–69. doi:10.3390/w6072056.

[31]   Shen X, Shamshina JL, Berton P, Gurau G, Rogers RD. Hydrogels based on cellulose and chitin: Fabrication, properties, and applications. Green Chem 2015;18:53–75. doi:10.1039/c5gc02396c.

[32]   Sawut A, Yimit M, Sun W, Nurulla I. Photopolymerisation and characterization of maleylatedcellulose-g- poly(acrylic acid) superabsorbent polymer. Carbohydr Polym 2014;101:231–9. doi:10.1016/j.carbpol.2013.09.054.

[33]   Gao J, Yang Q, Ran F, Ma G, Lei Z. Preparation and properties of novel eco-friendly superabsorbent composites based on raw wheat bran and clays. Appl Clay Sci 2016;132–133:739–47. doi:10.1016/j.clay.2016.08.021.

[34]   Olad A, Zebhi H, Salari D, Mirmohseni A, Reyhani Tabar A. Slow-release NPK fertilizer encapsulated by carboxymethyl cellulose-based nanocomposite with the function of water retention in soil. Mater Sci Eng 2018;90:333–40. doi:https://doi.org/10.1016/j.msec.2018.04.083.

[35]   Essawy HA, Ghazy MBM, El-Hai FA, Mohamed MF. Superabsorbent hydrogels via graft polymerization of acrylic acid from chitosan-cellulose hybrid and their potential in controlled release of soil nutrients. Int J Biol Macromol 2016;89:144–51. doi:10.1016/j.ijbiomac.2016.04.071.

[36]   Fang S, Wang G, Li P, Xing R, Liu S, Qin Y, et al. Synthesis of chitosan derivative graft acrylic acid superabsorbent polymers and its application as water retaining agent. Int J Biol Macromol 2018;115:754–61. doi:10.1016/j.ijbiomac.2018.04.072.

[37]   Hamed OA, Jaber F, Hamed EM, Adwan K, Jodeh S, Salghi R, et al. New routes to prepare superabsorbent polymers free of acrylate cross-linker. Iran Polym J (English Ed 2015;24:849–59. doi:10.1007/s13726-015-0373-9.

[38]   Marandi GB, Hariri S, Mahdavinia GR. Effect of hydrophobic monomer on the synthesis and swelling behaviour of a collagen-graft-poly[(acrylic acid)-co-(sodium acrylate)] hydrogel. Polym Int 2009;58:227–35. doi:10.1002/pi.2520.

[39]   Almeida FCR, Klemm AJ. Efficiency of internal curing by superabsorbent polymers (SAP) in PC-GGBS mortars. Cem Concr Compos 2018;88:41–51. doi:10.1016/j.cemconcomp.2018.01.002.

[40]   Snoeck D, Schaubroeck D, Dubruel P, De Belie N. Effect of high amounts of superabsorbent polymers and additional water on the workability, microstructure and strength of mortars with a water-to-cement ratio of 0.50. Constr Build Mater 2014;72:148–57. doi:10.1016/j.conbuildmat.2014.09.012.

[41]   Pourjavadi A, Fakoorpoor SM, Hosseini P, Khaloo A. Interactions between superabsorbent polymers and cement-based composites incorporating colloidal silica nanoparticles. Cem Concr Compos 2013;37:196–204. doi:10.1016/j.cemconcomp.2012.10.005.

[42]   Schröfl C, Mechtcherine V, Gorges M. Relation between the molecular structure and the efficiency of superabsorbent polymers (SAP) as concrete admixture to

mitigate autogenous shrinkage. Cem Concr Res 2012;42:865–73. doi:10.1016/j.cemconres.2012.03.011.

[43]   Secrieru E, Mechtcherine V, Schröfl C, Borin D. Rheological characterisation and prediction of pumpability of strain-hardening cement-based-composites (SHCC) with and without addition of superabsorbent polymers (SAP) at various temperatures. Constr Build Mater 2016;112:581–94. doi:10.1016/j.conbuildmat.2016.02.161.

[44]   Yang S, Wang Y, Lin S, Fan J, Liu C, Yan X. Facile surface-engineered polymeric absorbents for simultaneous adsorption and degradation of organic wastes. Chemosphere 2018;191:17–22. doi:10.1016/j.chemosphere.2017.10.019.

[45]   Lu Y, Yuan W. Superhydrophobic three-dimensional porous ethyl cellulose absorbent with micro/nano-scale hierarchical structures for highly efficient removal of oily contaminants from water. Carbohydr Polym 2018;191:86–94. doi:10.1016/j.carbpol.2018.03.018.

[46]   Venkatachalam D, Kaliappa S. Superabsorbent polymers: A state-of-art review on their classification, synthesis, physicochemical properties, and applications. Rev Chem Eng 2021. doi:10.1515/REVCE-2020-0102/ASSET/GRAPHIC/J_REVCE-2020-0102_FIG_015.JPG.

[47]   Naumann D'Alnoncourt R, Csepei LI, Hävecker M, Girgsdies F, Schuster ME, Schlögl R, et al. The reaction network in propane oxidation over phase-pure MoVTeNb M1 oxide catalysts. J Catal 2014. doi:10.1016/j.jcat.2013.12.008.

[48]   Centi G, Grasselli RK, Trifiro F. Propane ammoxidation to acrylonitrile - an overview. Catal Today 1992. doi:10.1016/0920-5861(92)80106-W.

[49]   Cuadri AA, Romero A, Bengoechea C, Guerrero A. Natural superabsorbent plastic materials based on a functionalized soy protein. Polym Test 2017. doi:10.1016/j.polymertesting.2016.12.024.

[50]   Zohuriaan-Mehr M, Motazedi Z, Kabiri K, Ershad-Langroudi A. New super-

absorbing hydrogel hybrids from gum arabic and acrylic monomers. J Macromol Sci - Pure Appl Chem 2005;42 A:1655–66. doi:10.1080/10601320500246859.

[51]   Moerdyk JP, Bielawski CW. Architectures of Polymers Synthesized using ROMP. Polym. Sci. A Compr. Ref. 10 Vol. Set, vol. 4, Elsevier; 2012, p. 523–50. doi:10.1016/B978-0-444-53349-4.00094-7.

[52]   Maiti S, Jana S. Polysaccharide carriers for drug delivery. Elsevier; 2019. doi:10.1016/C2017-0-02351-0.

[53]   Lu L, Yuan S, Wang J, Shen Y, Deng S, Xie L, et al. The Formation Mechanism of Hydrogels. Curr Stem Cell Res Ther 2018;13:490–6. doi:10.2174/1574888X12666170612102706.

[54]   Ratanavaraporn J, Rangkupan R, Jeeratawatchai H, Kanokpanont S, Damrongsakkul S. Influences of physical and chemical crosslinking techniques on electrospun type A and B gelatin fiber mats. Int J Biol Macromol 2010;47:431–8. doi:10.1016/J.IJBIOMAC.2010.06.008.

[55]   Mauri E, Giannitelli SM, Trombetta M, Rainer A. Synthesis of nanogels: Current trends and future outlook. Gels 2021;7. doi:10.3390/GELS7020036.

[56]   Singhal R, Gupta K. A Review: Tailor-made Hydrogel Structures (Classifications and Synthesis Parameters). Polym - Plast Technol Eng 2016;55:54–70. doi:10.1080/03602559.2015.1050520.

[57]   Blackman LD, Gunatillake PA, Cass P, Locock KES. Chem Soc Rev and applications in solution and at surfaces 2019:757–70. doi:10.1039/c8cs00508g.

[58]   Dobaj Štiglic A, Kargl R, Beaumont M, Strauss C, Makuc D, Egger D, et al. Influence of Charge and Heat on the Mechanical Properties of Scaffolds from Ionic Complexation of Chitosan and Carboxymethyl Cellulose. ACS Biomater Sci Eng 2021;7:3618–32. doi:10.1021/ACSBIOMATERIALS.1C00534/ASSET/IMAGES/LARGE/AB1C00 534_0009.JPEG.

[59]   Sahi A, Mahboub K El, Belem T, Maqsoud A, Mbonimpa M. Dewatering of mine tailings slurries using superabsorbent polymers (SAPs) reclaimed from industrial reject of baby diapers: A preliminary study. Minerals 2019;9. doi:10.3390/MIN9120785.

[60]   Abedi-Koupai J, Sohrab F, Swarbrick G. Evaluation of hydrogel application on soil water retention characteristics. J Plant Nutr 2008;31:317–31. doi:10.1080/01904160701853928.

[61]   Elliott M (BASF A. Superabsorbent Polymers Author : Mark Elliott Product Development Scientist for SAP BASF Aktiengesellschaft. 2014.

[62]   Dayal U, Metha SK, Choudhary MS, Jain RC. Synthesis of Acrylic Superabsorbents. J Macromol Sci Part C Polym Rev 2002;39:507–25. doi:10.1081/mc-100101426.

[63]   Seguela G, Littlewood JR, Karani G. Eco-engineering strategies for soil restoration and water conservation: Investigating the application of soil improvements in a semi-arid climate in a medical facility case study, Abu Dhabi. Ecol Eng 2018;121:53–64. doi:https://doi.org/10.1016/j.ecoleng.2017.07.020.

[64]   Koupai JA, Eslamian SS, Kazemi JA. Enhancing the available water content in unsaturated soil zone using hydrogel, to improve plant growth indices. Ecohydrol Hydrobiol 2008;8:67–75. doi:10.2478/v10104-009-0005-0.

[65]   Montesano FF, Parente A, Santamaria P, Sannino A, Serio F. Biodegradable Superabsorbent Hydrogel IncreasesWater Retention Properties of Growing Media and Plant Growth. Agric Agric Sci Procedia 2015;4:451–8. doi:10.1016/j.aaspro.2015.03.052.

[66]   Adhikari R, Bristow KL, Casey PS, Freischmidt G, Hornbuckle JW, Adhikari B. Preformed and sprayable polymeric mulch film to improve agricultural water use efficiency. Agric Water Manag 2016;169:1–13. doi:https://doi.org/10.1016/j.agwat.2016.02.006.

[67]   Yu J, Shi JG, Ma X, Dang PF, Yan YL, Mamedov AI, et al. Superabsorbent
       Polymer Properties and Concentration Effects on Water Retention under Drying
       Conditions. Soil Sci Soc Am J 2017;81:889. doi:10.2136/sssaj2016.07.0231.

[68]   Zhan F, Liu M, Guo M, Wu L. Preparation of superabsorbent polymer with slow-
       release phosphate fertilizer. J Appl Polym Sci 2004;92:3417–21.
       doi:10.1002/app.20361.

[69]   Ma X, Wen G. Development history and synthesis of super-absorbent polymers: a
       review. J Polym Res 2020;27:1–12. doi:10.1007/s10965-020-02097-2.

[70]   Zhang J, Wang L, Wang A. Preparation and properties of chitosan-g-poly(acrylic
       acid)/montmorillonite superabsorbent nanocomposite via in situ intercalative
       polymerization. Ind. Eng. Chem. Res., vol. 46, American Chemical Society ;
       2007, p. 2497–502. doi:10.1021/ie061385i.

[71]   Gooch JW. Superabsorbent Polymers. Encycl. Dict. Polym., New York, NY:
       Springer New York; 2011, p. 714–5. doi:10.1007/978-1-4419-6247-8_11417.

[72]   Stahl JD, Cameron MD, Haselbach J, Aust SD. Biodegradation of superabsorbent
       polymers in soil. Environ Sci Pollut Res 2000;7:83–8.
       doi:10.1065/espr199912.014.

[73]   Maldonado RA, Geraili A, Xing M, Mequanint K. Tissue engineering and
       regenerative therapeutics: The nexus of chemical engineering and translational
       medicine. Can J Chem Eng 2021. doi:10.1002/cjce.24094.

[74]   He M, Zhao Y, Duan J, Wang Z, Chen Y, Zhang L. Fast contact of solid-liquid
       interface created high strength multi-layered cellulose hydrogels with controllable
       size. ACS Appl Mater Interfaces 2014;6:1872–8. doi:10.1021/am404855q.

[75]   Campos EVR, de Oliveira JL, Fraceto LF, Singh B. Polysaccharides as safer
       release systems for agrochemicals. Agron Sustain Dev 2014;35:47–66.
       doi:10.1007/s13593-014-0263-0.

[76]   Rabat NE, Hashim S, Majid RA. Effect of Different Monomers on Water Retention Properties of Slow Release Fertilizer Hydrogel. Procedia Eng 2016;148:201–7. doi:10.1016/j.proeng.2016.06.573.

[77]   Essawy HA, Ghazy MBM, El-Hai FA, Mohamed MF. Superabsorbent hydrogels via graft polymerization of acrylic acid from chitosan-cellulose hybrid and their potential in controlled release of soil nutrients. Int J Biol Macromol 2016;89:144–51. doi:10.1016/j.ijbiomac.2016.04.071.

[78]   Fekete T, Borsa J, Takács E, Wojnárovits L. Synthesis and characterization of superabsorbent hydrogels based on hydroxyethylcellulose and acrylic acid. Carbohydr Polym 2017;166:300–8. doi:10.1016/j.carbpol.2017.02.108.

[79]   Sawut A, Yimit M, Sun W, Nurulla I. Photopolymerisation and characterization of maleylatedcellulose-g-poly(acrylic acid) superabsorbent polymer. Carbohydr Polym 2014;101:231–9. doi:10.1016/J.CARBPOL.2013.09.054.

[80]   Chen P, Zhang W, Luo W, Fang Y. Synthesis of superabsorbent polymers by irradiation and their applications in agriculture. J Appl Polym Sci 2004. doi:10.1002/app.20612.

[81]   Tufail T, Saeed F, Imran M, Arshad MU, Anjum M, Afzaal M, et al. International Journal of Food Properties Biochemical characterization of wheat straw cell wall with special reference to bioactive profile 2018. doi:10.1080/10942912.2018.1484759.

[82]   Wang Y, Wang X, Xie Y, Zhang K. Functional nanomaterials through esterification of cellulose: a review of chemistry and application. Cellul 2018 257 2018;25:3703–31. doi:10.1007/S10570-018-1830-3.

[83]   Klemm D, Heublein B, Fink HP, Bohn A. Cellulose: Fascinating biopolymer and sustainable raw material. Angew Chemie - Int Ed 2005;44:3358–93. doi:10.1002/anie.200460587.

[84]   Withanage SR, Ariyarathne U. Preparation and characterizations of swelling

behaviour and mechanical properties of γ-PGA/C-CNC hydrogelsγ- Polyglutamic acid. figshare, 2019. doi:10.6084/M9.FIGSHARE.9959843.V1.

[85]   Hasan AMA, Abdel-Raouf ME-S. Cellulose-Based Superabsorbent Hydrogels 2019:245–67. doi:10.1007/978-3-319-77830-3_11.

[86]   Zhang L, Zhong J, Ren X. Natural fiber-based biocomposites. Green Energy Technol 2017;0:31–70. doi:10.1007/978-3-319-46610-1_3.

[87]   Lee J, Park S, Roh H gyoo, Oh S, Kim S, Kim M, et al. Preparation and characterization of superabsorbent polymers based on starch aldehydes and carboxymethyl cellulose. Polymers (Basel) 2018;8:605. doi:10.3390/polym10060605.

[88]   Bao D, Chen M, Wang H, Wang J, Liu C, Sun R. Preparation and characterization of double crosslinked hydrogel films from carboxymethylchitosan and carboxymethylcellulose. Carbohydr Polym 2014;110:113–20. doi:10.1016/j.carbpol.2014.03.095.

[89]   Uyanga KA, Iamphaojeen Y, Daoud WA. Effect of zinc ion concentration on crosslinking of carboxymethyl cellulose sodium-fumaric acid composite hydrogel. Polymer (Guildf) 2021;225:123788. doi:10.1016/j.polymer.2021.123788.

[90]   Adair A, Kaesaman A, Klinpituksa P. Superabsorbent materials derived from hydroxyethyl cellulose and bentonite: Preparation, characterization and swelling capacities. Polym Test 2017;64:321–9. doi:10.1016/j.polymertesting.2017.10.018.

[91]   Kono H. Characterization and properties of carboxymethyl cellulose hydrogels crosslinked by polyethylene glycol. Carbohydr Polym 2014;106:84–93. doi:10.1016/j.carbpol.2014.02.020.

[92]   Klinpituksa P, Kosaiyakanon P. Superabsorbent Polymer Based on Sodium Carboxymethyl Cellulose Grafted Polyacrylic Acid by Inverse Suspension Polymerization. Int J Polym Sci 2017;2017:1–6. doi:10.1155/2017/3476921.

[93]   Sharma N, Bhardwaj NK, Singh RBP. Environmental issues of pulp bleaching and prospects of peracetic acid pulp bleaching: A review. J Clean Prod 2020;256:120338. doi:10.1016/J.JCLEPRO.2020.120338.

[94]   Shui T, Feng S, Chen G, Li A, Yuan Z, Shui H, et al. Synthesis of sodium carboxymethyl cellulose using bleached crude cellulose fractionated from cornstalk. Biomass and Bioenergy 2017;105:51–8. doi:10.1016/J.BIOMBIOE.2017.06.016.

[95]   Zhang W, Vinueza NR, Datta P, Michielsen S. Functional dye as a comonomer in a water-soluble polymer. J Polym Sci Part A Polym Chem 2015;53:1594–9. doi:10.1002/POLA.27592.

[96]   Lakshmi DS, Trivedi N, Reddy CRK. Synthesis and characterization of seaweed cellulose derived carboxymethyl cellulose. Carbohydr Polym 2017;157:1604–10. doi:10.1016/J.CARBPOL.2016.11.042.

[97]   González-López ME, Robledo-Ortíz JR, Manríquez-González R, Silva-Guzmán JA, Pérez-Fonseca AA. Polylactic acid functionalization with maleic anhydride and its use as coupling agent in natural fiber biocomposites: a review. Https://DoiOrg/101080/0927644020181439622 2018;25:515–38. doi:10.1080/09276440.2018.1439622.

[98]   Cichosz S, Masek A, Wolski K, Zaborski M. Universal approach of cellulose fibres chemical modification result analysis via commonly used techniques. Polym Bull 2019;76:2147–62. doi:10.1007/S00289-018-2487-7.

[99]   Bátori V, Jabbari M, Srivastava RK, Åkesson D, Lennartsson PR, Zamani A, et al. (Synthesis and characterization of maleic anhydride-grafted orange waste for potential use in biocomposites. BioResources 2018;13:4986–97.

[100]   Lacoste C, Lopez-Cuesta JM, Bergeret A. Development of a biobased superabsorbent polymer from recycled cellulose for diapers applications. Eur Polym J 2019;116:38–44. doi:10.1016/J.EURPOLYMJ.2019.03.013.

[101] Dehabadi VA, Buschmann HJ, Gutmann JS. Durable press finishing of cotton fabrics: An overview. Text Res J 2013;83:1974–95. doi:10.1177/0040517513483857.

[102] Mali KK, Dhawale SC, Dias RJ, Dhane NS, Ghorpade VS. Citric acid crosslinked carboxymethyl cellulose-based composite hydrogel films for drug delivery. Indian J Pharm Sci 2018.

[103] Siemens PR, Giauque WF. The entropies of the hydrates of sodium hydroxide. II. Low-temperature heat capacities and heats of fusion of NaOH·2H2O and NaOH·3.5H2O. J Phys Chem 1969;73:149–57. doi:10.1021/J100721A024/ASSET/J100721A024.FP.PNG_V03.

[104] Budtova T, Navard P. Cellulose in NaOH–water based solvents: a review. Cellul 2015 231 2015;23:5–55. doi:10.1007/S10570-015-0779-8.

[105] Egal M, Budtova T, Navard P. Structure of aqueous solutions of microcrystalline cellulose/sodium hydroxide below 0 °C and the limit of cellulose dissolution. Biomacromolecules 2007;8:2282–7. doi:10.1021/BM0702399/ASSET/IMAGES/MEDIUM/BM0702399N00001.GIF.

[106] Zhang L, Mao Y, Zhou J, Cai J. Effects of Coagulation Conditions on the Properties of Regenerated Cellulose Films Prepared in NaOH/Urea Aqueous Solution. Ind Eng Chem Res 2005;44:522–9. doi:10.1021/IE0491802.

[107] Huh E, Yang JH, Lee CH, Ahn IS, Mhin BJ. Thermodynamic analysis of cellulose complex in NaOH–urea solution using reference interaction site model. Cellulose 2020;27:6767–75. doi:10.1007/S10570-020-03202-W/FIGURES/6.

[108] Egal M, Budtova T, Navard P. The dissolution of microcrystalline cellulose in sodium hydroxide-urea aqueous solutions. Cellulose 2008;15:361–70. doi:10.1007/S10570-007-9185-1/FIGURES/6.

[109] Cai J, Zhang L. Rapid dissolution of cellulose in LiOH/urea and NaOH/urea aqueous solutions. Macromol Biosci 2005;5:539–48.

doi:10.1002/MABI.200400222.

[110] Laszkiewicz B, Cuculo JA. Solubility of cellulose III in sodium hydroxide solution. J Appl Polym Sci 1993;50:27–34. doi:10.1002/APP.1993.070500104.

[111] Yan L, Gao Z. Dissolving of cellulose in PEG/NaOH aqueous solution. Cellulose 2008;15:789–96. doi:10.1007/S10570-008-9233-5/FIGURES/9.

[112] Sadeghi GMM, Sayaf M. Nanostructure Formation in Block Copolymers. Nanostructured Polym Blends 2014:195–271. doi:10.1016/B978-1-4557-3159-6.00007-9.

[113] Pal P, Pandey JP, Sen G. Synthesis and Application as Programmable Water Soluble Adhesive of Polyacrylamide Grafted Gum Tragacanth (GT-g-PAM). Biopolym Grafting Appl 2018:153–203. doi:10.1016/B978-0-12-810462-0.00005-3.

[114] Khanlari S, Dubé MA. Effect of pH on Poly(acrylic acid) Solution Polymerization. Http://DxDoiOrg/101080/1060132520151050628 2015;52:587–92. doi:10.1080/10601325.2015.1050628.

[115] Ferreira DP, Cruz J, Fangueiro R. Surface modification of natural fibers in polymer composites. Green Compos Automot Appl 2019:3–41. doi:10.1016/B978-0-08-102177-4.00001-X.

[116] Lutz H, Weitzel HP, Huster W. Aqueous Emulsion Polymers. Polym Sci A Compr Ref 10 Vol Set 2012;10:479–518. doi:10.1016/B978-0-444-53349-4.00280-6.

[117] Kumar D, Pandey J, Raj V, Kumar P. A Review on the Modification of Polysaccharide Through Graft Copolymerization for Various Potential Applications. Open Med Chem J 2017;11:109–26. doi:10.2174/1874104501711010109.

[118] Masuda F, Ueda Y. Superabsorbent Polymers. Encycl Polym Nanomater 2014:1–18. doi:10.1007/978-3-642-36199-9_129-1.

[119] Gibas I, Janik H. Review: Synthetic Polymer Hydrogels for Biomedical Applications. Chem Chem Technol 2010;4:297–304. doi:10.23939/CHCHT04.04.297.

[120] Cheng B, Pei B, Wang Z, Hu Q. Advances in chitosan-based superabsorbent hydrogels. RSC Adv 2017. doi:10.1039/c7ra07104c.

[121] Mondal MIH, Haque MO. Cellulosic Hydrogels: A Greener Solution of Sustainability, 2019, p. 3–35. doi:10.1007/978-3-319-77830-3_4.

[122] Adhikari S, Nam H, Chakraborty JP. Conversion of Solid Wastes to Fuels and Chemicals Through Pyrolysis. Waste Biorefinery Potential Perspect 2018:239–63. doi:10.1016/B978-0-444-63992-9.00008-2.

[123] Lal R. World crop residues production and implications of its use as a biofuel. Environ Int 2005;31:575–84. doi:10.1016/J.ENVINT.2004.09.005.

[124] Williams CL, Emerson RM, Tumuluru JS. Biomass Compositional Analysis for Conversion to Renewable Fuels and Chemicals. Biomass Vol Estim Valorization Energy 2017. doi:10.5772/65777.

[125] Hayes DJM. Biomass Composition and Its Relevance to Biorefining. Role Catal Sustain Prod Bio-Fuels Bio-Chemicals 2013:27–65. doi:10.1016/B978-0-444-56330-9.00002-4.

[126] Haghighi Mood S, Hossein Golfeshan A, Tabatabaei M, Salehi Jouzani G, Najafi GH, Gholami M, et al. Lignocellulosic biomass to bioethanol, a comprehensive review with a focus on pretreatment. Renew Sustain Energy Rev 2013;27:77–93. doi:10.1016/J.RSER.2013.06.033.

[127] Thoresen PP, Matsakas L, Rova U, Christakopoulos P. Recent advances in organosolv fractionation: Towards biomass fractionation technology of the future. Bioresour Technol 2020;306:123189. doi:10.1016/J.BIORTECH.2020.123189.

[128] Alonso DM, Hakim SH, Zhou S, Won W, Hosseinaei O, Tao J, et al. Increasing

the revenue from lignocellulosic biomass: Maximizing feedstock utilization. Sci Adv 2017;3. doi:10.1126/SCIADV.1603301.

[129] Philippini RR, Martiniano SE, Ingle AP, Franco Marcelino PR, Silva GM, Barbosa FG, et al. Agroindustrial Byproducts for the Generation of Biobased Products: Alternatives for Sustainable Biorefineries. Front Energy Res 2020;8:152. doi:10.3389/FENRG.2020.00152/BIBTEX.

[130] Oriez V, Peydecastaing J, Pontalier PY. Lignocellulosic Biomass Fractionation by Mineral Acids and Resulting Extract Purification Processes: Conditions, Yields, and Purities. Molecules 2019;24. doi:10.3390/MOLECULES24234273.

[131] Xu J, Li C, Dai L, Xu C, Zhong Y, Yu F, et al. Biomass Fractionation and Lignin Fractionation towards Lignin Valorization. ChemSusChem 2020;13:4284–95. doi:10.1002/CSSC.202001491.

[132] Zhou Z, Lei F, Li P, Jiang J. Lignocellulosic biomass to biofuels and biochemicals: A comprehensive review with a focus on ethanol organosolv pretreatment technology. Biotechnol Bioeng 2018;115:2683–702. doi:10.1002/BIT.26788.

[133] Li MF, Sun SN, Xu F, Sun RC. Formic acid based organosolv pulping of bamboo (Phyllostachys acuta): Comparative characterization of the dissolved lignins with milled wood lignin. Chem Eng J 2012;179:80–9. doi:10.1016/J.CEJ.2011.10.060.

[134] Shui T, Feng S, Yuan Z, Kuboki T, Xu C. Highly efficient organosolv fractionation of cornstalk into cellulose and lignin in organic acids. Bioresour Technol 2016. doi:10.1016/j.biortech.2016.07.054.

[135] Dammer L, Carus M, Raschka A, Scholz L. Market Developments of and Opportunities for biobased products and chemicals. Mark Trends Bio-Based Prod 2013.

[136] Wang M, Leitch M, (Charles) Xu C. Synthesis of phenol-formaldehyde resol resins using organosolv pine lignins. Eur Polym J 2009. doi:10.1016/j.eurpolymj.2009.10.003.

[137] Wood S, Layzell D. A Canadian Biomass Inventory: Feedstocks for a Bio-based Economy\rFinal Report. BIOCAP Canada Found 2003.

[138] Wells TP, Hallett JP, Williams CK, Welton T. Esterification in ionic liquids: the influence of solvent basicity n.d.

[139] Jin B, Duan P, Xu Y, Wang B, Wang F, Zhang L. Lewis acid-catalyzed in situ transesterification/esterification of microalgae in supercritical ethanol. Bioresour Technol 2014;162:341–9. doi:10.1016/j.biortech.2014.03.157.

[140] Suman T, Srinivas S, Mahajani SM. Entrainer based reactive distillation for esterification of ethylene glycol with acetic acid. Ind Eng Chem Res 2009;48:9461–70. doi:10.1021/IE801886Q.

[141] Huang F, Xu S, Li T, Zhu D. Innovative Ethylene Glycol Diacetate synthesis process in a single reactive distillation column. Chem Eng Process - Process Intensif 2016;109:80–9. doi:10.1016/J.CEP.2016.08.017.

[142] Gadekar-Shinde S, Reddy B, Khan M, Chavan S, Saini D, Mahajani S. Reactive distillation for the production of methoxy propyl acetate: Experiments and simulation. Ind Eng Chem Res 2017;56:832–43. doi:10.1021/ACS.IECR.6B03489/SUPPL_FILE/IE6B03489_SI_001.PDF.

[143] Keogh J, Tiwari MS, Manyar H. Esterification of Glycerol with Acetic Acid Using Nitrogen-Based Brønsted-Acidic Ionic Liquids. Ind Eng Chem Res 2019;58:17235–43. doi:10.1021/ACS.IECR.9B01223/SUPPL_FILE/IE9B01223_SI_001.PDF.

[144] Patidar P, Mahajani SM. Esterification of fusel oil using reactive distillation. Part II: Process alternatives. Ind Eng Chem Res 2013;52:16637–47. doi:10.1021/IE401553Z.

[145] Singh A, Hiwale R, Mahajani SM, Gudi RD, Gangadwala J, Kienle A. Production of Butyl Acetate by Catalytic Distillation. Theoretical and Experimental Studies. Ind Eng Chem Res 2005;44:3042–52. doi:10.1021/IE049659U.

[146] Cho M, Jo S, Kim G, Han M. Entrainer-enhanced reactive distillation for the production of butyl acetate. Ind Eng Chem Res 2014;53:8095–105. doi:10.1021/IE403049Z.

[147] Kulkarni AA, Zeyer KP, Jacobs T, Kienle A. Miniaturized systems for homogeneously and heterogeneously catalyzed liquid-phase esterification reaction. Ind Eng Chem Res 2007;46:5271–7. doi:10.1021/IE060411.

[148] Kantam ML, Bhaskar V, Choudary BM. Direct Condensation of Carboxylic Acids with Alcohols: The Atom Economic Protocol Catalysed by Fe3+-Montmorillonite. Catal Lett 2002 781 2002;78:185–8. doi:10.1023/A:1014993809745.

[149] Yadav GD, Mehta PH. Heterogeneous Catalysis in Esterification Reactions: Preparation of Phenethyl Acetate and Cyclohexyl Acetate by Using a Variety of Solid Acidic Catalysts. Ind Eng Chem Res 1994;33:2198–208. doi:10.1021/IE00033A025.

[150] Barbosa SL, Dabdoub MJ, Hurtado GR, Klein SI, Baroni ACM, Cunha C. Solvent free esterification reactions using Lewis acids in solid phase catalysis. Appl Catal A Gen 2006;313:146–50. doi:10.1016/J.APCATA.2006.07.015.

[151] Lindman B, Medronho B, Alves L, Costa C, Edlund H, Norgren M. The relevance of structural features of cellulose and its interactions to dissolution, regeneration, gelation and plasticization phenomena. Phys Chem Chem Phys 2017;19:23704–18. doi:10.1039/C7CP02409F.

[152] Klemm D, Philpp B, Heinze T, Hewinze U, Wagenknecht W. Comprehensive cellulose chemistry. Volume 2: Functionalization of cellulose. Compr Cellul Chem Vol 2 Funct Cellul 1998.

[153] Fox SC, Li B, Xu D, Edgar KJ. Regioselective esterification and etherification of cellulose: A review. Biomacromolecules 2011;12:1956–72. doi:10.1021/BM200260D/ASSET/IMAGES/LARGE/BM-2011-00260D_0006.JPEG.

[154] Illy N, Fache M, Ménard R, Negrell C, Caillol S, David G. Phosphorylation of bio-based compounds: the state of the art. Polym Chem 2015;6:6257–91. doi:10.1039/C5PY00812C.

[155] Esterification of Polysaccharides. Esterification of Polysaccharides 2006. doi:10.1007/3-540-32112-8.

[156] Bátori V, Jabbari M, Srivastava RK, Åkesson D, Lennartsson PR, Zamani A, et al. Synthesis and characterization of maleic anhydride-grafted orange waste for potential use in biocomposites. BioResources 2018;13:4986–97.

[157] Hamcerencu M, Desbrieres J, Popa M, Khoukh A, Riess G. New unsaturated derivatives of Xanthan gum: Synthesis and characterization. Polymer (Guildf) 2007;48:1921–9. doi:10.1016/J.POLYMER.2007.01.048.

[158] Almeida E, Facchi SP, Martins AF, Nocchi S, Schuquel ITA, Nakamura C V., et al. Synthesis and characterization of pectin derivative with antitumor property against Caco-2 colon cancer cells. Carbohydr Polym 2015;115:139–45. doi:10.1016/J.CARBPOL.2014.08.085.

[159] Ragab S, Eleryan A, El Nemr A. Ferric perchlorate hydrate as a new catalyst for highly efficient esterification of cellulose at room temperature. Sci Reports 2022 121 2022;12:1–13. doi:10.1038/s41598-022-09669-w.

[160] Kong PS, Aroua MK, Daud WMAW, Lee HV, Cognet P, Pérès Y. Catalytic role of solid acid catalysts in glycerol acetylation for the production of bio-additives: a review. RSC Adv 2016;6:68885–905. doi:10.1039/C6RA10686B.

[161] Liu T, Qian L, Li B, Li J, Zhu K, Deng H, et al. Homogeneous synthesis of chitin-based acrylate superabsorbents in NaOH/urea solution. Carbohydr Polym 2013. doi:10.1016/j.carbpol.2013.01.010.

[162] Liu TG, Wang YT, Guo J, Liu TB, Wang X, Li B. One-step synthesis of corn starch urea based acrylate superabsorbents. J Appl Polym Sci 2017. doi:10.1002/app.45175.

[163] Luo Y, Peng H, Wu J, Sun J, Wang Y. Novel amphoteric pH-sensitive hydrogels derived from ethylenediaminetetraacetic dianhydride, butanediamine and amino-terminated poly(ethylene glycol): Design, synthesis and swelling behavior. Eur Polym J 2011. doi:10.1016/j.eurpolymj.2010.11.001.

[164] Marani D, Hjelm J, Wandel M. Use of Intrinsic Viscosity for evaluation of polymer-solvent affinity. Nord Rheol Soc Annu Trans 2013.

[165] Lisperguer J, Nuñez C, Perez-Guerrero P. Structure and thermal properties of maleated lignin-recycled polystyrene composites. J Chil Chem Soc 2013. doi:10.4067/S0717-97072013000400005.

[166] Smith BC. The C=O bond, Part IV: Acid anhydrides. Spectrosc (Santa Monica) 2018.

[167] Abderrahim B, Abderrahman E, Mohamed A, Fatima T, Abdesselam T, Krim O. Kinetic Thermal Degradation of Cellulose, Polybutylene Succinate and a Green Composite: Comparative Study. World J Environ Eng Vol 3, 2015, Pages 95-110 2015. doi:10.12691/WJEE-3-4-1.

[168] Zuluaga R, Putaux J-L, Cruz J, Veléz J, Mondragón I, Gañan P. Cellulose microfibrils from banana rachis: Effect of alkaline treatments on structural and morphological features Related papers. Carbohydr Polym 2009;26:51–9. doi:10.1016/j.carbpol.2008.09.024.

[169] Zohuriaan-Mehr MJ, Kabiri K. Superabsorbent polymer materials: A review. Iran Polym J 2008;17:451–77.

[170] Mignon A, De Belie N, Dubruel P, Van Vlierberghe S. Superabsorbent polymers: A review on the characteristics and applications of synthetic, polysaccharide-based, semi-synthetic and 'smart' derivatives. Eur Polym J 2019;117:165–78. doi:10.1016/J.EURPOLYMJ.2019.04.054.

[171] Chiaregato CG, França D, Messa LL, dos Santos Pereira T, Faez R. A review of advances over 20 years on polysaccharide-based polymers applied as enhanced

efficiency fertilizers. Carbohydr Polym 2022;279:119014. doi:10.1016/J.CARBPOL.2021.119014.

[172] Kamath KR, Park K. Biodegradable hydrogels in drug delivery. Adv Drug Deliv Rev 1993;11:59–84. doi:10.1016/0169-409X(93)90027-2.

[173] Hokkanen S, Bhatnagar A, Sillanpää M. A review on modification methods to cellulose-based adsorbents to improve adsorption capacity. Water Res 2016;91:156–73. doi:10.1016/j.watres.2016.01.008.

[174] Murali Mohan Y, Keshava Murthy PS, Mohana Raju K. Preparation and swelling behavior of macroporous poly(acrylamide-co-sodium methacrylate) superabsorbent hydrogels. J Appl Polym Sci 2006;101:3202–14. doi:10.1002/APP.23277.

[175] Işik B. Swelling Behavior and Determination of Diffusion Characteristics of Acrylamide-Acrylic Acid Hydrogels. J Appl Polym Sci 2004;91:1289–93. doi:10.1002/APP.13270.

[176] Yoshimura T, Matsuo K, Fujioka R. Novel biodegradable superabsorbent hydrogels derived from cotton cellulose and succinic anhydride: Synthesis and characterization. J Appl Polym Sci 2006. doi:10.1002/app.22794.

[177] Llanes L, Dubessay P, Pierre G, Delattre C, Michaud P. Biosourced Polysaccharide-Based Superabsorbents. Polysaccharides 2020, Vol 1, Pages 51-79 2020;1:51–79. doi:10.3390/POLYSACCHARIDES1010005.

[178] Hasan AMA, Abdel-Raouf ME-S. Cellulose-Based Superabsorbent Hydrogels 2018:1–23. doi:10.1007/978-3-319-76573-0_11-1.

[179] Senna AM, Novack KM, Botaro VR. Synthesis and characterization of hydrogels from cellulose acetate by esterification crosslinking with EDTA dianhydride. Carbohydr Polym 2014;114:260–8. doi:10.1016/J.CARBPOL.2014.08.017.

[180] Liu TG, Wang YT, Li B, Deng HB, Huang ZL, Qian LW, et al. Urea free synthesis

of chitin-based acrylate superabsorbent polymers under homogeneous conditions: Effects of the degree of deacetylation and the molecular weight. Carbohydr Polym 2017. doi:10.1016/j.carbpol.2017.06.108.

[181]   Mali KK, Dhawale SC, Dias RJ, Dhane NS, Ghorpade VS. Citric acid crosslinked carboxymethyl cellulose-based composite hydrogel films for drug delivery. Indian J Pharm Sci 2018;80:657–67. doi:10.4172/PHARMACEUTICAL-SCIENCES.1000405.

[182]   Dai Q, Kadla JF. Effect of nanofillers on carboxymethyl cellulose/hydroxyethyl cellulose hydrogels. J Appl Polym Sci 2009;114:1664–9. doi:10.1002/APP.30789.

[183]   Zhang K, Feng W, Jin C. Protocol efficiently measuring the swelling rate of hydrogels. MethodsX 2020;7:100779. doi:10.1016/j.mex.2019.100779.

[184]   Craciun G, Ighigeanu D, Manaila E, Stelescu MD. Synthesis and characterization of Poly(Acrylamide-Co-Acrylic Acid) flocculant obtained by electron beam irradiation. Mater Res 2015;18:984–93. doi:10.1590/1516-1439.008715.

[185]   Chang C, Duan B, Cai J, Zhang L. Superabsorbent hydrogels based on cellulose for smart swelling and controllable delivery. Eur Polym J 2010;46:92–100. doi:10.1016/J.EURPOLYMJ.2009.04.033.

[186]   Zhang C, Keten S, Derome D, Carmeliet J. Hydrogen bonds dominated frictional stick-slip of cellulose nanocrystals. Carbohydr Polym 2021;258:117682. doi:10.1016/J.CARBPOL.2021.117682.

[187]   Wang H, Zhang C, Chu X, Zhu P. Mechanism of Antiwrinkle Finishing of Cotton Fabrics Using Mixed Polycarboxylic Acids. Int J Polym Sci 2020;2020. doi:10.1155/2020/3876595.

[188]   Li Y, Liu Y, Liu Y, Lai W, Huang F, Ou A, et al. Ester Crosslinking Enhanced Hydrophilic Cellulose Nanofibrils Aerogel. ACS Sustain Chem Eng 2018;6:11979–88. doi:10.1021/ACSSUSCHEMENG.8B02284/SUPPL_FILE/SC8B02284_SI_007.A

VI.

[189] De Sterck B, Vaneerdeweg R, Du Prez F, Waroquier M, Van Speybroeck V. Solvent effects on free radical polymerization reactions: The influence of water on the propagation rate of acrylamide and methacrylamide. Macromolecules 2010;43:827–36. doi:10.1021/MA9018747/SUPPL_FILE/MA9018747_SI_001.PDF.

[190] Dankar I, Haddarah A, Omar FEL, Pujolà M, Sepulcre F. Characterization of food additive-potato starch complexes by FTIR and X-ray diffraction. Food Chem 2018;260:7–12. doi:10.1016/J.FOODCHEM.2018.03.138.

[191] Czarnecka E, Nowaczyk J. Synthesis and Characterization Superabsorbent Polymers Made of Starch, Acrylic Acid, Acrylamide, Poly(Vinyl Alcohol), 2-Hydroxyethyl Methacrylate, 2-Acrylamido-2-methylpropane Sulfonic Acid. Int J Mol Sci 2021;22. doi:10.3390/IJMS22094325.

[192] Abdallah AM. The effect of hydrogel particle size on water retention properties and availability under water stress. Int Soil Water Conserv Res 2019;7:275–85. doi:10.1016/J.ISWCR.2019.05.001.

[193] Ma X, Wen G. Development history and synthesis of super-absorbent polymers: a review. J Polym Res 2020;27:1–12. doi:10.1007/S10965-020-02097-2/FIGURES/9.

[194] Zhang S, Peng Y, Jiang R, Liu W, Yang H, Yun N, et al. Predicting the Swelling Behavior of Acrylic Superabsorbent Polymers Used in Diapers. Adv Polym Technol 2021;2021:1–7. doi:10.1155/2021/9999826.

[195] Vishal Gupta N, Shivakumar HG. Investigation of Swelling Behavior and Mechanical Properties of a pH-Sensitive Superporous Hydrogel Composite. Iran J Pharm Res 2012;11:481. doi:10.22037/ijpr.2012.1097.

[196] Takeuchi A, Inoue A. Classification of bulk metallic glasses by atomic size difference, heat of mixing and period of constituent elements and its application to

characterization of the main alloying element. Mater Trans 2005;46:2817–29. doi:10.2320/MATERTRANS.46.2817.

[197] Abou-Baker NH, Ouis M, Abd-Eladl M, Ibrahim MM. Transformation of Lignocellulosic Biomass to Cellulose-Based Hydrogel and Agriglass to Improve Beans Yield. Waste and Biomass Valorization 2020;11:3537–51. doi:10.1007/s12649-019-00699-6.

[198] Li X, Li Q, Su Y, Yue Q, Gao B, Su Y. A novel wheat straw cellulose-based semi-IPNs superabsorbent with integration of water-retaining and controlled-release fertilizers. J Taiwan Inst Chem Eng 2015;55:170–9. doi:10.1016/j.jtice.2015.04.022.

[199] Ibrahim MM, Abd-Eladl M, Abou-Baker NH. Lignocellulosic biomass for the preparation of cellulose-based hydrogel and its use for optimizing water resources in agriculture. J Appl Polym Sci 2015;132:42652. doi:10.1002/app.42652.

[200] Zhang H, Luan Q, Huang Q, Tang H, Huang F, Li W, et al. A facile and efficient strategy for the fabrication of porous linseed gum/cellulose superabsorbent hydrogels for water conservation. Carbohydr Polym 2017;157:1830–6. doi:10.1016/j.carbpol.2016.11.070.

[201] Ghazy MBM, El-Hai FA, Mohamed MF, Essawy HA. Potassium fulvate as co-interpenetrating agent during graft polymerization of acrylic acid from cellulose. Int J Biol Macromol 2016;91:1206–14. doi:10.1016/j.ijbiomac.2016.06.088.

[202] Zhang M, Zhang S, Chen Z, Wang M, Cao J, Wang R. Preparation and characterization of superabsorbent polymers based on sawdust. Polymers (Basel) 2019;11:1891. doi:10.3390/polym11111891.

[203] Wang Z, Ning A, Xie P, Gao G, Xie L, Li X, et al. Synthesis and swelling behaviors of carboxymethyl cellulose-based superabsorbent resin hybridized with graphene oxide. Carbohydr Polym 2017;157:48–56. doi:10.1016/j.carbpol.2016.09.070.

[204] Fekete T, Borsa J, Takács E, Wojnárovits L. Synthesis of carboxymethylcellulose/acrylic acid hydrogels with superabsorbent properties by radiation-initiated crosslinking. Radiat Phys Chem 2016;124:135–9. doi:10.1016/j.radphyschem.2015.09.018.

[205] Wen P, Han Y, Wu Z, He Y, Ye BC, Wang J. Rapid synthesis of a corncob-based semi-interpenetrating polymer network slow-release nitrogen fertilizer by microwave irradiation to control water and nutrient losses. Arab J Chem 2017;10:922–34. doi:10.1016/j.arabjc.2017.03.002.

[206] Karami Z, Naderi P, Kabiri K, Zohuriaan-Mehr MJ. Epoxidized and Cyclocarbonated Star-Shaped Macromolecules as Bio-Based Internal and External Crosslinkers for Superabsorbent Polymer Hydrogels. J Polym Environ 2020;28:1684–95. doi:10.1007/S10924-020-01718-7/FIGURES/4.

[207] Jafari M, Najafi GR, Sharif MA, Elyasi Z. Superabsorbent polymer composites derived from polyacrylic acid: Design and synthesis, characterization, and swelling capacities. Polym Polym Compos 2020;29:733–9. doi:10.1177/0967391120933482.

[208] Tomar RS, Gupta I, Singhal R, Nagpal AK. Synthesis of Poly (Acrylamide-co-Acrylic Acid) based Superabsorbent Hydrogels: Study of Network Parameters and Swelling Behaviour. Polym Plast Technol Eng 2007;46:481–8. doi:10.1080/03602550701297095.

[209] Filiciotto L, Rothenberg G. Biodegradable Plastics: Standards, Policies, and Impacts. ChemSusChem 2021;14:56–72. doi:10.1002/CSSC.202002044.

[210] Lim XZ. Microplastics are everywhere - but are they harmful? Nature 2021;593:22–5. doi:10.1038/D41586-021-01143-3.

[211] Du N, Dal-Cin MM, Robertson GP, Guiver MD. Decarboxylation-Induced Cross-Linking of Polymers of Intrinsic Microporosity (PIMs) for Membrane Gas Separation † n.d. doi:10.1021/ma300751s.

[212] Xu Y, Odelius K, Hakkarainen M. One-pot synthesis of lignin thermosets exhibiting widely tunable mechanical properties and shape memory behavior. ACS Sustain Chem Eng 2019;7:13456–63. doi:10.1021/ACSSUSCHEMENG.9B02921/SUPPL_FILE/SC9B02921_SI_001.PDF.

[213] López-Carrasquero F, Rangel-Rangel E, Cárdenas M, Torres C, Dugarte N, Laredo E. Copolymers of long-side-chain di-n-alkyl itaconates or methyl n-alkyl itaconates with styrene: Synthesis, characterization, and thermal properties. Polym Bull 2013;70:131–46. doi:10.1007/S00289-012-0788-9.

[214] Ferdosian F, Yuan Z, Anderson M, Xu CC. Thermal performance and thermal decomposition kinetics of lignin-based epoxy resins. J Anal Appl Pyrolysis 2016;119:124–32. doi:10.1016/J.JAAP.2016.03.009.

[215] Mahon R, Balogun Y, Oluyemi G, Njuguna J. Swelling performance of sodium polyacrylate and poly(acrylamide-co-acrylic acid) potassium salt. SN Appl Sci 2020;2:1–15. doi:10.1007/S42452-019-1874-5/TABLES/4.

[216] Rosa F, Casquilho M. Effect of synthesis parameters and of temperature of swelling on water absorption by a superabsorbent polymer. Fuel Process Technol 2012;103:174–7. doi:10.1016/J.FUPROC.2011.09.004.

[217] Gao J, Liu J, Peng H, Wang Y, Cheng S, Lei Z. Preparation of a low-cost and eco-friendly superabsorbent composite based on wheat bran and laterite for potential application in Chinese herbal medicine growth. R Soc Open Sci 2018;5. doi:10.1098/RSOS.180007.

[218] Abdel Bary EM, Harmal AN. A novel method to prepare three-component hydrogels as neural tissue engineering. Polym Bull 2019;76:4451–68. doi:10.1007/S00289-018-2617-2.

[219] Bachra Y, Grouli A, Damiri F, Talbi M, Berrada M. A Novel Superabsorbent Polymer from Crosslinked Carboxymethyl Tragacanth Gum with Glutaraldehyde:

Synthesis, Characterization, and Swelling Properties. Int J Biomater 2021;2021. doi:10.1155/2021/5008833.

[220] Anwar Z, Gulfraz M, Irshad M. Agro-industrial lignocellulosic biomass a key to unlock the future bio-energy: A brief review. J Radiat Res Appl Sci 2014;7:163–73. doi:10.1016/J.JRRAS.2014.02.003.

[221] Oriez V, Peydecastaing J, Pontalier PY. Lignocellulosic Biomass Mild Alkaline Fractionation and Resulting Extract Purification Processes: Conditions, Yields, and Purities. Clean Technol 2020, Vol 2, Pages 91-115 2020;2:91–115. doi:10.3390/CLEANTECHNOL2010007.

[222] Borand MN, Karaosmanoğlu F. Effects of organosolv pretreatment conditions for lignocellulosic biomass in biorefinery applications: A review. J Renew Sustain Energy 2018;10. doi:10.1063/1.5025876.

[223] Hazwan Hussin M, Trache D, Hui Chuin CT, Nurul Fazita MR, Mohamad Haafiz MK, Sohrab Hossain M. Extraction of cellulose nanofibers and their eco-friendly polymer composites. Sustain Polym Compos Nanocomposites 2019:653–91. doi:10.1007/978-3-030-05399-4_23/COVER.

[224] Rabelo SC, Nakasu PYS, Scopel E, Araújo MF, Cardoso LH, Costa AC da. Organosolv pretreatment for biorefineries: Current status, perspectives, and challenges. Bioresour Technol 2023;369:128331. doi:10.1016/J.BIORTECH.2022.128331.

[225] Wang T, Zhao Y. Optimization of bleaching process for cellulose extraction from apple and kale pomace and evaluation of their potentials as film forming materials. Carbohydr Polym 2021;253:117225. doi:10.1016/J.CARBPOL.2020.117225.

[226] Shui T, Feng S, Yuan Z, Kuboki T, Xu C. Highly efficient organosolv fractionation of cornstalk into cellulose and lignin in organic acids. Bioresour Technol 2016;218:953–61. doi:10.1016/J.BIORTECH.2016.07.054.

[227] Sluiter A, Hames B, Ruiz R, Scarlata C, Sluiter J, Templeton D, et al.

Determination of Structural Carbohydrates and Lignin in Biomass Laboratory Analytical Procedure (LAP) Issue Date: 7/17/2005 2008.

[228] Tumuluru JS, Sokhansanj S, Hess JR, Wright CT, Boardman RD. A review on biomass torrefaction process and product properties for energy applications. Ind Biotechnol 2011;7:384–401. doi:10.1089/IND.2011.7.384.

[229] Reddy KO, Maheswari CU, Shukla M. Physico-chemical characterization of cellulose extracted from ficus leaves. J Biobased Mater Bioenergy 2013;7:496–9. doi:10.1166/JBMB.2013.1342.

[230] Sun XF, Xu F, Sun RC, Fowler P, Baird MS. Characteristics of degraded cellulose obtained from steam-exploded wheat straw. Carbohydr Res 2005;340:97–106. doi:10.1016/J.CARRES.2004.10.022.

[231] Sun XF, Sun RC, Su Y, Sun JX. Comparative Study of Crude and Purified Cellulose from Wheat Straw. J Agric Food Chem 2004;52:839–47. doi:10.1021/JF0349230/ASSET/IMAGES/LARGE/JF0349230F00005.JPEG.

[232] Liu H, Liu D, Yao F, Wu Q. Fabrication and properties of transparent polymethylmethacrylate/cellulose nanocrystals composites. Bioresour Technol 2010;101:5685–92. doi:10.1016/J.BIORTECH.2010.02.045.

[233] Bian J, Peng F, Peng X-P, Peng P, Xu F, Sun R-C. Purification of bagasse cellulose. BioResources 2012;7:4626–39.

[234] Zuo Y, Gu J, Yang L, Qiao Z, Tan H, Zhang Y. Synthesis and characterization of maleic anhydride esterified corn starch by the dry method. Int J Biol Macromol 2013;62:241–7. doi:10.1016/J.IJBIOMAC.2013.08.032.

[235] Jandura P, Kokta B V, Riedl B. Fibrous Long-Chain Organic Acid Cellulose Esters and Their Characterization by Diffuse Reflectance FTIR Spectroscopy, Solid-State CP/MAS 13 C-NMR, and X-Ray Diffraction. 2000. doi:10.1002/1097-4628.

[236] Tang L, Huang B, Lu Q, Wang S, Ou W, Lin W, et al. Ultrasonication-assisted manufacture of cellulose nanocrystals esterified with acetic acid. Bioresour Technol 2013;127:100–5. doi:10.1016/J.BIORTECH.2012.09.133.

[237] Hivechi A, Bahrami SH, Arami M, Karimi A. Ultrasonic mediated production of carboxymethyl cellulose : Optimization of conditions using response surface methodology. Carbohydr Polym 2015;134:278–84. doi:10.1016/j.carbpol.2015.07.045.

[238] Bochek AM, Zabivalova NM, Petropavlovskii GA. Determination of the esterification degree of polygalacturonic acid. Russ J Appl Chem 2001. doi:10.1023/A:1012701219447.

[239] Cumpstey I, Cumpstey I. Chemical Modification of Polysaccharides, Chemical Modification of Polysaccharides. Int Sch Res Not Int Sch Res Not 2013. doi:10.1155/2013/417672, 10.1155/2013/417672.

Appendices

Appendix A: Back titration procedure

The –COOH grafted to a sample (pure cellulose, starch, or crude cellulose) following an esterification was obtained through back titration in which the –COOH concentration of a sample reacted with a known mass of NaOH standard solution. Then, this mixture (sample and NaOH standard solution) was titrated with a HCl standard solution. Finally, the volume of wasted HCl standard solution neutralized the mixture that was used to calculate the DS of –COOH in the esterified sample (Figure 68).
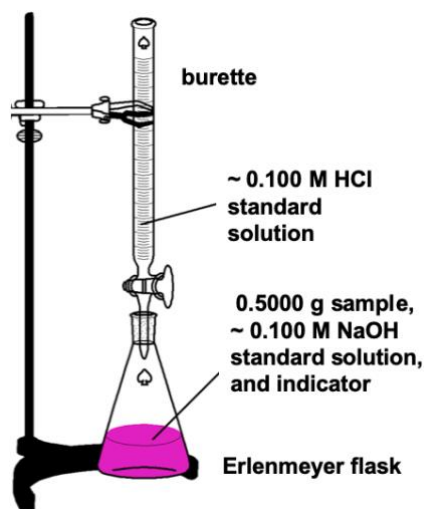
Figure 68: Titration of esterified pure cellulose/starch

First, standard solutions of NaOH and HCl were prepared [132] using the following procedure. To obtain a NaOH ~0.100 M solution, a 50% w/w NaOH solution was first prepared in order to remove the dissolved CO_2 through precipitation of Na_2CO_3 overnight. Distilled water was boiled for 5 min to expel the CO_2 and then left to cool down. Next, the boiled distilled water was used to dilute 5.30 mL of 50% w/w NaOH solution to prepare the ~0.100 M NaOH solution. To standardize the prepared ~0.100 M NaOH solution, potassium hydrogen phthalate was pre-dried for 1 h at 110°C and then stored in a desiccator. A 0.5100 g portion of potassium hydrogen phthalate was weighed and then dissolved in 25 mL of distilled water in a flask; subsequently, three drops of phenolphthalein were added. Then, the ~0.100 M NaOH solution was poured into the flask through a graduated burette until the mixture appeared pink for 15 consecutive seconds. The titration of the potassium hydrogen phthalate with the ~0.100 M NaOH solution was performed in triplicate.

A standard solution of ~0.100 M of HCl was prepared by adding 8.20 mL of 37% w/v HCl solution to 1 L of distilled water. Sodium carbonate, as the primary standard, was pre-dried at 110°C for 1 h and then cooled down in a desiccator. In a procedure similar to the standardization of the ~0.100 M NaOH solution, a sodium carbonate sample was weighed and then mixed with 25 mL of distilled water and three drops of bromocresol purple. Then, the mixture was titrated through a burette with the ~0.100 M HCl solution;

at the endpoint of titration, the mixture's colour changed from purple to yellow. Then, the titrated sample was boiled to expel CO_2; during this process, the mixture's colour turned purple again. Next, more HCl from the burette was added to the sample solution, turning the colour back to yellow. The final volume of ~0.100 M HCl solution that was needed to make the sample permanently yellow was used to calculate the exact molarity of the standard solution of HCl. The titration of the sodium carbonate with the ~0.100 M HCl solution, including the expulsion of CO_2, was performed in triplicate.

Subsequently, titration was performed by mixing 0.5000 g of esterified pure cellulose/starch with 30.00 mL of the ~0.100 M NaOH standard solution and stirring for 20 min. Then, three drops of phenolphthalein were added, tinting the mixture a pale pink colour. Finally, the ~0.100 M HCl standard solution was added until the mixture was colourless. The titration of the esterified sample was performed in triplicate. The total volume of the ~0.100 M HCl standard solution that was added to the mixture was recorded; this datum, which represents the neutralization of the mixture, was then used to measure the DS of the sample [238] using the following equation:

$$\overline{\text{n HCl}} = \frac{[\text{NaOH}] \times 30\text{g}}{1000} - \frac{[\text{NaOH}] \times \overline{\text{sample mass}}}{1000} \quad \textbf{Equation 17}$$

Equation 17 means that the average number of moles of HCl used to neutralize carboxylic acid groups is equal to the average number of moles of HCl needed to neutralize a 30.00 mL neat NaOH solution subtracted by the average number of moles of HCl needed to neutralize the 30.00 mL NaOH solution in the presence of the esterified pure cellulose/starch sample.

From the average number of moles of HCl calculated using Equation 17, the DS of the esterified sample was calculated via successive iteration using Equation 18 by taking the molecular mass of the esterification agent as the initial estimation of the mass of the grafted esterification agent per mole of cellulose/starch unit at the first iteration:

$$DS^1 = \frac{\overline{\frac{n\ HCl}{sample\ mass}}}{esterification\ agent\ molecular\ mass\frac{g}{mol} + cellulose\ or\ satrch\ molecular\ mass\ \frac{g}{mol}}$$ **Equation 18**

The iteration was performed by changing the mass of the grafted esterification agent per mole of cellulose/starch until the difference between the DS^n calculated and DS^{n-1} approximated from the previous iteration was ≤ 0.001.

Cellulose/starch has three hydroxyl groups per monomer; therefore, in a cellulose/starch substitution, all three –OH groups can be functionalized, and the maximum DS is 3 [239].

Appendix B: Kinetics of esterification reaction between cellulose and maleic anhydride

The experimental data of the esterification reaction between cellulose and maleic anhydride were obtained by monitoring the reaction at 0, 2, 3, 4, 5, and 6 hours. The experiment was held in a 250 mL three neck flask, where the following substances were added and stirred: 49.92 g of cellulose, 30.00 g of maleic anhydride, 3.19 g of zinc chloride, and up to 200 mL of acetone. The concentration of the samples was analyzed using an Agilent 7890 GC/5975 MS equipped with an HP-5MS capillary column (30 m $\times$ 0.25 mm id., 0.25 µm film thickness) (Agilent Technologies, California, USA). For each GC–MS run, 1 µL of a sample was injected at 280°C with a split ratio of 20:1. Helium was used as a carrier gas with a flow rate of 2.64 mL/min. The GC oven temperature was programmed as follows: held at 60°C for 2 min, then ramped to 280°C with a heating rate of 20°C/min, and held for 10 min.

The sample concentration's data are reported in Table 23. The experimental data were used to create three graphs (Figure 69) to evaluate the best kinetic order. The data were plotted as follows: maleic anhydride (MA) concentration versus time (t) (order zero), ln[MA] versus t (first order), and 1/[MA] versus t (second order).

Table 23: Concentration of maleic anhydride taken while monitoring the esterification reaction throughout 6 hours

t (h)	ppm (mg /L)	[MA] mol/L	ln[MA]	1/[MA]
0	15000	0.153	-1.88	6.54
2	14800	0.151	-1.89	6.63
3	14500	0.148	-1.91	6.76
4	14250	0.145	-1.93	6.88
5	14000	0.143	-1.95	7.00
6	14000	0.143	-1.95	7.00
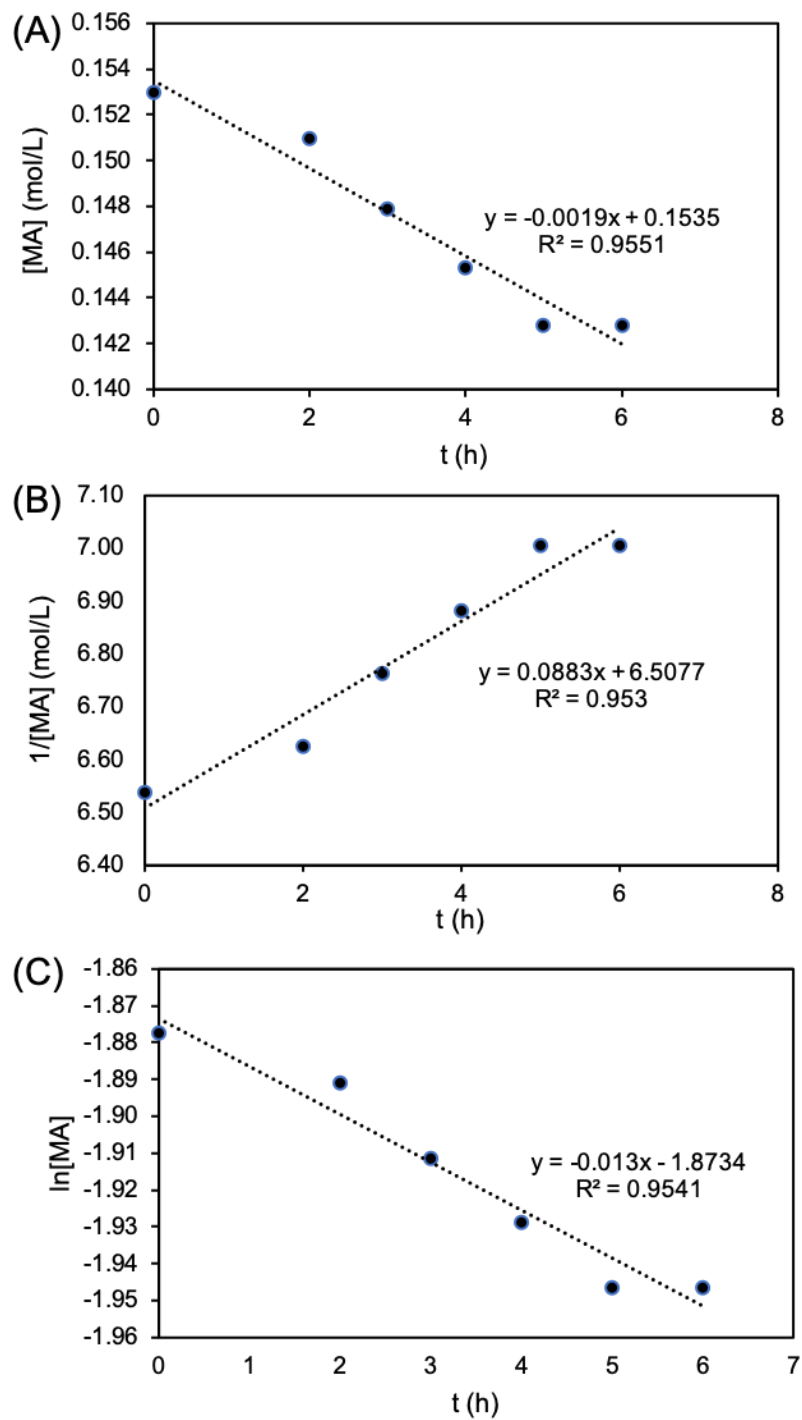
Figure 69: Experimental data plots of (A) zero-, (B) first- and(C) second-order reactions

Appendix C: Licence agreement to use published paper

License Number	5454350066092
License date	Dec 22, 2022
Licensed Content Publisher	John Wiley and Sons
Licensed Content Publication	Canadian Journal of Chemical Engineering
Licensed Content Title	Performance of a novel, eco-friendly, cellulose-based superabsorbent polymer (Cellulo-SAP): Absorbency, stability, reusability, and biodegradability
Licensed Content Author	Rosa Arredondo, Zhongshun Yuan, Dennise Sosa, et al
Licensed Content Date	Sep 19, 2022
Licensed Content Volume	0
Licensed Content Issue	0
Licensed Content Pages	10
Type of use	Dissertation/Thesis
Requestor type	Author of this Wiley article
Format	Electronic
Portion	Full article
Will you be translating?	No
Title	Production of cellulose-based superabsorbent polymers for soil water retention
Institution name	Western University

Expected
presentation date   Dec 2022

Requestor Location London, ON
                    Canada
                    Attn: Miss Rosa Arredondo
Publisher Tax ID   EU826007151

Appendix D: Swelling kinetics of Cellulo-SAP

The experimental data obtained from the swelling absorption behaviour of Cellulo-SAP in deionized water and in 1.0 mol/L solutions of $MgSO_4$, NaCl, and $CaCl_2$ were used to generate a model equation.

The swelling absorption accurately described the following second-order equation:

$$W_t = \frac{At}{t+B} \qquad \textbf{Equation 16}$$

where W_t (g) is the weight of the absorbed liquid at time t (min); A (g) and B (min) are constant values. To calculate the constant values, Equation 19 was changed to its linear form, as follows:

$$\frac{t}{W_t} = \frac{1}{A}t + \frac{B}{A} \qquad \textbf{Equation 19}$$

Then, using the experimental data of the swelling absorption of Cellulo-SAP, the parameters of the second-order equation for deionized water and the solutions were calculated from the resultant linear equations of their corresponding graphs, which are shown in Figures 70–73.

t (min)	w_t (g)	t/w_t (min/g)
0	0	0
30	17.0	1.8
60	20.6	2.9
90	21.9	4.1
120	22.9	5.2
150	23.5	6.4
180	23.8	7.6
210	23.9	8.8
240	23.9	10.0
270	23.9	11.3
300	23.9	12.5

(A)

(B)

$y = 0.041x + 0.339$
$R^2 = 0.999$

Parameters of second order kinetic model in deionized water				
1/A	B/A	A (g)	B (min)	R2
0.041	0.339	24.39	8.268	0.999
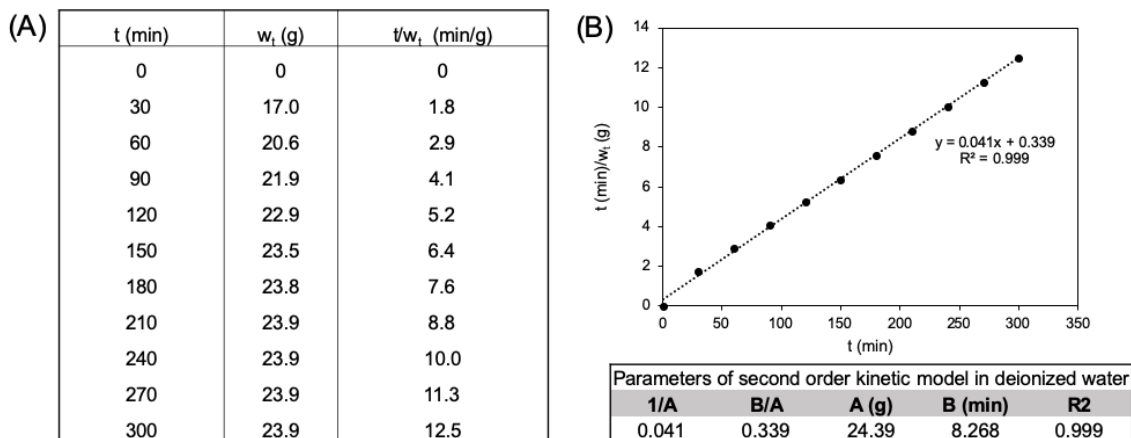
Figure 70: (A) Experimental data of swelling absorption of Cellulo-SAP in deionized water; (B) graph and parameters of second order kinetic model

t (min)	w_t (mg)	t/w_t (min/mg)
0	0	0
30	11437	0.1
60	13232	0.1
90	10046	0.2
120	10024	0.2
150	11012	0.3
180	11471	0.4
210	7693	0.4
240	995	0.5
270	4297	0.5
300	3657	0.6

(A)

(B)

$y = 0.002x + 0.021$
$R^2 = 0.997$

Parameters of second order kinetic model of Cellulo-SAP in 1.0 mol/L solution of $MgSO_4$				
1/A	B/A	A (mg)	B (min)	R²
0.002	0.021	560.32	11.61	0.997
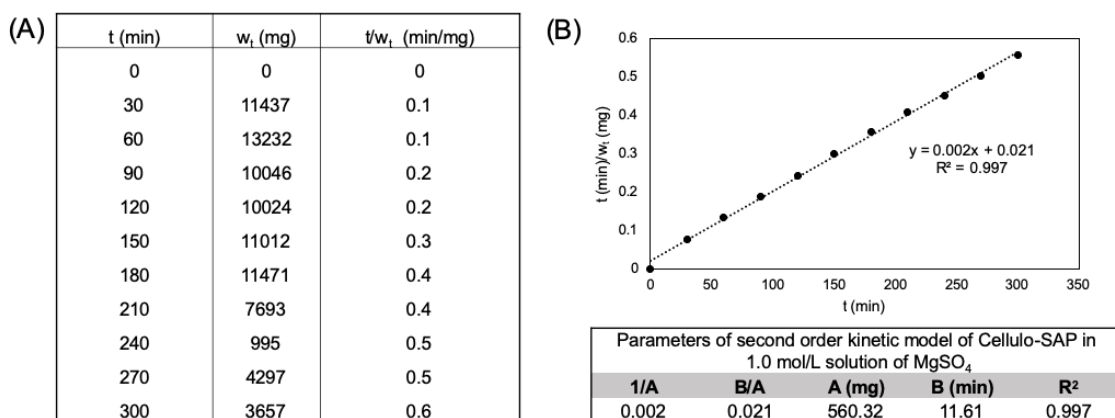
Figure 71: (A) Experimental data of swelling absorption of Cellulo-SAP in 1.0 mol/L solution of MgSO4; (B) graph and parameters of second order kinetic model

(A)

t (min)	w_t (mg)	t/w_t (min/mg)
0	0	0
30	335.1	0.1
60	402.3	0.1
90	423.3	0.2
120	430.4	0.3
150	433.3	0.3
180	435.5	0.4
210	435.9	0.5
240	438.2	0.5
270	444.7	0.6
300	449.2	0.7

(B)

$y = 0.002x + 0.014$
$R^2 = 0.999$

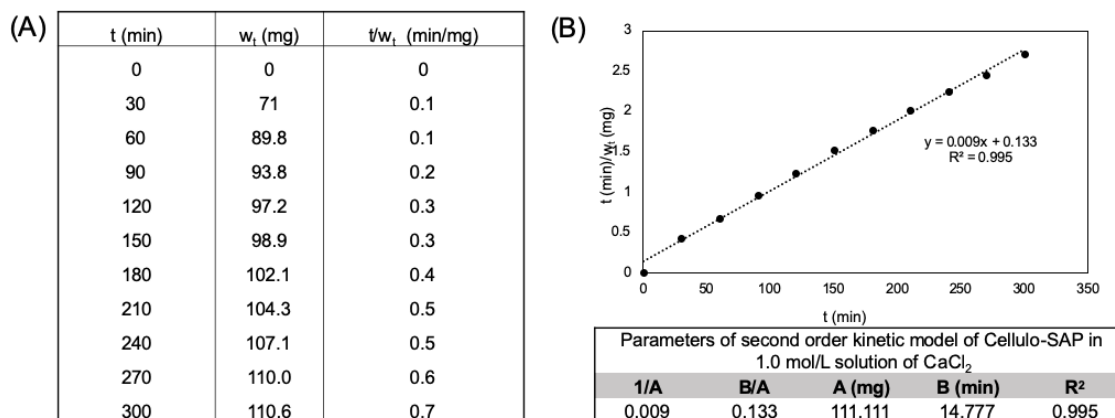| Parameters of second order kinetic model of Cellulo-SAP in 1.0 mol/L solution of NaCl				
1/A	B/A	A (mg)	B (min)	R^2
0.002	0.014	450.32	6.304	0.999
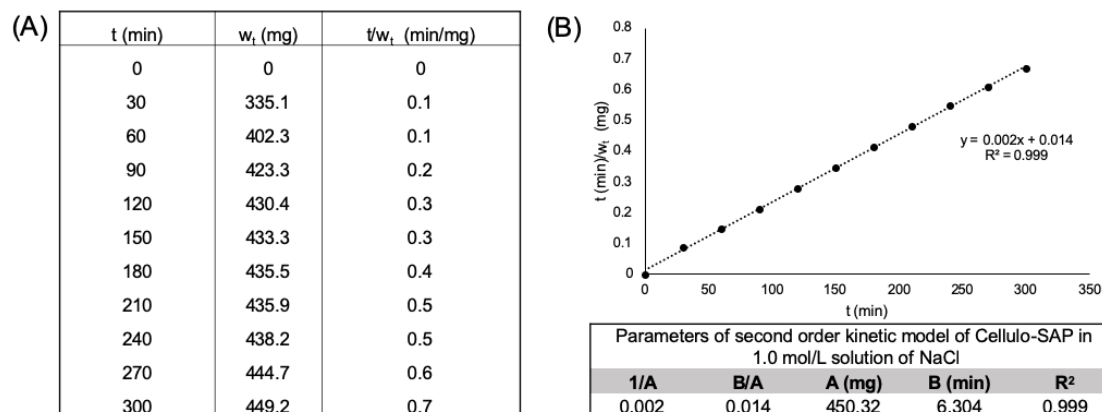
Figure 72: (A) Experimental data of swelling absorption of Cellulo-SAP in 1.0 mol/L solution of NaCl; (B) graph and parameters of second order kinetic model

(A)

t (min)	w_t (mg)	t/w_t (min/mg)
0	0	0
30	71	0.1
60	89.8	0.1
90	93.8	0.2
120	97.2	0.3
150	98.9	0.3
180	102.1	0.4
210	104.3	0.5
240	107.1	0.5
270	110.0	0.6
300	110.6	0.7

(B)

$y = 0.009x + 0.133$
$R^2 = 0.995$

Parameters of second order kinetic model of Cellulo-SAP in 1.0 mol/L solution of $CaCl_2$				
1/A	B/A	A (mg)	B (min)	R^2
0.009	0.133	111.111	14.777	0.995

Figure 73: (A) Experimental data of swelling absorption of Cellulo-SAP in 1.0 mol/L solution of $CaCl_2$; (B) graph and parameters of second order kinetic model

Curriculum vitae

Rosa María Arredondo Ramírez

Post-secondary education and degrees

2018–2022: **Ph.D. in chemical engineering**
Western University
London, Canada

2013–2015: **M.Sc. in environmental engineering**
University Michoacana de San Nicolás de Hidalgo
Morelia, Mexico

2015: **Graduate student exchange**
University of Manchester
Manchester, England

2007–2012: **B.Sc. in chemical engineering**
University Michoacana de San Nicolás de Hidalgo
Morelia, Mexico

Honours and awards

2018–2022: **Mexican Overseas Science & Technology Ph.D. Scholarship**
Government of Mexico, National Council of Science and Technology
(CONACyT-SENER)

2019: **First Place Speech in 3-Minute Thesis Competition**
Research Bridges Competition (Green and Environmental Engineering)
Chemical and Biochemical Engineering Department of Western University

2013–2015: **Mexican National Science & Technology M.Sc. Scholarship**
Government of Mexico, National Council of Science and Technology
(CONACyT)

Related work experience

2018–2021: **Graduate teaching assistant**
Western University
London, Canada

2017–2018: **University instructor and laboratory supervisor**
University Tecnológica de la Construcción
Morelia, Mexico

2016–2018: **University instructor and laboratory supervisor**
University Tecnológica de Morelia
Morelia, Mexico

Peer-reviewed publications

2022: **Principal author of "Performance of a novel, eco-friendly, cellulose-based, superabsorbent polymer (Cellulo-SAP): Absorbency, stability, reusability, and biodegradability"** (*Canadian Journal of Chemical Engineering*, 2022)

2022: **Co-author of "Functionalized wood as bio-based advanced materials: Properties, applications, and challenges"** (*Renewable and Sustainable Energy Reviews*, 2021)

Podium presentations

2021: **Development of cellulose-based superabsorbent polymers (SAPs)**
Canadian Chemical Engineering Conference
Montreal, Canada

2019: **Bio-based superabsorbent polymers for agricultural soil water retention**
Wood Pellet Association of Canada Annual General Meeting & Conference
Ottawa, Canada

2014: **Polymer emulsion obtained from post-consumer expanded polystyrene with application in mortars**
International Materials Research Congress
Cancún, Mexico